Evaluation of Linear Multiinput-Multioutput Feedback Control for a Human Arm Model

by

Steve G. Massaquoi

A.B., Harvard University (1978)
M.D., Harvard Medical School (1983)

Submitted to the Department of Electrical Engineering and Computer Science
in partial fulfillment of the requirements for the degree of

Master of Science in Computer Science and Engineering

at the

MASSACHUSETTS INSTITUTE OF TECHNOLOGY

September 1993

Author ...
.....
Department of Electrical Engineering and Computer Science
September 3, 1993

Certified by .....
Munther Dahleh
Associate Professor
Thesis Supervisor

Accepted by .....
Frederic R. Morgenthaler
Chairman, Departmental Committee on Graduate Students

Evaluation of Linear Multiinput-Multioutput Feedback Control for a Human Arm Model

by

Steve G. Massaquoi

Submitted to the Department of Electrical Engineering and Computer Science
on September 3, 1993, in partial fulfillment of the
requirements for the degree of
Master of Science in Computer Science and Engineering

Abstract

In this thesis, I define and simulate a human arm model and a feedback linearization control scheme based on established and hypothesized neurophysiology of the cerebellum and its connections. The arm model employs variable rest-length springs as actuators and the control signal consists of the intended trajectory in angular coordinates, a feedback correction signal and several types of additional feedforward signals chosen to cancel or, partially cancel, plant nonlinearities. The feedback signal is generated by a linear, multiinput-multioutput controller which is taken to represent the action of the medial cerebellum in the processing of angular position and angular velocity error signals. The performance of several different linear MIMO controller designs, including H_2, H_∞ and PD structures, is evaluted in several regulation and tracking tasks with several different plant variations. Evaluation is made in terms of integrated square input and state error costs, and various standard time-domain measures. The effects of changing the feedforward signal and of saturating the actuators are studied as well. The goals of the investigation are to determine whether certain linear feedback matrix structures offer systematic advantages under various conditions and according to various criteria, and to identify any implications which these findings may have for cerebellar function and performance.

Thesis Supervisor: Munther Dahleh
Title: Associate Professor

Contents

Chapter 1

Introduction

1.1 Motivation

The brain of every animal which needs to generate quick, accurate movements has a cerebellum, and significant damage to the organ invariably results in clumsiness and incoordination. Drunken stagger, loss of manual dexterity and slurring of speech are classic manifestations of cerebellar dysfunction due to the effect of alcohol on the cerebellum. As cerebellar damage never produces paralysis, the structure is felt to be involved chiefly in the coordination and modulation of movements rather than in their origination.

The cerebellum does not appear to operate primarily at the conceptual or strategic level, but rather at the level of unconscious execution. In particular, the more lateral parts of the cerebellum are thought to be involved in facilitating the timely execution of motor program components specified by other brain regions. The more medial parts of the cerebellum participate in reinforcing and coordinating muscular activity patterns to stabilize, and otherwise optimize body movement as it proceeds.

Neuroanatomically, the organ is well-organized for such functions. It is richly connected to almost all major motor and sensory processing centers via high-speed nerves. In particular, it receives massive position, velocity and force/torque information from virtually all moving body parts, and has outflow to the motor areas of the cerebral cortex, brainstem and spinal cord. On the other hand, the cerebellum itself has a fairly simple and extremely uniform ultrastructure which has been conserved across most vertebrates, from fish and amphibians to birds and mammals. This clearly suggests that its computation is basic and of universal importance to animal motor control.

An important aspect of cerebellar control is that it is adaptive. This feature presumably enables the animal's motor control system to adjust to changes in loads and actuator (muscle) properties, as well as perhaps to the aging, and slowing, of the nervous system itself. Evidently, cerebellum-mediated adaptation is a principle component of general behavioral motor learning.

Because of its significance to all animal motor control, its relatively easy accessibility to direct neuronal electrophysiologic study and its well-understood, fairly simple architecture, in addition to the fact that many humans suffer from its dysfunction, the cerebellum has been the subject of much investigation and modelling. Work has been done by neurophysiologists, neurologists, psychologists, as well as by engineers and biophysicists. While many of the latter apparently are motivated by the desire to assist physiologists, some have approached the subject with an independent interest in its possible applications to more general parallel networks for adaptive control. Both of these motivations underlie this investigation.

1.2 Existing Models

1.2.1 Cerebellar Models

Figure 1-1 depicts the essential functional gross and ultrastructural neuroanatomy of the cerebellum in the human motor system. Grossly, the cerebellum is massively connected to the sensorimotor areas of the cerebrum where volitional movement is conceived and directed, as well as to subcortical, brainstem, and spinal sites where more primitive reflex responses originate and diverse sensory signals are processed. Virtually all conceptions of cerebellar function suggest that the cerebellum operates by modulating inflowing signals, which are conveyed by mossy fibers, by the action of a side loop which traverses parallel fibers and Purkinje cells. The net output is transmitted via the nuclear cells to other sites in the nervous system. For clarity, the figure depicts only one instance of each cell and fiber type. Since, in actuality, the destinations of the mossy fibers and their branches are widely distributed throughout the cerebellum, there is great divergence of information to great numbers of parallel fibers. And since thousands of parallel fibers contact each Purkinje cell, there is subsequently great convergence of information prior to output.

The synaptic connections between the parallel fibers and the Purkinje cells have modi-

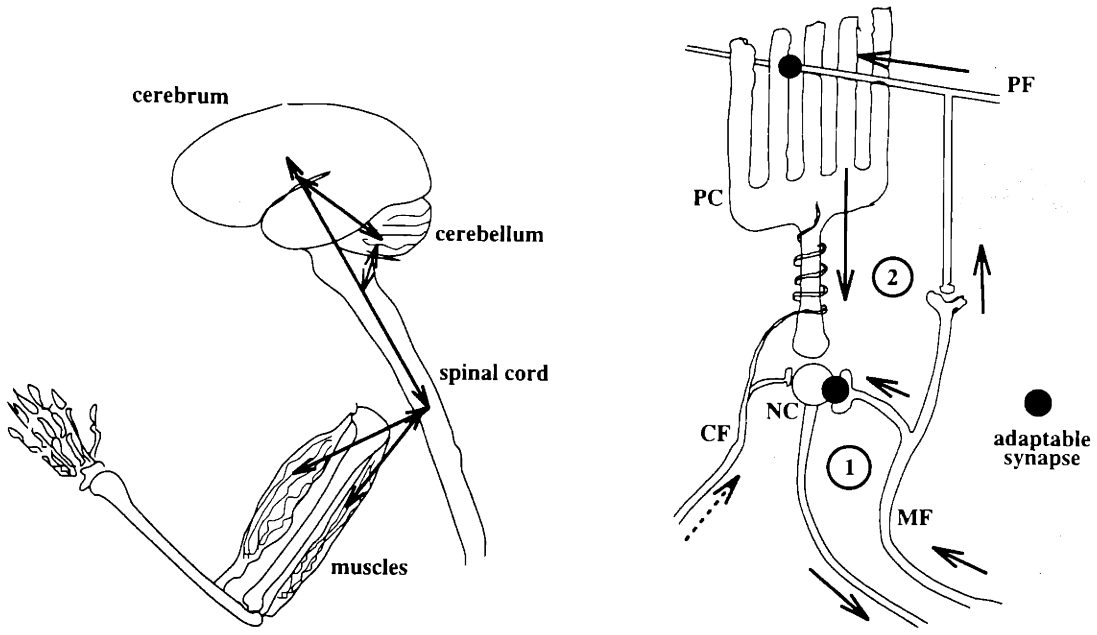

Figure 1-1: Functional neuroanatomy (schematic) of the cerebellum. Left) major motor system signal flows; Right) cerebellar ultrastructure and major internal signal flows: PC, Purkinje Cell; NC, Nuclear Cell; PF, Parallel Fiber; CF, Climbing Fiber; MF, Mossy Fiber. Loops labelled "1" and "2" represent main input/output and main side loops, respectively.

fiable transmission strengths, as possibly do the connections between the mossy fibers and nuclear cells. In particular, changes in connection strength are thought to be precipitated by simultaneous activity in the parallel fiber and the climbing fiber (which activates the Purkinje cell).

As will be elaborated in chapter 2, this thesis assumes that the primary inflowing signals represent position and velocity error information, and the primary outflow consists of feedback correction signals. The net gain of this feedback loop and possibly its predictive capacity, then, is regulated by the side loop which is controlled by the climbing fibers which convey "behavioral" error signals. These are error signals which indicate that *behaviorally significant* error has occurred and therefore adaptation should be effected in an effort to improve the feedback Since the climbing fiber activity gates the adaptation of the main circuitry, it can be viewed as form of a "learning supervisor" in the sense of abstract neural network learning theory (see section 1.2.2 below).

A host of mathematical models have been developed to account for cerebellar function, including the perceptron models of Marr [16] and Albus [1], the tensor model of Pellionisz

[22] and the adjustable pattern generator model of Houk, et. al [13] . Each of these tends to stress a different important aspect of cerebellar physiology: Marr and Albus point out its abilities to spatially integrate signals and to learn patterns over time, Pellionisz emphasizes that the organ is inherently massively multiinput and multioutput and serves to perform a coordinate transformation from covariant sensory vectors to contravariant motor vectors; and Houk suggests that the cerebellum and its closely associated motor centers comprise an adaptive motor pattern generator in response to trigger signals from other areas.

All of these features, however, can be largely subsumed by the view that the organ is fundamentally an adaptive MIMO feedforward/feedback controller which is probably at least in part dynamic. The bases for this general framework can be seen in the adaptive filter model proposed by Fujita[8], and the models of Neilson[18, 19] and Kawato [14]. The latter, in particular, serves as a point of departure for this work.

Briefly, these control models each suggest how the cerebellum adaptively weights neural signals to generate control inputs appropriate for minimizing tracking error between a body part and its intended trajectory. While the theories do not purport to account for all aspects of cerebellar function, they do give reasonable models for the role of the lateral cerebellum in generating appropriate feedforward signals to the muscles. Indeed, especially because the dynamics of body parts are typically quite nonlinear, the accuracy of the feedforward control signal *may* be of great importance to effective body control.

On the other hand, effective control must also utilize feedback information because of possible error in estimating the plant dynamics and/or because of exogenous disturbances. Since the cerebellum critically assists in both trajectory formation and postural stabilization, as in maintaining upright balance, one expects that it would participate in both feedforward and feedback control. Kawato alludes to this latter role when he hypothesizes that the medial cerebellum assists in generating predictive feedback signals to compensate for transmission delays from the periphery. However, he does not otherwise discuss how the cerebellum might distribute these signals to yield more optimal MIMO feedback control.

1.2.2 Relationship to General Neural Network Models

It is important to note that while *a priori* there is no compelling reason that the medial cerebellum must have a linear input/output relationship, parsimony and practicality dictate that initial inquiries consider the possibility that it does. Though neurons clearly have

strongly nonlinear input/output relationships overall (since they have firing thresholds and output saturation limits), many have sigmoidal input/output relationships which, like those of transistors, are quite linear over much of their practical operating ranges. Within this linear range the output firing levels are very often well-modelled by being considered linear combinations of weighted input signals.

Just as important in practice, is the fact that at the present time adaptive control is, in general, only understood in terms of adaptation of linear combinations of signals. Thus, to the extent that cerebellar adaptation is to be understood, it will be in this linear framework. This has therefore been the approach used by Kawato.

On the other hand, the consideration that the adaptation of the connection (synaptic) weights is fundamentally a nonlinear process, being essentially a correlation of input and output signals, is generalized from the actual neurophysiology of plastic changes in neural connections. This feature need not, and should not be simplified.

The combination of these linear and nonlinear features gives rise to the abstract neural elements used by many current neural network models. The correlation property of synaptic adaptation is the basis of the Hebb rule used to update connection weights in some artificial neural networks. Alhough there is general agreement that these processing elements represent an extremely gross simplification of neuronal operation, they already provide considerable richness in processing capability and are sufficiently realistic to yield important initial insights into the behavior of actual neural circuits.

The models studied by the investigators mentioned above, and in this thesis, are consistent with this type of abstract neural network theory. These cerebellar models, however, due to the nature of the underlying process being investigated, analyze the dynamic behavior of the neural network signals during its operation, not just the pattern and stability of connection weight adaptation which is the emphasis of most neural net studies not involving control applications.

1.3 Linear Feedback Optimization for Nonlinear Plants

Kawato's model, in particular, can be closely mapped to a feedback linearization control scheme outlined by Slotine and Li [24, pages 208-213] in which a combined nonlinear feedforward (computed torque), and an additional, explicit linear feedback term comprise a

control law for a 2-link robot arm. In principle, the nonlinear feedforward signal should perfectly anticipate (and cancel) the plant nonlinearities and thereby "linearize" any tracking error which may be due, for example, to initial conditions. The linearized error is fed back through a (time-invariant) linear feedback matrix (LFBM) to provide a correction signal. In an example [24, pages 404-405], Slotine and Li use a proportional-derivative controller as the LFBM. The PD controller used is "local" in the sense that position and velocity feedback from each joint is fed back to the same joint and not to the other joint. This yields a nonlinear-linear control law for which global system stability can readily be demonstrated. However, it is not suggested that this choice of feedback gain matrices is unique. In fact, an example of an alternative LFBM is given which takes advantage of the positive definite property of the system's moment of inertia matrix.

Thus, the general question emerges as to whether the linear feedback control matrix in a feedback linearization scheme can be optimized for a given system to improve its performance in tracking and disturbance rejection, as well as its robustness to feedforward dynamics misestimation. While it is possible that time-varying feedback control is used *in vivo*, for reasons of simplicity it is reasonable to first consider the time-invariant case. In particular, the following questions can be asked:

- 1) Are LFBMs which are designed to optimize performance with respect to the true linearized plant using some standard synthesis strategy (such as H_2/H_∞) stabilizing?
- 2) Do they, or any other controller design, perform better than the simple local PD LFBM with respect to any standard performance measures when used in conjunction with imperfect feedforward control?
- 3) If there are significant differences in performance between controllers, are these differences maintained across variations in plant structure or quality of feedforward signal?

If the answers to these questions are affirmative, then aside from the possibility of identifying an LFBM which may improve the performance of general feedback linearization schemes, we may gain further insight into cerebellar structure and function.

Specifically, if it becomes evident that global PD (GPD) control (incorporating interjoint feedback signals) is superior in some important regard to local PD (LPD) control, even (or especially) for a nonlinear plant such as an arm, we obtain a rationale for the presence of the large-scale convergence and divergence of signals between the cerebellum and different body parts. Moreover, if it appears that different MIMO gain ratios are clearly superior under different plant conditions or tasks, then the importance of specific types of gain adaptation

may be demonstrated.

Together, such findings would provide further theoretical support for the hypothesis that the cerebellum functions at least to some extent as an adaptive MIMO feedback controller. And if the performance of such simulated linear controllers corresponds well to that of humans, these findings would support the hypothesis that cerebellar feedback control may, in fact be substantially linear.

On the other hand, if there is no consistent advantage seen in the use of global linear control, the hypotheses regarding cerebellar function must be reevaluated. Perhaps, the cerebellum provides improved motor performance by exerting specifically *nonlinear* control. Or perhaps the the structure does not function as a feedback controller at all.

1.4 Thesis Findings

The simulations performed herein show that indeed, several LFBM's besides the LPD design are stabilizing and can be used to advantage. Not surprisingly, the preference for design of LFBM depends on the performance measure which is to be optimized. Both H_2 and H_∞ designs often perform comparably and appear to be best at minimizing an total cost functional which weights integrated (square) input magnitude as well as (square) error magnitude. This performance advantage occurs even in the face of plant nonlinearities.

In fact, a major finding of the study is that within the range of normal human arm velocities, the presence of dynamic nonlinearities does not dramatically degrade tracking or regulation performance in the presence feedback controllers having large but reasonable gains as measured by closed-loop crossover frequency. This observation and others may also explain why gainscheduling across angular velocity-space does not confer any particular performance advantage to the H_∞ or H_2 designs.

On the other hand, time domain measures, such as peak angular and Cartesian excursion, and angular and Cartesian settling time, are not optimally minimized by H_2, H_∞ or LPD controller designs. Instead, most often GPD designs which use significant levels of interjoint feedback (for example, larger than those of the H_2 and H_∞ controllers), perform best for a given limit of closed-loop crossover frequency. It appears that the presence of interjoint feedback acts to suppress secondary reactions at remote joints to the application of feedback correction at a given joint. Since the secondary reactions are typically un-

desirable, especially in tracking tasks, interjoint feedback typically enhances performance. Certain interjoint feedback also tends to have advantageous effects on closed-loop frequency response.

While the findings appear to be general across several plant variations, the useful controller gain values varied which suggests that gain adaptation in response to plant parameter changes may be important. Moreover, the importance of the LFBM structure was found to depend sensitively on the nature of the feedforward signal. Essentially, as might be expected, LFBM structure is most important where the feedforward signal is poor at anticipating, and hence poor at cancelling the effects of plant nonlinearities. All LFBMs tested performed well when the feedforward signal was accurate.

The latter observations especially, illustrate the significance of feedback matrix design to the performance of the particular feedback linearization scheme studied. While not extensive enough to provide an evaluation of its general importance, the simulations indicate that there are circumstances under which the LFBM structure is not a negligible consideration.

Together, the results do support the possiblity that the cerebellum functions at least partially as a MIMO feedback controller. They therefore encourage the incorporation of this control concept into the current theories of equilibrium trajectory movement control and the application of this model to explain actual limb movement data from normal human subjects as well as those who suffer from cerebellar impairment.

Chapter 2

Definitions

2.1 System Description

2.1.1 The Plant

The equations of motion of a 2-link rotary joint arm moving across a horizontal surface (thereby neglecting the effects of gravity), and having no intrinsic joint viscosity or other joint rotation resistance are:

$$\begin{cases} \tau_1 = h_1\ddot{\theta}_1 + h_2\ddot{\theta}_2 + h_3\dot{\theta}_1^2 + h_4\dot{\theta}_2^2 + h_5\dot{\theta}_1\dot{\theta}_2 \\ \tau_2 = h_6\ddot{\theta}_1 + h_7\ddot{\theta}_2 + h_8\dot{\theta}_1^2 \end{cases} \tag{2.1}$$

where

$h_1 = I_1 + I_2 + m_2 l_1^2 + 2m_2 C_2 l_1 \bar{l}_2$
$h_2 = h_6 = I_2 + m_2 C_2 l_1 \bar{l}_2$
$h_3 = 0$
$h_4 = -h_8 = -m_2 S_2 l_1 \bar{l}_2$
$h_5 = -2m_2 S_2 l_1 \bar{l}_2$
$h_7 = I_2$

and

$C_i = \cos\theta_i, \quad S_i = \sin\theta_i,$
τ_i is the (external) torque applied to joint i,
I_i and m_i are the moment of inertia and mass, respectively, of link i,
l_i and $\bar{l}_i$ are the length and distance to center of mass, respectively, of link i (see Fig. 2-1).

The system (2.1) can be rewritten:

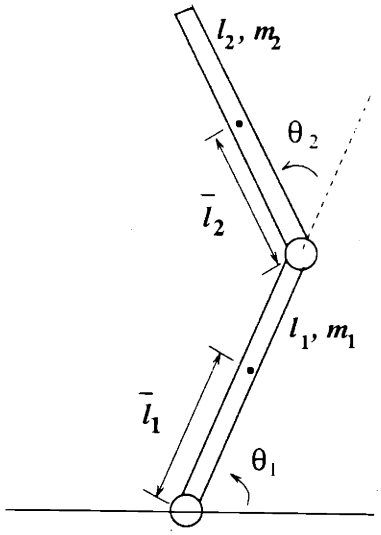

Figure 2-1: 2-link, rotary joint manipulator with parameters as defined in text.

$$\begin{bmatrix} \tau_1 \\ \tau_2 \end{bmatrix} = \begin{bmatrix} h_1 & h_2 \\ h_6 & h_7 \end{bmatrix} \begin{bmatrix} \ddot{\theta}_1 \\ \ddot{\theta}_2 \end{bmatrix} + \begin{bmatrix} h_4\dot{\theta}_2 & h_4(\dot{\theta}_1 + \dot{\theta}_2) \\ h_8\dot{\theta}_1 & 0 \end{bmatrix} \begin{bmatrix} \dot{\theta}_1 \\ \dot{\theta}_2 \end{bmatrix}$$

or

$$\boldsymbol{\tau} = H\ddot{\boldsymbol{\theta}} + C\dot{\boldsymbol{\theta}} \tag{2.2}$$

where:

$\boldsymbol{\tau}$ is the vector of applied joint torques: $[\tau_1, \tau_2]^T$,
$\boldsymbol{\theta}$ is the vector of joint angles: $[\theta_1, \theta_2]^T$,
H is the nonlinear, angular position-dependent moment of inertia matrix, and
C is a nonlinear, angular position and velocity-dependent matrix which includes Coriolis force effects.

Actual human or animal muscles, to a first approximation, behave as very lightly damped springs whose active length can be controlled via neural signals. They are typically arranged in antagonistic pairs which return joints to a specified equilibrium (reference) setpoint (See appendix A). This can be taken into account by augmenting (2.2) as:

$$\boldsymbol{\tau} = H\ddot{\boldsymbol{\theta}} + C\dot{\boldsymbol{\theta}} + K(\boldsymbol{\theta} - \boldsymbol{\theta}_{ref}) \tag{2.3}$$

where:

K is the symmetric (angular) stiffness matrix. In practice, K is positive definite.
$\boldsymbol{\theta}_{ref}$ are the possibly time-dependent intended joint angles (equilibrium setpoint trajec-

tories).

Muscles also have passive mechanical viscosity separate from the velocity-dependent torque components associated with C. However, the values of resting joint viscosities are small[1] and therefore we will consider (2.3) which ignores additional viscosity terms, to be a reasonable model of animal arm dynamics.[2]

Rearranging and generalizing, we may obtain the state space representation of the plant, $\mathcal{P}$:

$$\mathcal{P}: \qquad \dot{\mathbf{q}} = A\mathbf{q} + B_1\boldsymbol{\tau} + B_2\boldsymbol{\theta}_{ref}$$

or

$$\mathcal{P}: \qquad \dot{\mathbf{q}} = A\mathbf{q} + B_1\boldsymbol{\tau}_d + B_2\mathbf{u}_p \tag{2.4}$$

where:

$\mathbf{q}$ is the state vector: $[\theta_1, \theta_2, \dot{\theta}_1, \dot{\theta}_2]^T = [\boldsymbol{\theta}, \dot{\boldsymbol{\theta}}]^T$.

$\boldsymbol{\tau}_d$ is the vector of applied joint torques now explicitly identified with direct, nonmuscular disturbance torques,

$\mathbf{u}_p$ is the control signal sent to the muscle pairs at each joint.[3] In (2.3) this was simply $\boldsymbol{\theta}_{ref}$ but it may be a more general signal which includes feedforward components.

A is the nonlinear matrix representing the angular motions of the two masses (the two links).

B_1 is the nonlinear matrix reflecting the effect of direct torques on the angular motions.

B_2 is the nonlinear matrix reflecting the effect of joint angle equilibrium setpoints on the angular motions.

In particular,

$$A = \begin{bmatrix} 0 & I_2 \\ -H^{-1}K & -H^{-1}C \end{bmatrix}, \quad B_1 = \begin{bmatrix} 0 \\ H^{-1} \end{bmatrix} \quad \text{and} \quad B_2 = \begin{bmatrix} 0 \\ H^{-1}K \end{bmatrix}$$

where I_2 is the 2 by 2 identity matrix. We can be assured that the "mobility" matrix, H^{-1}, exists because inertia matrices are always positive definite.

---

[1] Estimated: 0.02-0.2 N-m-s [28] and these investigators confirmed that there were no significant changes in trajectory simulations over this range.

[2] To be sure, there is evidence that both the stiffness and effective viscosity of muscles changes (increases) with activation[15, 5], but, as discussed in section 2.1.2, we will treat these effects as being due to the action of the controller.

[3] Since the arm has there main pairs of muscles there are potentially three input signals. Assuming a simple constraint, however, the potentially problematic effects of muscle redundancy can be eliminated. See appendix A.

2.1.2 The Control System

Because of the great complexity of natural motor control systems, a considerable amount of abstraction is required to render them tractable to system analysis. The following simplifications are made with the recognition that results are likely to not be fully representative of actual system behavior, but with the belief that the major features will be retained from which basic organizing principles may be derivable.

Plant Input and Output Signals

The specific input signal to an animal muscle, $\mathbf{u}_m$, is a stream of neural impulses which are conveyed from the spinal cord along motor neuron fibers (Fig. 2-2). The impulses are of fixed amplitude and the strength of $\mathbf{u}_m$ is determined by the impulse frequency.. For a fixed-length muscle, there is a monotonic relationship between the frequency of these impulses and the intensity of muscle fiber contraction. Hence, for a stationary limb, there is a monotonic relationship between $\mathbf{u}_m$ and the torques developed at the joints which the muscle spans. However, since muscle fibers are of different sizes and types, and since muscles have various position-dependent mechanical actions at each joint, there is considerable nonlinearity in the relationship between $\mathbf{u}_m$ and the torque developed. That is, K in (2.3) is itself, in fact, an increasing function of $\mathbf{u}_m$. Moreover, there are small transmission delays and velocity dependencies in torque production. There is also evidence, however, [4],[12, page 307] that local spinal circuitry serves to compensate for much nonlinearity so that the descending input to the *spinal* circuitry, $\mathbf{u}_{sp}$, is *incrementally*[4] *nearly proportional to the joint torque developed* especially for small signals, modulo a small transmission delay. Significant nonlinearity is encountered most markedly for torque signals resulting from commands to abruptly change the joint angle by more than about 20 degrees [12, pages 292-284].

Therefore, as a significant simplification, it will be assumed herein that from the perspective of the brain (including the cerebellum), K is square and constant with respect to $\mathbf{u}_{sp}$. Thus, in the absence of active muscular cocontraction, any effective change in arm stiffness during movement is taken to be due to the action of the controller (see appendix A for further discussion). In this case, we can take $\mathcal{P}$ to represent the *entire spinomuscu-*

[4]Net torque only develops when $\mathbf{u}_{sp}$ does not match the current position specification.

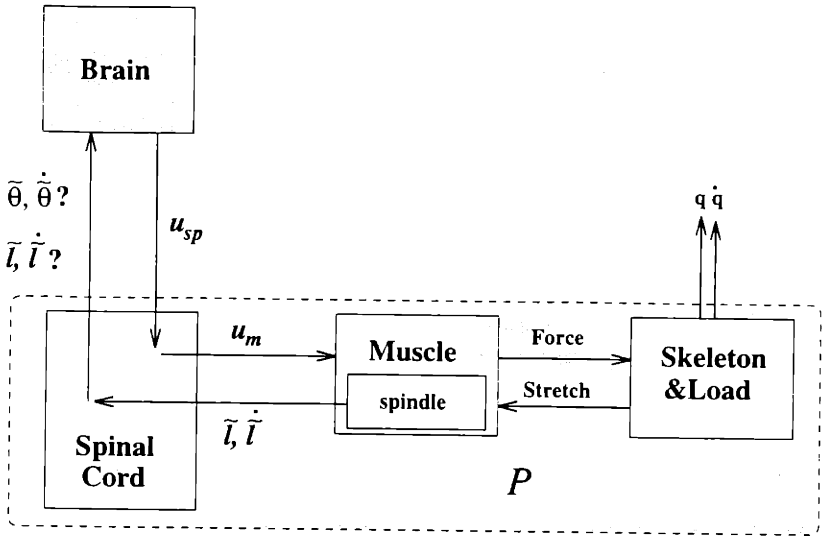

Figure 2-2: Schematic diagram of spinomuscular apparatus which controls limb movement. $\mathcal{P}$ defines plant being controlled. Path variables are defined in text.

loskeletal system, and identify $\mathbf{u}_p$ as $\mathbf{u}_{sp}$. It will also be assumed, as indicated in section 2.1.1, that intrinsic plant viscosity is constant (and negligible). All system viscosity, then, is modeled to derive from the controller.

To further simplify the analysis significantly, it will also be assumed that there are no transmission delays. However, as suggested above, this is ultimately an unacceptable assumption for any realistic natural control model. In a human, for instance, the typical round-trip transit time for a feedback signal controlling the arm via the brain is on the order of 80-100 milliseconds. It is, in fact, accepted by many current neurophysiologists and modellers that natural motor systems must therefore include a mechanism for prediction to compensate for these delays. Several investigators [8, 22, 14] have already discussed mechanisms by which the cerebellar circuitry could generate predictive signals and it is assumed herein that some such mechanism is indeed operative.

The sensory signals from fixed-length muscles (from the muscle spindles) include signals proportional to muscle length, its rate of change and to the force developed. This is especially the case for small amplitude displacements. This observation, along with the recognition that the spindles can be actively biased by descending neural input, has led several physiologists to hypothesize that the sensory signals are muscle length, length-rate

and force *errors* relative to the bias signal. Presumably, the bias signal represents the intended, or reference variable values [12, pages 265-266, 268].[5] It is likely that ascending nerve fibers[6] convey signals representing mixtures of these error variables to the brain [3, page 738]. Recent evidence [21] is consistent with the hypothesis that at least the length and length-rate signals are combined linearly[7].

Muscle length and lengthening rate are usually monotonically related to the angles and angular velocities of the joints which are spanned, but for straightforward geometrical reasons, this relationship is not linear. While it is known that the length and length-rate signals from the muscles undergo preprocessing in the spinal cord before ascending, it is not known whether this processing translates the signals into joint coordinates. As a third simplification, however, it will be assumed that the conversion is made and hence full linear state (angular) error information is available to the control system from $\mathcal{P}$. To the extent that the translation is not performed, the results herein will only have strong applicability to the (fairly large) regions of the workspace in which the geometrical nonlinearities are small; that is, where joint angles are near $\pi/2$.

The Role of the Cerebellum in Tracking and Regulation

As mentioned in the introduction, the gross connectivity of the cerebellum as well as numerous physiologic experiments suggest that the cerebellum participates in both feedforward and feedback control. In a complex control system which includes several levels of control loops, however, feedforward and feedback are terms which relative to the depth of loop nesting. Therefore, some clarification of these ideas is important.

To be sure, as concerns the human, or more generally mammalian, motor control system there has been longstanding debate regarding the precise role of the cerebellum in motor control. The structure clearly participates in several control loops and appears to be partitioned, by virtue of its input/output connectivity pattern, into a lateral (hemispheric)

[5] Although this formulation has not been established definitively, it will be adopted here for simplicity. Whether the spindle sends an error signal, or an absolute signal from which a reference value is subtracted elsewhere to generate the error, is not important to distinguish at this point. It is simply important to consider that, ultimately, error information is generated and that the cerebellum is intimately involved in the feedback control based on these errors.

[6] Specifically, the dorsal spinocerebellar tract (DSCT)

[7] In the study cited, at least 85 percent of the variance in these signals can be accounted for by a linear combination of 3 component waveforms. By my interpretation of the data which is presented, the first signal is consistent with length, the second and third add to represent lengthening velocity.

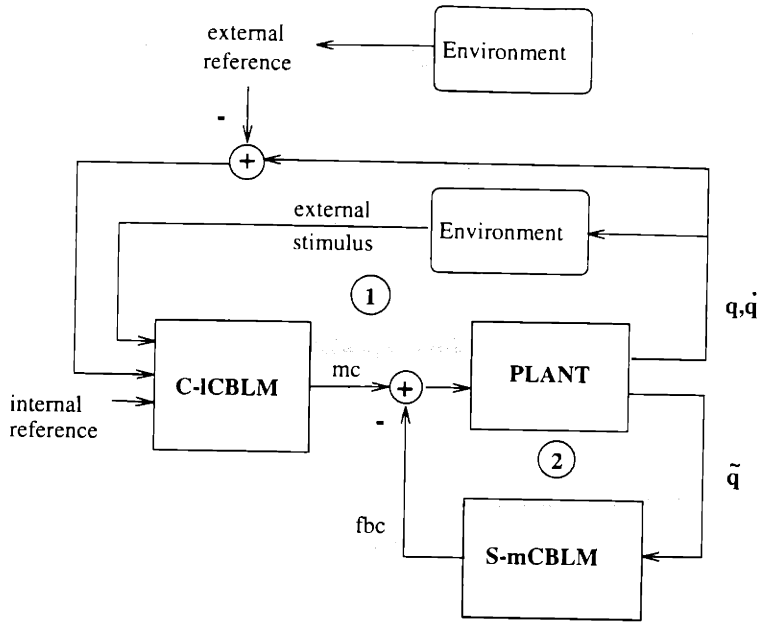

Figure 2-3: General formulation of the role of the cerebellum in motor control. Loop 1) Behavioral feedback loop. Loop 2) Stabilizing feedback loop. **mc**, motor command; **fbc** feedback correction.

portion, which communicates reciprocally with the cerebrum, and a medial portion which communicates reciprocally with especially the spinal cord, and to some extent with the cerebrum as well.

There remains considerable disagreement regarding the functions of these two cerebellar subsystems because there has been much apparently conflicting data. For the purposes of this thesis, a very general model structure will be adopted which is consistent with most physiological studies and with Kawato's model in particular.

The general scheme as outlined in Figure 2-3 considers two main control loops. The outer loop is the consciously, or semi-consciously mediated "behavioral" or "S-R" (stimulus-response) loop which enables accurate motor responses to consciously perceived external and internal stimuli [12, pages 269-270]. This loop, when closed, yields continuous updating of intended movements relative to consciously perceived performance errors or other events. Examples would include so-called "hand-eye coordination" tasks, which may involve tracking an external reference trajectory, and "skilled" balancing tasks, i.e. tasks such as bicycle riding or ice-skating for which a repertoire of special "reflexes" to external events must be learned.

Alternatively, the forward path of the loop may function in open-loop mode wherein volitional movements are made according to an internal stimulus (reference plan) and correction on the basis of external stimuli is suppressed. Examples would include the performance of "wrote" movement patterns such as instrument playing or handwriting, but also any volitional movement for which ongoing conscious correction will be suppressed, e.g. "ballistic" flailing of the arms.

There is considerable evidence, which will not be reviewed here, that suggests that the lateral cerebellum cooperates with the cerebrum to execute this loop. Damage to this part of the cerebellum is associated with slowed reaction times and disordered timing of volitional movement sequences. Kawato suggests that the lateral cerebellum assists the cerebrum in generating accurate signals which anticipate the nonlinearities of the plant. This will be discussed in greater detail below.

Such signals from the cerebro-lateral cerebellar system (C-lCBLM), whether in response to internal or external stimuli, are feedforward relative to the inner, subconscious stabilizing loop which involves principally the interaction between the medial cerebellum and spinal cord (probably with contributions from the cerebrum, though the details are not clear). The inner loop apparently serves to match actual body position with that instructed by the C-lCBLM. As such, it is important both in tracking and postural stabilization. Damage to this system manifests itself chiefly as delayed initiation and underdamped termination of movements. Sometimes a persistent tremor results [29, 27].

Within the inner loop, the medial cerebellum facilitates error feedback control in some fashion. Kawato suggests that it is by providing a predicted position signal based on an acquired dynamical model. Others [9, 10], argue that it modulates the strength of spindle feedback signals. In either case, the entire spino-medial cerebellar system (S-mCBLM)[8] appears to function as a MIMO feedback controller with sufficient predictive capacity to neutralize the effects of transmission delays.

It is from this perspective that the cerebellum can be considered to be involved in both feedforward and feedback control. Much of the confusion in the interpretation of physiological experiments involving cerebellar lesions may be due to the fact for most tasks both loops operate in concert. Moreover, some experimental tasks involve the behavioral loop in closed-loop mode, while others involve it in open-loop mode. In any case, this

[8]The possible contribution of the cerebrum is recognized, but not emphasized in this abbreviation.

investigation focuses on the role of the S-mCBLM in the inner stabilizing loop. Therefore, "tracking" refers to following the internally generated feedforward signal from the C-lCBLM, not tracking of an exernal stimulus.

In principle, feedback is essential for regulation tasks, where the feedforward signal is constant and unpredictable disturbances are to be rejected. Thus, postural stabilization can be considered to be most fundamentally dependent on feedback control, while volitional movement may utilize a combination of feedforward and feedback signals. Since successful maintenance of posture is logically a prerequisite to successful body trajectory formation (intended body trajectory tracking) it would appear, then, that postural stabilization is the most fundamental function of especially the medial cerebellum.[9] On the other hand, it may be suspected that good disturbance rejection properties of medial cerebellar circuits will serve well to minimize tracking errors as well.

Accepting this general framework, as does Kawato, we can detail the cerebellar control system as shown in Fig. 2-4. Here the C-lCBLM generates a feedforward signal $\mathbf{u}_{ff}$ consisting of reference trajectory, $\boldsymbol{\theta}_{ref}$, (again, for our purposes in joint coordinates, but in actuality quite possibly in muscle length coordinates) and an additional feedforward input signal $\mathbf{u}_{dyn}$. The net input signal, $\mathbf{u}_{sp}$, is seen to be the difference between $\mathbf{u}_{ff}$ and $\mathbf{u}_{fb}$, the feedback signal from the S-mCBLM processing of the error signal $\tilde{\mathbf{q}} = \mathbf{q} - \mathbf{q}_{ref}$. The S-mCBLM is represented as the linear feedback controller, G. If we take $G = [G_1 \quad G_2]$, where G_i are the angular position and angular velocity feedback components respectively, we may extend (2.4) to include the action of the S-mCBLM:

$$\dot{\mathbf{q}} = A\mathbf{q} + B_1\boldsymbol{\tau}_d + B_2(\mathbf{u}_{ff} - \mathbf{u}_{fb})$$

or

(2.5)
$$\dot{\mathbf{q}} = A\mathbf{q} + B_1\boldsymbol{\tau}_d + B_2(\mathbf{u}_{ff} - G\tilde{\mathbf{q}})$$

or

[9]The spinomuscular apparatus itself participates in the regulation of muscle stiffness via the monosynaptic spinal "knee jerk" reflex. Hence, it contributes to postural stability at a low level. Numerous physiologists have argued, however, that the spinal reflex does not comprise the major portion of posture regulation. Analysis of electromyographic data (muscle electrical activity) clearly shows that there are significantly larger "long loop" responses to muscular stretch (an equivalent to postural disturbance) which occur at latencies consistent with processing at levels higher than the spinal cord [12, page 280], i.e. in the brain.

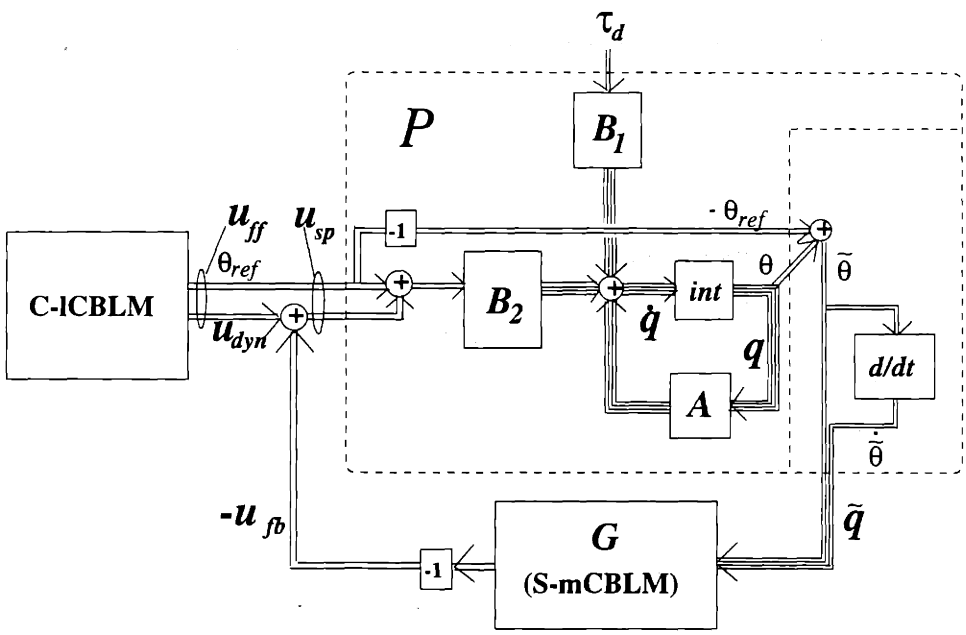

Figure 2-4: The cerebellar control system as a feedback linearizing scheme. The plant, $\mathcal{P}$, is the spinomusculoskeletal system of Figure 2.2 with the hypothesized function of the muscle spindle represented by the subregion at right. C-lCBLM is the cerebro-lateral cerebellar system. S-mCBLM is the spino-medial cerebellar system. Matrices A, B_1, B_2 and path variables are as in equations 2.5 and 2.6. "*int*" reprsents an integrator.

$$\dot{\mathbf{q}} = A\mathbf{q} + B_1\tau_d + B_2(\boldsymbol{\theta}_{ref} + \mathbf{u}_{dyn} - G\tilde{\mathbf{q}}) \tag{2.6}$$

This system can now be interpreted in terms of the similar feedback linearization schemes of Kawato, and of Slotine and Li [14, 24]. In feedback linearization, to the extent that $\mathbf{u}_{ff}$ anticipates the plant dynamics (including nonlinearities), $\tilde{\mathbf{q}}$ will be determined chiefly by τ_d. We can see this from (2.4) by expanding the system as:

$$\begin{cases} \dot{\boldsymbol{\theta}} &= \dot{\boldsymbol{\theta}} \\ H\ddot{\boldsymbol{\theta}} &= -KG_2\dot{\tilde{\boldsymbol{\theta}}} - K(I_2 + G_1)\tilde{\boldsymbol{\theta}} - C\dot{\boldsymbol{\theta}} + \tau_d + K\mathbf{u}_{dyn} \end{cases}$$

Here we see that if $\mathbf{u}_{dyn} = K^{-1}(\hat{H}\ddot{\boldsymbol{\theta}}_{ref} + \hat{C}\dot{\theta}_{\text{ref}} - \hat{\tau}_d)$, where $\hat{H}$, $\hat{C}$ and $\hat{\tau}_d$ are the estimates of H, C and, if possible, τ_d, respectively, then the dynamics can be written:

$$H\dot{\tilde{\boldsymbol{\theta}}} = -(KG_2 + C)\dot{\tilde{\boldsymbol{\theta}}} - K(I_2 + G_1)\tilde{\boldsymbol{\theta}} + \mathbf{u}_{err}$$

where

$\mathbf{u}_{err} = \tilde{H}\ddot{\boldsymbol{\theta}}_{ref} + \tilde{C}\dot{\boldsymbol{\theta}}_{ref} - \tilde{\tau}_d$,
$\tilde{H} = \hat{H} - H$, $\tilde{C} = \hat{C} - C$ and $\tilde{\tau} = \hat{\tau} - \tau_d$.

This indicates that aside from errors generated by initial conditions, state errors are driven by misestimation of forward dynamics and failure to anticipate disturbances (indeed, typically $\hat{\tau}_d$=0); and assuming that G is a stabilizing controller, errors will tend to zero in the absence of a moving reference trajectory and torque disturbances.

In the adaptive versions of this scheme, the model of the plant dynamics which is used by the C-1CBLM to generate $\mathbf{u}_{dyn}$ is adaptively improved over time through practice so that the S-mCBLM eventually becomes exclusively concerned with the rejection of unpredicted disturbances (including the effects of unanticipated initial conditions).

Kawato and Slotine's formulations differ slightly in the manner in which the feedforward model is adapted, but neither discusses extensively the adaptation or optimization of G. It is reasonable to consider, however, that for any given plant, even – or especially – nonlinear ones, some choices of G yield better performance than others. The subject of this investigation, then, is the advantageous selection of G given $\mathcal{P}$.

2.2 Optimizing Feedback Gains

2.2.1 Physiological Considerations

The cerebellum is essential for optimal muscle coordination and smoothness for virtually all motor tasks. We can therefore hypothesize that it tends to optimize some very basic cost criterion which is of general significance to the whole motor control system. This criterion may not be easy to define, however. Nevertheless, we can hope to gain some insight by considering some candidate cost functionals which are both simple and physiologically reasonable, and try to determine whether associated optimal controllers could be implemented by the cerebellar structure.

It is reasonable to assume that in most circumstances large tracking error, defined as the difference between the desired and the actual trajectory (whether in movement or in posture maintenance) is undesirable. Therefore, it is likely that the motor system seeks to minimize the magnitude of $\tilde{\mathbf{q}}$ to the extent possible. Since under non-pathological conditions, animal control systems are grossly stable[10] and since relatively large amplitude tremor is a frequent result of cerebellar damage, it is apparent that G is a stabilizing controller.

Stability maintenance and tracking error minimization are naturally desirable goals for any control system. These goals are at some level, however, always traded off against the costs of control input. In animal systems, however, the understanding of these tradeoffs is still quite incomplete. Several studies of normally-coordinated human movement have attempted to identify control cost optimization in human movement. Minimized variables have included peak velocity, acceleration, force, total energy [20], and most recently time-integrated square torque-change cost [28]. The latter empirically gives the best accounting for the smooth, gently curved trajectories of many "natural" (relatively low-effort) human arm movements. On the other hand, it is also evident that very straight, abrupt, effortful, yet well-coordinated movements can be made at will. And in general, there are also well-described speed/accuracy tradeoffs in human movement [6] such that movement time minimization and accuracy maximization are both clearly possible optimizations; individuals apparently may vary the relative importance between control and error cost for different movements. Thus, the total optimization of a movement likely depends on a very

[10] The most common normal instability, "physiologic" tremor occurs typically at very low amplitude – a few millimeters peak to peak at the fingertips – and appears to be related to disturbances originating in muscles and not control loop instability [7].

task-dependent hierarchy of constraints, the interrelationships of which are not yet well identified.

It is recognized, furthermore, that during motor learning neural changes occur at multiple sites in the motor control system such that optimization involves tuning of the entire system, not just the cerebellum. The task-dependent nature of torque-change optimization suggests that this level of optimization involves strategic decisions and, hence, may primarily involve the C-lCBLM. In any case, it is quite possible that the S-mCBLM, with its role in feedback stabilization, is concerned with other types of input cost.

2.2.2 Linear Controller Design

Without a clearer indication from the physiology to suggest a particular cost functional to minimize, we turn to control theory to suggest candidate controller designs. While a rich theory exists for optimizing the feedback control of linear systems, there is no general theory for optimizing linear control of nonlinear systems. We can nevertheless consider at least three reasonable approaches.

First, Slotine [24, pages 89-90] points out that a controller of form $[G_P\ G_D]$ where G_P and G_D are positive definite matrices, is always globally stabilizing for a mechanical system such as an arm. Indeed, this type of controller with G_P and G_D diagonal is the (local) "PD" used extensively in industrial robot control applications. The LPD controller, then, will be a stabilizing controller for $\mathcal{P}$ and can serve here as a reference against which to evaluate other controller designs.

The four-input, two-output LPD controller, leaves four degrees of freedom (the off-diagonal elements of G_P and G_D) potentially underutilized. It would be reasonable to consider that, especially for a plant having significant interactions between the state variables, certain MIMO synthesis strategies may be able to employ the additional degrees of freedom advantageously.

To this end, as a second approach, we can consider $\mathcal{P}$ to be a family of linear, time-invariant plants, $\mathcal{P}_{lti}(\mathbf{q}_i)$, each defined at a different point $\mathbf{q}_i$ within the state-space. Any linear controller design method can be used to find optimal controller at each point. Each such controller, G_i, could then be switched into use according to the current state of the system. In practice, we would consider deriving optimal controllers at a finite number of benchmark state-space coordinates. Then the instantaneous controller, G, would be defined

as an interpolation between the G_i determined by the instantaneous distance of the system state from the different benchmarks.

Specifically, we can consider using the H_2 methodology which minimizes the cost functional:

$$\mathcal{J} = \int_0^\infty (\tilde{\mathbf{q}}^T Q \tilde{\mathbf{q}} + \mathbf{u}_{sp}^T R \mathbf{u}_{sp}) \tag{2.7}$$

where

Q is a positive semidefinite state error weighting matrix, and
R is a positive definite input cost weighting matrix.

Assuming observability and controllability of the system[11], this method always generates stabilizing controllers, and if the system nonlinearities are reasonably slowly varying, we can then expect the whole gainscheduling scheme to be stabilizing. On the other hand, it is not necessarily true that if the G_i minimize $\mathcal{J}$ for each of the $\mathcal{P}_{lti}(\mathbf{q}_i)$, the interpolations will do so for $\mathcal{P}$ overall.

An alternative approach is to recast the nonlinear control problem as an H_∞ problem by regarding the nonlinear plant as a linear plant associated with an uncertainty due to its nonlinear components. A linear controller may then be defined to be robust to the "worst-possible" anticipated nonlinearity. Such a design would be stabilizing over the region of uncertainty because H_∞ controllers are always stabilizing. Moreover, we expect that the derived controller would be the linear time-invariant feedback controller which minimizes $\mathcal{J}$ in the face of the worst nonlinearity anticipated. However, especially for other, non- "worst-case" limb configurations in which the nonlinear effects are less severe, the H_∞ design may be less effective at minimizing $\mathcal{J}$ than other controllers, such as the one resulting from the first procedure outlined above.

Both approaches, especially the latter, have the advantage of utilizing wellunderstood techniques for designing controllers to optimize a cost functional which penalizes both state error and input magnitude. Moreover, because of the flexibility in the specification of Q and R, a wide range of controllers can be generated to enable modelling a range of input/error cost tradeoffs. It is also of note, that all controllers generated by H_2 and H_∞ methods are not only globally stabilizing for linear plants, but are such that when used as the LFBM in

[11] Both of these conditions hold for the system at hand which is verified in Appendix B.

the appropriate adaptive feedback linearization scheme, are globally stabilizing for plants similar to $\mathcal{P}$ (see Appendix B).

On the other hand, $\mathcal{J}$ is optimized by $H_{2/\infty}$ methods only when $\mathbf{q}_{ref}$ is constant; that is, for the regulator problem. While it is reasonable to expect good regulators to operate well as servos, especially when the input to be tracked is slowly varying relative to the regulator's settling time, optimal regulators may not be ideal for tracking rapidly changing inputs. In fact, since there does not exist a general theory for designing optimal servo controllers, we must evaluate servo performance empirically. Therefore, we will employ a number of standard time-domain measures (see Chapter 3) in addition to $\mathcal{J}$ to assess controller performance.

Finally, while integrated total cost is a useful formal tool for optimal design, it is not necessarily meaningful in practical human or robotic movement where avilable input energy is not strongly limited and more restrictive constraints appear in terms of $\hat{J}_q$ and/or time-domain indices.

2.3 Formal Summary of Problem

In an effort to gain insight into the possible role of the S-mCBLM in motor control and the general problem of optimizing linear feedback control of nonlinear plants, we have made the following simplifying assumptions regarding the structure and operation of the animal motor control system:

Assumption 1 *The plant, $\mathcal{P}$, is taken to be the entire spinomusculoskeletal apparatus as diagrammed in Fig. 2-2 and it is considered to have a square stiffness matrix, negligible intrinsic viscosity and a linear response to descending neural inputs, $\mathbf{u}_{sp}$.*

Assumption 2 *The brain, including the cerebellum, generates the muscle force commands necessary to track, possibly stationary, intended joint angle trajectories. To a first approximation, we may take the spinomuscular command signals, $\mathbf{u}_{sp}$ to consist of three terms, two feedforward: a reference trajectory vector,$\boldsymbol{\theta}_{\mathrm{ref}}$, and, $\mathbf{u}_{dyn}$, which anticipates the plant dynamics to minimize tracking error, and a feedback input signal, $\mathbf{u}_{fb}$, derived by linearly processing the state error $\tilde{\mathbf{q}}$.*

Assumption 3 *Initially, we assume that there are no signal transmission delays, or equivalently, that all transmission delays can be effectively compensated for by additional circuitry*

present in the physiologic motor system.

Assumption 4 *The ascending output of the plant consists of linear combinations of joint angle and angular velocity error signals. Thus, full state error feedback, $\tilde{\mathbf{q}}$, is available to the brain for control.*

Assumption 5 *The S-mCBLM functions as a linear feedback controller, G, having output $\mathbf{u}_{fb}$, has a critical role in postural stabilization and disturbance rejection during tracking tasks.*

Given these premises, the questions for this investigation become:

How do G's derived from H_2, H_∞ and possibly other methods, with and without gain-scheduling, compare with PD control in terms of regulation and tracking performance for $\mathcal{P}$? Can these be demonstrated empirically and perhaps theoretically to be stabilizing? Specifically, does any one control scheme minimize $\mathcal{J}$ and time-domain measures most effectively accross different disturbances and tracking tasks? Does varying the plant in terms of the elimination of nonlinearities or the changing of mechanical parameters change the relative performances of the different controllers with regard to these measures? Does the inclusion of different types of feedforward signals change the relative performances of the different controllers?

Chapter 3

Methods

3.1 Simulation Scheme

Simulations of the control system used the MATLAB CAD software package on the MIT athena computing system. Overall, 432 simulations were performed in 12 runs representing combinations of various plants, tasks, feedforward signals and controller designs. Within each run, imulations are referred to in terms of these components as summarized in Table 3.1.

3.2 Plant Specification

Initially, a "standard" plant was used with parameters comparable to a human arm (Table 3.2). These runs are designated: "PLANT(1)".

Run Number	Plant Type	Task Type	Feedforward Signal	Controller
1	PLANT(0)	TASKS(1-4)	FFTYP(0)	$CTLRS_1$(1-12)
2	PLANT(0)	TASKS(5-8)	FFTYP(1)	$CTLRS_1$(1-12)
3	PLANT(1)	TASKS(1-4)	FFTYP(0)	$CTLRS_1$(1-12)
4	PLANT(1)	TASKS(5-8)	FFTYP(1)	$CTLRS_1$(1-12)
5	PLANT(1)	TASK(5)	FFTYPS(1-4)	$CTLRS_1$(1-10)
6	PLANT(2)	TASKS(1-4)	FFTYP(0)	$CTLRS_2$(1-3,5,7,9-12)
7	PLANT(2)	TASKS(5-8)	FFTYP(1)	$CTLRS_2$(1-3,5,7,9-12)
8	PLANT(3)	TASKS(1-4)	FFTYP(0)	$CTLRS_3$(1,3,13-17)
9	PLANT(3)	TASKS(5-8)	FFTYP(1)	$CTLRS_3$(1,3,13-17)
10	PLANT(3)	TASK(5)	FFTYPS(1-4)	$CTLRS_3$(1,3,13-17)
11	PLANT(3c)	TASKS(1-4)	FFTYP(0)	$CTLRS_{3c}$(1,3,13-17)
12	PLANT(3c)	TASKs(5-8)	FFTYP(1)	$CTLRS_{3c}$(1,3,13-17)

Table 3.1: Summary of simulations performed. The definitions are presented in the sections below.

Parameter	Value(s)	Units	Note
l_1	0.25	meters	From[28]
l_2	0.35	meters	From[28]
$\bar{l}_1$	0.11	meters	From[28]
$\bar{l}_2$	0.15, 0.2	meters	First value from[28] used for PLANT(1). Second value used for PLANT(2)
m_1	0.9	kg	From[28]
m_2	1.1, 3.0	kg	First value from[28] used for PLANT(1). Second value used for PLANT(2)
$\bar{m}_1$	0.065	kg-m^2	From[28]
$\bar{m}_2$	0.1, 0.3	kg-m^2	First value from[28] used for PLANT(1). Second value used for PLANT(2)
K	$\begin{bmatrix} 20 & 10 \\ 10 & 20 \end{bmatrix}, \begin{bmatrix} 20 & 0 \\ 0 & 20 \end{bmatrix}$	N-m/rad	First matrix: Values approximate those derived from human measurements and used in simulations by Flash [26]. Second matrix used for PLANTS(3,3c)
$\bar{H}$	$\begin{bmatrix} 0.2726 & 0.1043 \\ 0.1043 & 0.1 \end{bmatrix}$	kg-m^2	Values based on $[\theta_1, \theta_2]^T_{initial} = [1.25, 1.49]^T$.

Table 3.2: Numerical values for plant parameters.

To assess the effect of the system nonlinearities on controller performance, all tasks were repeated using the same controllers designed for PLANT(1) but controlling instead a linear, time-invariant version of $\mathcal{P}$ defined by setting C to zero in (2.2) and using fixed values for h_1, h_2, h_6 and h_7 (thus defining $\bar{H}$) as in section 3.3.1 below, yielding:

$$\mathcal{P}_{lti}: \quad \dot{\mathbf{x}} = \bar{A}\mathbf{x} + \bar{B}_1\boldsymbol{\tau}_d + \bar{B}_2\mathbf{u}_{sp}$$

where

$$\bar{A} = \begin{bmatrix} 0 & I_2 \\ -\bar{H}^{-1}K & 0 \end{bmatrix}, \quad \bar{B}_1 = \begin{bmatrix} 0 \\ \bar{H}^{-1} \end{bmatrix} \quad \text{and} \quad \bar{B}_2 = \begin{bmatrix} 0 \\ \bar{H}^{-1}K \end{bmatrix}.$$

These simulation runs are designated with: "PLANT(0)". A third set of simulations was performed using $m_2 = 3.0$, $\bar{m}_2 = 0.3$ and $\bar{l}_2 = 0.2$ instead of 1.1, 0.1 and 0.15, respectively, to simulate the presence of a load at the end of link 2. These simulation runs are designated with: "PLANT(2)". PLANTS(1,2) represent the "Full (human) Arm Model" (FAM). After preliminary analysis of the results of the first three sets of simulations, two more sets of simulations were undertaken to focus on the dependence of integrated state error and

time-domain performance measures on the presence or absence of interjoint control. These included a fourth set of simulations which used a diagonal stiffness matrix K to represent the situation where there are no biarticular muscles and hence all interjoint feedback must be due to the controller. This is referred to as the "Reduced (human) Arm Model" (RAM). The fifth set of simulations uses the RAM and repeats most of the simulations of the fourth set, but clips the the controller torque signal if it exceeds a fixed upper limit, thereby simulating the effect of actuator saturation. These two cases are designated PLANT(3) and PLANT(3c), respectively.

3.3 Controller Specification

3.3.1 H_2 Controller and Gainscheduling

As the simulations, especially TASKS(1-4) (defined in section 3.4) utilized only perturbations which resulted in relatively small angular displacements ($\simeq$ .3 rad) but significantly larger angular velocities (up to 10 rad/sec), the major plant nonlinearities were introduced through the velocity-dependent terms (in matrix C in (2.2)), and not through the inertia terms (h_j in (2.1)). As such, *solely for the purposes of controller calculation* and *linear system simulation* (see section 3.2 above), *fixed* values for the h_j (defined at $[\theta_1, \theta_2]_{initial}$) were picked. This yields a constant matrix $\bar{H}$ and I then gainscheduled across the 2-dimensional angular velocity-space to define the different matrices, C_i. In particular, I considered 9 benchmark angular velocity states for the system:

$$\left[\begin{array}{c}\dot{\theta}_1\\ \dot{\theta}_2\end{array}\right]_i = \left[\begin{array}{c}0\\0\end{array}\right], \left[\begin{array}{c}10\\10\end{array}\right], \left[\begin{array}{c}10\\-10\end{array}\right], \left[\begin{array}{c}-10\\10\end{array}\right], \left[\begin{array}{c}-10\\-10\end{array}\right], \left[\begin{array}{c}10\\0\end{array}\right], \left[\begin{array}{c}-10\\0\end{array}\right], \left[\begin{array}{c}0\\10\end{array}\right], \left[\begin{array}{c}0\\-10\end{array}\right]$$

yielding C_i, (i=0,...,8), respectively. The magnitude of 10 rad/sec was chosen semi-arbitrarily to (generously) represent the upper limit of joint angular velocities produced by humans moving under their own power. Since our controllers are stabilizing, we expect that the system will very likely remain within the region of velocity space bounded by states 1-8 throughout the course of its movement making the interpolation scheme (3.2) below, a reasonable one.

Given C_i and $\bar{H}$, the A_i are defined as:

$$\bar{A}_i = \begin{bmatrix} 0 & I_2 \\ -\bar{H}^{-1}K & -\bar{H}^{-1}C_i \end{bmatrix}$$

and $\bar{B}_2$ is as in section 3.2. Nine time-invariant H_2 problems are then solved by solving the algebraic Riccati equations:

$$0 = X_i A_i + A_i{}^T X_i + Q - X_i \bar{B}_2 R^{-1} \bar{B}_2^T X_i, \qquad i = 0, ...8$$

for the matrix X_i. For simulation Q was taken to be:

$$Q = \begin{bmatrix} 1 & 0 & 0 & 0 \\ 0 & 1 & 0 & 0 \\ 0 & 0 & .1 & 0 \\ 0 & 0 & 0 & .1 \end{bmatrix}$$

as it was shown empirically to generate mild underdamping as characteristic of the human arm. and $R = \rho I$ where the method of determining ρ is explained in section 3.3.3. The set of optimal linear feedback controllers, G_i, for the benchmark states is then given by:

$$\{ G_i \mid G_i = R^{-1} \bar{B}_2^T X_i \mid i = 0, ..8 \} \tag{3.1}$$

Finally, if d_i is the distance from the current velocity state to each of the benchmarks, then the current controller used is given by the weighted sum:

$$G = \frac{\sum_{i=0}^{8} (1/d_i)(G_i)}{\sum_{i=0}^{8} (1/d_i)} \tag{3.2}$$

which interpolates between the G_i, becoming equal to G_i when $d_i = 0$.[1]

3.3.2 The H_∞ Controller

If we continue to neglect the nonlinearity in the dependence of H on θ, the problem of controlling $\mathcal{P}$ can be recast as an H_∞ problem as diagrammed in Figure 3-1. Here, the nominal linear time-invariant plant $\mathcal{P}_{lti}$, defined as in section 3.2, is subjected to a disturbance, δ, of uncertain direction (represented by the random rotation matrix Δ, with $\|\Delta\|_\infty = 1$), and

[1] For actual computation, denominators were cleared to prevent NaN/overflow errors.

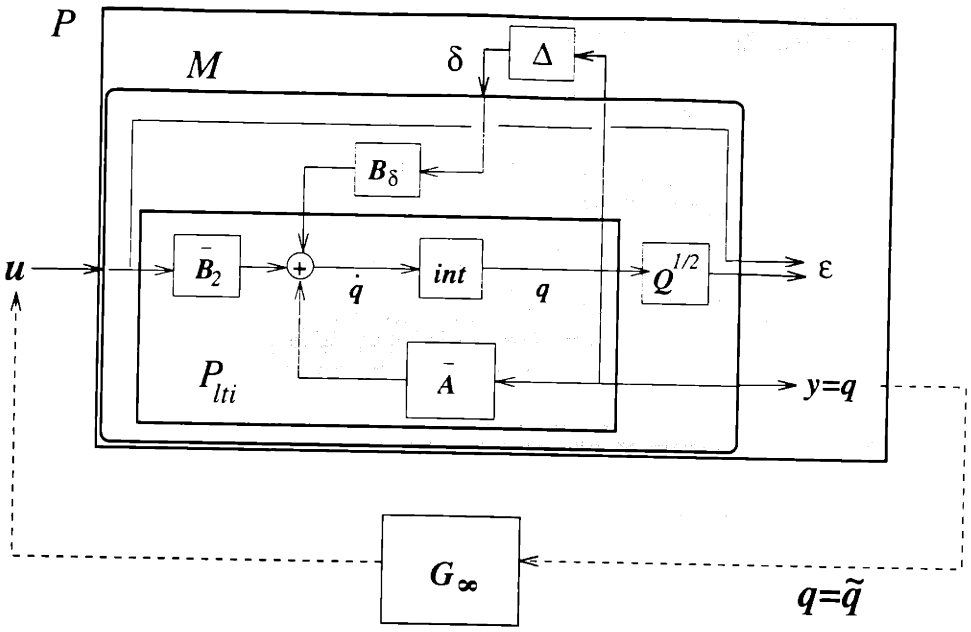

Figure 3-1: The nonlinear plant $\mathcal{P}$ represented as a linear plant, $\mathcal{P}_{lti}$, plus uncertainty, δ, which is generated by the plant state and a random rotation matrix Δ, and whose effect is modulated by B_δ. The formal representation of the H_∞ problem given in equation 3.2 is in terms of the system matrices M, G_∞, and system variables $\mathbf{q}$, δ, $\mathbf{u}$, ϵ and $\mathbf{y}$ identified here. The block labelled "*int*" is an integrator.

of magnitude which is $\leq \|B_\delta\|_\infty \|\mathbf{q}\|$, where

$$B_\delta = \begin{bmatrix} 0 & 0 \\ 0 & \bar{H}^{-1}C \end{bmatrix}.$$

Therefore, $\delta = B_\delta \Delta \mathbf{q}$ represents the uncertain effect of the major (velocity-dependent) nonlinearities. This arrangement can be represented as the formal system in Figure 3-1 having the matrix representation:

$$\begin{bmatrix} \dot{\mathbf{q}} \\ \varepsilon \\ \mathbf{y} \end{bmatrix} = M \begin{bmatrix} \mathbf{q} \\ \delta \\ \mathbf{u} \end{bmatrix} = \left[\begin{array}{c|cc} \bar{A} & B_\delta & \bar{B}_2 \\ \hline \sqrt{Q} & 0 & I \\ I & 0 & 0 \end{array}\right] \begin{bmatrix} \mathbf{q} \\ \delta \\ \mathbf{u} \end{bmatrix}.$$

The H_∞ controller, G_∞, is that which for any fixed value for C minimizes $\sup_s |T_{\delta\epsilon}(s)|_\infty$, the closed-loop transfer function from $\boldsymbol{\delta} \rightarrow \boldsymbol{\epsilon}$. Note that for the regulator problem, $\mathbf{q} = \tilde{\mathbf{q}}$. Because C, and therefore B_δ, is dependent on velocity terms, gainscheduling can be used in a manner very similar to that described in the previous subsection. Specifically, we define:

PLANT	ρ_0	γ_{min}
PLANT(1)	20	0.348
PLANT(2)	35	1.339
PLANT(3)	5	0.119

Table 3.3: H_∞ problem parameters.

$$\bar{B}_{\delta(i)} = \begin{bmatrix} 0 & 0 \\ 0 & \bar{H}^{-1}C_i \end{bmatrix}$$

to be the constant B_δ matrix defined at the ith benchmark point, i=1,...,8. Because the H_∞ problem inherently considers the "worst-case" disturbance, $\bar{B}_\delta$ is constrained to be nonzero, hence the 0th benchmark controller is not included in the gainscheduling. Otherwise, the set of H_∞ controllers, $\{G_{\infty(i)}\}$, is calculated by iteratively solving the modified Riccati equations:

$$0 = X_{\gamma(i)}\bar{A} + \bar{A}^T X_{\gamma(i)} + Q - X_{\gamma(i)}(\frac{1}{\rho_0}\bar{B}_2\bar{B}_2^T - \frac{1}{\gamma^2}\bar{B}_{\delta(i)}\bar{B}_{\delta(i)}^T)X_{\gamma(i)}$$

for $X_{\gamma(i)}$ using successively smaller values of γ to asymptotically approximate γ_{min}, the limiting value which avoids all three H_∞ algorithm termination criteria[2]. The $G_{\infty(i)}$, $i = 1,,,8$ are then obtained by setting $X_i = X_{\gamma(i)}$ and $R = \rho_0 I$ in (3.1). For the non-gainscheduled controller, an extreme benchmark controller $G_{\infty(1)}$ (which is also identical to $G_{\infty(4)}$) was used as it was most specifically designed for the worst-case to be encountered in the simulations. In practice, controllers obtained by using γ extremely close to γ_{min} are very high gain. Controllers with excessively high gain may be undesirable for several reasons outlined below, in addition to the numerical instabilities which may result during computer simulations. Therefore, the program sets $\gamma = 1.2 * \gamma_{min}$. The specific numerical values used are given in Table 3.3.

[2]These are, specifically that 1) the matrix X becomes asymmetric or no longer positive definite, 2) that the matrix $[\bar{A} + \frac{1}{\gamma^2}B_\delta B_\delta^T X_\gamma - \frac{1}{\rho_0}\bar{B}\bar{B}_2^T X_\gamma]$ becomes unstable, or 3) that the Hamiltonian matrix:

$$\begin{bmatrix} \bar{A} & \frac{1}{\gamma_2}\bar{B}_2\bar{B}_2^T \\ -Q & -\bar{A} \end{bmatrix}$$

develops eigenvalues on the $j\omega$-axis. For the purposes of this study, γ_{min} was considered reached when the real parts of the closest Hamiltonian eigenvalues to the $j\omega$-axis were less than 0.01.

3.3.3 Controller Normalization

Theoretical Considerations

The measures outlined in section 3.4 describe a controller's characteristics in a given system. However, in general controller performance will depend sensitively on controller gain. In order to better compare the performances of different controller designs it would be desirable to normalize for the controller gain in some fashion. Since there is no standard way to do this for a MIMO controller, the problem was addressed by considering different practical measures of controller "strength". Although *ad hoc*, the measures allow evaluation of different controllers under different assumptions about which constraints may be significant in the design of the natural system.

Several practical considerations limit the allowable gain for a controller. These include importantly: 1) a limitation in the gain of the amplifiers, 2) a limitation in the peak signals able to be accepted by actuators or other components in the system, or 3) a limitation in the allowable high-frequency responsiveness of the system because of concern for sensor noise or unmodelled dynamics (including transmission delays).

Each of these is a legitimate concern in a biological control system. The first, however, is *a priori* least likely to be the most significant constraint since synaptic gain can be flexibly adjusted over a very large range. Nevertheless, any physical system does have practical limits on its range of effective amplification. With regard to actuators, muscles clearly do have output limitations and within these limits, unnecessarily high activity levels are disadvantageous from both energy utilization and material stress points of view. Moreover, any controller which saturates actuators will have degraded performance, though this event is not necessarily catastrophic.[3] Finally, though we have argued that (2.4) does not leave major dynamics unmodelled, this is always an important issue. Furthermore, there is clearly considerable sensor noise in biological systems. So, the consequences of excess gain in terms of decreased robustness are potentially quite great.

Therefore, the three following factors are used for control gain normalization:

$$g_{max1} = \max_{i,j} |g_{ij}|,$$

[3]Indeed, though sustained high levels of neural and/or muscular firing may exhaust cells, transient output saturation is typically well tolerated by nerves and muscles.

$$g_{max2} = \max_i \left\{ \sum_{j=1}^{2} 0.03|(g_\tau)_{ij}| + \sum_{j=3}^{4} |(g_\tau)_{ij}| \right\} \quad \text{and}$$

$$\omega_c,$$

where g_{ij} are the elements of G, and $(g_\tau)_{ij}$ are the elements of $G_\tau = K([I_2\ 0] + G)$, the matrix determining the total feedback torque, and

ω_c is the crossover frequency of the closed-loop system (2.1.2) with the plant at rest at the initial position.[4]

Thus, g_{max1} is a measure of the maximum gain element in the controller and g_{max2} is proportional the maximum torque signal which would be generated by the feedback controller *if it is assumed that the state error remains in the region:* $|\dot{\tilde{\theta}}_i| \leq 10$ and $|\tilde{\theta}_i| \leq 0.3$. To be sure, since the output signal of the controller depends directly on the state error, it is in principle unbounded. g_{max2} is a sensible measure only for strongly stabilizing controllers which bring the system to zero within the specified region. Preliminary simulations indicated that this was the case, or very nearly the case, for all of the controllers under consideration.

Normalization Procedure

In the simulations, the normalization is done as follows: given Q as defined above (section 3.3.1), the H_∞ problem is solved with $R = \rho_0 I_2$, where ρ_0 is empirically specified for each plant to yield a reasonable G_∞.[5] The numerical values of ρ which were used are given in Table 3.3 above. Next, g_{max1}, g_{max2} and ω_c are calculated. The H_2 problem is then solved iteratively twice at each benchmark point with $R = \rho I_2$, by adjusting ρ until g_{max1} and g_{max2} are each closely approximated. This yields two sets of H_2 controllers: $\{G_i'\}$, and $\{G_i''\}$ which have approximate maximal element and maximal output signal equivalence to G_∞,

[4] Crossover frequencies were calculated for the system at rest, and at each of the extreme angular velocity benchmark points. The values were extremely close (within 4 radians). The rest values were taken because they were the largest, and hence the most conservative values. The variation in ω_c with angular position was not examined, however. Thus, significant changes in arm configuration may significantly alter this normalization factor.

[5] For the current study, "reasonable" implied that 1) the peak torques produced during the simulations did not exceed reasonable physiologic values. Peak elbow torques for average persons are on the order of 50-60 N-m/rad.[5] Shoulder values could be different, but were assumed to be the same for this purpose. 2) that ω_c is less than 600 rad/sec since sensor noise develops significant energy above 100 Hz, and 3) that the settling time and level of damping appered roughly physiologic by inspection.

respectively. Evaluation of closed-loop crossover frequencies for these controllers reveals that H_2 controllers matched for g_{max2} are also nearly matched for ω_c as well, so a third set of H_2 controllers was not derived.

Simulation indicates that H_2 controllers normalized according to g_{max1} generate considerably larger (by a factor of 3) torques than do the other controllers. While this may be acceptable in an artificial arm system, such torque levels are not realistic for human voluntary movement. If the cerebellum functioned as such a controller, actuator saturation would occur. Therefore, to explore the consequences of this type of event, additional simulation runs were performed in which the torque output was simply clipped at peak values of 65 N-m/rad.

To narrow the large number of LPD controllers which could be compared with the H_∞ and H_2 controllers, the following (somewhat arbitrary) procedure was followed. First, the ratios, r_∞ and r_2 were defined from the elements of G_∞ and G_0', respectively, as:

$$r = \frac{\sum_{i=1,j=1}^{2,2} |g_{ij}|}{\sum_{i=1,j=3}^{2,4} |g_{ij}|}$$

The LPD controller is then defined as:

$$\begin{bmatrix} \rho & 0 & \rho r & 0 \\ 0 & \rho & 0 & \rho r \end{bmatrix}$$

and ρ is adjusted iteratively to match g_{max1} or g_{max2} for different r values. For simplicity, but arbitrarily, the two elements along each diagonal were taken to be equal, and the value of 1 was tried for r in addition to $r = r_2$ and $r = r_\infty$. This yields four controllers G'_{pd-a}, G''_{pd-a}, G'_{pd-b} and G'_{pd-c}. The controllers are specifically defined such that comparison of the first two isolates the significance of different normalizations for a fixed value of $r = r_\infty$. Comparison of the first, third and fourth, isolates the significance of the choice of different values for r, for a fixed type of normalization. Examination of all four, seeks to identify the importance, or lack of importance, of having off-diagonal elements in controlling the FAM. The controllers used with PLANT(0) and the FAM PLANTS(1,2) are summarized in Table 3.4. Note that for $\rho > 0$ and $r > 0$, the controllers are stabilizing according to the arguments of Slotine (see section 2.2.2).

It was also considered that a LPD design which was normalized according to crossover

Controller Design	Type	Designation[1]
G_∞	H_∞ non-gainscheduled	$\text{CTLR}_p(1)$
$\{G_{\infty(i)}\}$	H_∞ gainscheduled	$\text{CTLR}_p(2_i)$
G_0'	H_2 non-gainscheduled, matching g_{max1}	$\text{CTLR}_p(3)$
$\{G_i'\}$	H_2 gainscheduled, matching g_{max1}	$\text{CTLR}_p(4_i)$
G_0'	H_2 non-gainsched., matching g_{max1}, actuator sat.	$\text{CTLR}_p(5)$
$\{G_i'\}$	H_2 gainsched., matching g_{max1}, actuator sat.	$\text{CTLR}_p(6_i)$
G_0''	H_2 non-gainscheduled, matching g_{max2} (and nearly ω_c)	$\text{CTLR}_p(7)$
$\{G_i''\}$	H_2 gainscheduled, matching g_{max2} (and nearly ω_c)	$\text{CTLR}_p(8_i)$
G_{pd-a}'	LPD using $r = r_\infty$ and matching g_{max1}	$\text{CTLR}_p(9)$
G_{pd-a}''	LPD using $r = r_\infty$ and matching g_{max2}	$\text{CTLR}_p(10)$
G_{pd-b}'	LPD using $r = r_2$, matching g_{max1}	$\text{CTLR}_p(11)$
G_{pd-c}'	LPD using $r = 1$, matching g_{max1}	$\text{CTLR}_p(12)$

Table 3.4: Controller designs for PLANTS(0-2). [1]Where p is the number of the plant on which the design is based.

frequency should be tested. However, preliminary simulations indicated that, across all of the r values used, performance of such a controller matched for ω_c was significantly poorer than all other controllers tested with the FAM in terms of $\hat{\mathcal{J}}$ minimization. Therefore, analysis of such a crossover frequency-normalized controller was deferred to the RAM study.

The study of the RAM was undertaken to identify the controller structure requirements for maximal error suppression. Since the H_∞ and H_2 controllers are not designed to minimize error alone, these were not likely to have the greatest error suppression. Therefore, only one H_∞ and one H_2 controller were used in these simulations. Because K is different in the RAM, in order to obtain peak torque values which were reasonable in the sense defined in section 3.3.3, the H_∞ problem was re-solved using a reduced value of ρ_0 (5 instead of 20). The resulting G_∞ controller determined g_{max1} which was used in turn to define the g_{max1}-normalized H_2 controller in the same manner as described above for PLANTS(0-2). These controllers, however, served primarily to provide reference performances. The main RAM analysis involved five other (semi-arbitrary) controllers summarized in Table 3.5.

Controller $G_0'^*$ is defined in terms of G_0' by replacing the latter's near-zero off-diagonal elements with one-half of the average of its on-diagonal elements. This proportion was selected because it is simple, it produces matrices with significant off-diagonal gains, and it avoids very large off-diagonal elements which were empirically seen to degrade performance in exploratory simulations.[6] Controller $G_{pd-c}'^*$ is defined in terms of G_{pd-c}', which

[6]In fact, since the on-diagonal elements were always positive with ratios between 0.072 and 13.93 these *ad hoc* controllers are guaranteed to be stabilizing (see section B.3).

Controller Design	Type	Designation[1]
G_∞	H_∞ (for reference and defining g_{max1})	$CTLR_3(1)$
G'_0	H_2 matching g_{max1} (for reference)	$CTLR_3(3)$
G'_{pd-c}	LPD using $r = 1$ and matching g_{max1} (and defining ω'_c)	$CTLR_3(12)$
G'^*_0	H_2 matching g_{max1}, off-diag gains added	$CTLR_3(13)$
G'^*_{pd-c}	G'_{pd-c}, matching g_{max1}, off-diag gains added	$CTLR_3(14)$
G'^{**}_{pd-c}	G'^*_{pd-c}, rescaled to match ω'_c (no longer matches g_{max1})	$CTLR_3(15)$
G'^{**}_{pd-c}	G'^*_{pd-c}, rescaled ω'_c (no longer matches g_{max1}), actuator sat.	$CTLR_3(16)$

Table 3.5: Controller Designs for PLANTS(3,3c). [1]The same controllers when used with clipped torque signals are designated with subscript 3c.

is $CTLR_p(12)$ defined above, by replacing the latter's zero off-diagonal gains with one-half the average of its on-diagonal elements. Finally, G^{**}_{pd-c} was defined by normalizing G'^*_{pd-c} by ω'_c, where ω'_c is the closed loop crossover frequency using G'_{pd-c}. The rescaling was done by simply multiplying the entire controller by a constant gain sufficient to produce ω'_c equalization. No gainscheduling was studied with the RAM.

Although ultimately arbitrary, the above controllers were decided upon according to a specific rationale prompted by preliminary results from the FAM. Between the g_{max1}-normalized, and g_{max2}-normalized H_2 controllers defined above, the former display higher ω_c and considerably better error suppression in terms of measures $\hat{J}_q$, $\tilde{\theta}_{max}$, $\tilde{x}_{max}$, σ_θ and σ_x (see section 3.4 below) than the latter. Therefore, for the RAM, normalization by g_{max2} was not used. It was also noted that among the PD controllers studied with the FAM, that $CTLR_1(12)$ for which $r = 1$, displayed the best error suppression. So this controller design was used with the RAM and designated $CTLR_3(12)$. For the fixed value of g_{max1} any increase in r above unity (actually, any increase in *either* of the velocity feedback gains in $CTLR_3(12)$) causes the crossover frequency to exceed ω'_c. On the other hand, any increase in the position feedback gains of $CTLR_3(12)$ increases g_{max1}. Therefore, at least for the RAM, G'_{pd-c} is the highest-performance PD controller design for the given g_{max1} and ω'_c in terms of the performance measures mentioned.

Comparison of controllers G'_{pd-c} and G'^*_{pd-c}, then, identifies whether the addition of off-diagonal gains while still matching g_{max1} (because the off-diagonal elements, determined as described above, are necessarily smaller in absolute value than the largest controller gain) provides any improvement over PD performance. Comparison of controllers G'_{pd-c} and G^{**}_{pd-c}, on the other hand, identifies whether the addition of off-diagonal gains while maintaining ω'_c (and not g_{max1}) provides any improvement over PD performance. Finally,

the last controller, $CTLR_3(16)$, is identical to the previous controller except that the effect of actuator saturation is simulated to indicate whether the performance of $CTLR_3(15)$ is senstive to actuator saturation.

The RAM simulations were repeated for all controllers to determine the sensitivity of the results to actuator saturation. These results are designated as using $CTLRS_{3c}(1,3,12\text{-}15)$.[7]

Controller (G)	Elements of G			
$CTLR_1(4_1)$	0.799	0.471	0.567	0.176
	-0.471	0.799	-0.141	0.4649
$CTLR_1(4_2)$	-0.002	0.124	0.027	0.014
	-0.124	-0.002	0.003	0.044
$CTLR_1(4_3)$	0.002	0.123	0.071	0.027
	-0.123	0.002	0.015	0.045
$CTLR_1(4_4)$	0.800	0.651	0.457	0.154
	-0.651	0.800	-0.153	0.516
$CTLR_1(8_1)$	0.040	0.186	0.173	0.059
	-0.186	0.040	0.008	0.104
$CTLR_1(8_2)$	0.075	0.314	0.153	0.051
	-0.314	0.075	-0.047	0.160
$CTLR_1(8_3)$	0.045	0.272	0.153	0.053
	-0.272	0.045	-0.152	0.127
$CTLR_1(8_4)$	0.116	0.327	0.144	0.056
	-0.327	0.116	-0.038	0.202

Table 3.6: Selected gainscheduled controller element values.

[7]Thus, $CTLR_3(16)$ is identical to $CTLR_{3c}(15)$. The separate notations are used to facilitate graphical presentation later. This should not cause any confusion.

Controller (G)	Elements of G				Elements of $G_r = K([I_2\ 0] + G)$				g_{max1}, g_{max2}	ω_c, r
$CTLR_1(1)$	-0.099	0.800	0.190	0.055	12.434	25.664	3.614	1.994	0.8	323
	-0.559	-0.033	-0.020	0.089	-2.174	27.330	1.514	2.326	6.75	0.237
$CTLR_1(3,5)$	0.801	0.570	0.509	0.163	30.313	29.414	8.647	8.149	0.8,	530
	-0.570	-0.801	-0.154	0.489	6.602	41.718	2.021	11.416	18.59	0.480
$CTLR_1(7)$	0.078	0.306	0.167	0.056	18.503	16.906	2.978	2.711	0.31	314
	-0.306	0.078	-0.036	0.159	4.659	24.626	0.945	3.736	6.75	0.544
$CTLR_1(9)$	0.801	0	0.190	0	36.016	8.008	3.802	1.901	0.8	504
	0	0.801	0	0.190	18.008	16.016	1.901	3.802	7.32	0.237
$CTLR_1(10)$	0.730	0	0.173	0	34.590	17.295	3.463	1.732	0.73	485
	0	0.730	0	0.173	17.295	34.590	1.732	3.463	6.75	0.237
$CTLR_1(11)$	0.801	0	0.384	0	36.016	18.008	7.679	3.840	0.8	508
	0	0.801	0	0.384	18.008	36.016	3.840	7.699	13.14	0.475
$CTLR_1(12)$	0.801	0	0.801	0	36.016	18.008	16.016	8.008	0.8	512
	0	0.801	0	0.801	18.008	36.016	8.008	16.017	25.64	1.00
$CTLR_2(1)$	-0.031	0.674	0.184	0.072	15.064	23.882	3.954	2.635	0.67	122
	-0.431	0.040	0.028	0.120	1.060	27.541	2.404	3.118	7.76	0.343
$CTLR_2(3,5)$	0.674	0.454	0.485	0.141	28.941	25.826	8.566	7.340	0.67	189
	-0.454	0.674	-0.113	0.451	7.657	38.025	2.594	10.441	17.55	0.527
$CTLR_2(7)$	0.110	0.257	0.193	0.062	19.633	16.237	3.607	3.075	0.257	125
	-0.2568	0.110	-0.025	0.1836	5.964	24.769	1.424	4.292	7.76	0.632
$CTLR_2(9)$	0.674	0	0.231	0	33.477	16.738	4.623	2.312	0.67	181
	0	0.674	0	0.231	16.738	33.477	2.312	4.623	8.44	0.343
$CTLR_2(10)$	0.613	0	0.210	0	32.253	16.127	4.204	2.102	0.61	176
	0	0.613	0	0.210	16.127	32.253	2.102	4.204	7.76	0.343
$CTLR_2(11)$	0.674	0	0.355	0	33.477	16.738	7.106	3.553	0.67	182
	0	0.674	0	0.355	16.738	33.477	3.55	7.106	12.16	0.527
$CTLR_2(12)$	0.674	0	0.674	0	33.477	16.738	13.477	6.738	0.67	183
	0	0.674	0	0.674	16.738	33.477	6.738	13.477	21.72	1.00
$CTLR_3(1)$	0.057	0.361	0.284	0.033	21.135	7.224	5.686	0.654	0.36	440
	-0.328	0.077	-0.037	0.163	-6.555	21.541	-0.740	3.266	7.19	0.629
$CTLR_3(3)$	0.361	0	0.308	0.006	27.227	0	6.169	0.124	0.36	539
	0	0.361	0.006	0.298	0	27.227	0.124	5.964	7.11	0.857
$CTLR_3(12)$	0.361	0	0.361	0	27.227	0	7.227	0	0.36	539
	0	0.361	0	0.361	0	27.224	0	7.227	8.04	1.00
$CTLR_3(13)$	0.361	0.181	0.308	0.152	27.227	3.614	6.169	3.033	0.36	489
	0.181	0.361	0.152	0.308	3.614	27.227	3.033	6.169	10.12	0.839
$CTLR_3(14)$	0.361	0.181	0.361	0.181	27.227	3.614	7.227	3.614	0.36	489
	0.181	0.361	0.181	0.361	3.614	27.227	3.614	7.227	11.77	1.00
$CTLR_3(15)$,	0.542	0.271	0.542	0.271	30.841	5.421	10.841	5.421	0.54	536
$CTLR_3(16)$	0.271	0.542	0.271	0.542	5.421	30.841	5.421	10.841	17.35	1.00

Table 3.7: Non-gainscheduled controller element values and specifications.

3.4 Task Specifications and Controller Performance Assessment

Tasks

To specifically assess disturbance rejection properties, perturbations were chosen to represent exogenous torque impulses applied to one or more of the joints as if an obstacle has been encountered during movement. An impulse of torque applied to a joint produces a step in angular velocity and a ramp of angular displacement, the magnitude and slope, respectively, of which are inversely related to the moment of inertia. If we assume that the impulse acts instantaneously, this is equivalent, for the purposes of simulation, to initializing the system at its starting position, but with a non-zero angular velocity equal to torque/inertia. The initial position was taken to be in the near the center of the workspace with the arm in a position "typical" for arm function with $\theta_1 = 1.25$ rad. and $\theta_2 = 1.49$ rad. as shown in Fig. 2-1. Four combinations of initial angular velocities were studied:

$$\left[\begin{array}{c}\dot{\theta}_1\\ \dot{\theta}_2\end{array}\right]_{initial}, \left[\begin{array}{c}10\\ 10\end{array}\right], \left[\begin{array}{c}10\\ -10\end{array}\right], \left[\begin{array}{c}-10\\ 10\end{array}\right], \left[\begin{array}{c}-10\\ -10\end{array}\right]$$

These correspond to the four most extreme benchmark states used for gainscheduling (see section 3.3.1). The combinations were selected with the idea that together they yielded representative behavior of the system throughout the region of state-space interest. In the simulations, these conditions are designated as "TASKS(1-4)", respectively. Since regulation involves no feedforward signal, these tasks are assigned FFTYP(0).

To specifically assess tracking performance, four cases were explored. The first is with $u_{dyn} = 0$ and, hence, $u_{ff} = \boldsymbol{\theta}_{ref}$ so that the descending command is merely the reference trajectory and there is no anticipation of plant dynamics. In this case, $\boldsymbol{\theta}_{ref}$ was set up to consist of four double-ramp patterns (see Fig. 3-2) in which the arm moves away from and then returns to its starting position (the same as defined above). A velocity step amplitude of 5 was chosen to represent an effortful tracking task for a human. A ramp duration and inter-joint time lag were chosen so that the second joint-movement in the sequence occurs during the first joint-movement. This tends to provoke maximal interaction between the joint dynamics.

Together, the 4 patterns represent extremes of ramp tracking tasks, having angular

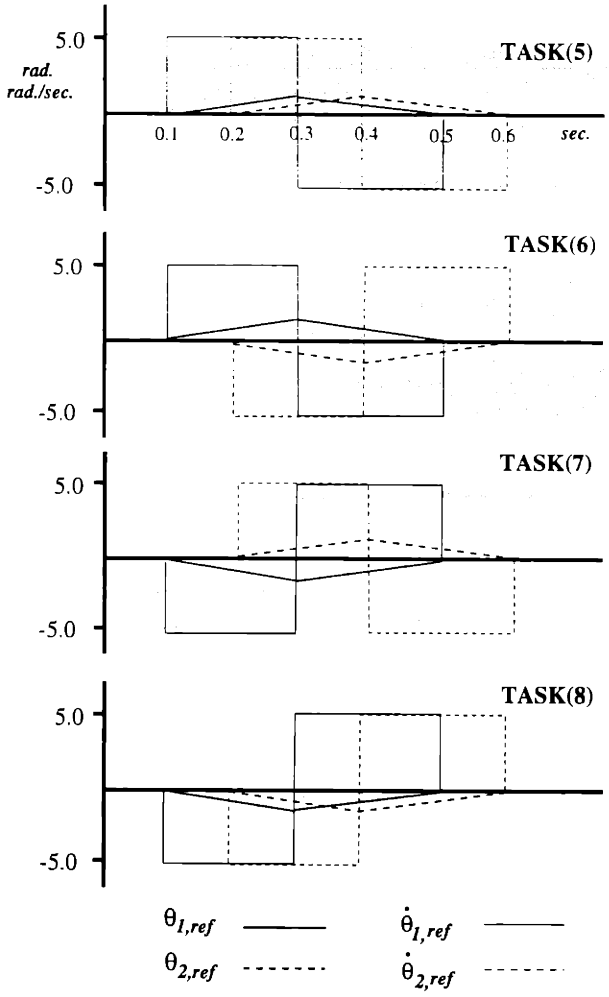

Figure 3-2: Angle ramp (and velocity step) patterns used for θ_{ref} (and implicitly for $\dot{\theta}_{ref}$ in tracking TASKS(5-8).

velocity amplitude of 5 which an arm could be asked to do in the specified region of the workspace. Simulations of these tasks are designated as "TASKS(5-8)", respectively and were assigned "FFTYP(1)".

The second case is with $u_{dyn} = K^{-1}\bar{H}\ddot{\theta}_{ref}$. In this case, the descending command, u_{ff}, is the reference trajectory plus a signal designed to approximately anticipate the torque requirements due to moments of inertia, but neglecting the angle-dependent inertia nonlinearities and the velocity-dependent terms. For this case, the first of the double-ramp patterns described above was used. This was designated "FFTYP(2)". Because velocity steps were used, the reference accelerations are, in principle, Dirac delta distributions.

These were approximated by narrow rectangular impulses having area=5 (a pulse of 0.02 sec duration with height 250 was used).

The third case is with $u_{dyn} = K^{-1}H\ddot{\theta}_{ref}$. This is very similar to FFTYP(2), except that the angle-dependent nonlinearities in H are no longer neglected. The velocity-dependent matrix C is still not included, however. The reference accelerations are again the narrow rectangular pulses. This case is designated FFTYP(3).

Finally, to check for overall accuracy of the simulations, the case where

$$u_{dyn} = K^{-1}(H\ddot{\theta}_{ref} + C\dot{\theta}_{ref})$$

is examined. Since this form correctly anticipates all plant dynamics, to the extent that the rectangular pulse represents a good approximation to a delta distribution, the tracking should be perfect. This case is designated FFTYP(4).

Performance Measures

For all tasks, performance was quantified in terms of the following five measures:

- The cost functional $\mathcal{J}$, approximated as:

$$\hat{\mathcal{J}} = \int_0^{t_f} (\tilde{\mathbf{q}}^T Q \tilde{\mathbf{q}} + \mathbf{u}_{sp}{}^T R \mathbf{u}_{sp}) \tag{3.3}$$

where t_f is a time at which the system has essentially come to rest completely. For convenience, the components $\hat{\mathcal{J}}_q$ and $\hat{\mathcal{J}}_u$ are also defined as $\int_0^{t_f} \tilde{\mathbf{q}}^T Q \tilde{\mathbf{q}}$ and $\int_0^{t_f} \mathbf{u}_{sp}{}^T R \mathbf{u}_{sp}$, respectively.

- σ_θ, the angular position settling time; defined as the length time from zero after which $\|\tilde{\boldsymbol{\theta}}(t)\|$ remains smaller than 0.01 rad. Since peak excursions for the average controllers are on the order of .5 rad, this represents a settling of around 98%.

- σ_x, the Cartesian position settling time; defined as the length time from zero after which the magnitude of the cartesian position error vector $\tilde{\mathbf{x}}(t) = [x(t) - x_{ref}(t), y(t) - y_{ref}(t)]^T$ remains smaller than 0.005 meters. Since typical peak excursions are on the order of 25 cm, this represents a settling of approximately 98%.

- $\tilde{\theta}_{max} = \max_{t\epsilon[0,t_f]} \|\tilde{\boldsymbol{\theta}}(t)\|$, the peak angular position error (peak angular excursion).

- $\tilde{x}_{max} = \max_{t\epsilon[0,t_f]} \|\tilde{\mathbf{x}}(t)\|$, the peak Cartesion position error (peak Cartesian excursion).

- $\tau_{max} = \max_{t\epsilon[0,t_f]} \|K\mathbf{u}_{sp}(t)\|$, the peak applied (input) torque (which does not include internal torques due to mechanical interactions between the links).

Chapter 4

Results

4.1 The Full Arm Model

4.1.1 Regulation Tasks

As expected, all design strategies produced stabilizing controllers. Their performances differed, however, with respect to the various measures used.

The Effect of Gainscheduling

A central result is that overall, the gainscheduling schemes affected performance measures comparatively little. This was especially true for TASKS(1,4) in which both joints began with initial velocities in the same direction. In TASKS(2,3) gainscheduling tended to reduce peak torque, τ_{max}, integrated input cost, $\hat{\mathcal{J}}_u$, and total cost,$\hat{\mathcal{J}}$, while it correspondingly somewhat increased peak excursions, $\tilde{\theta}_{max}$ and $\tilde{x}_{max}$, and integrated weighted state error, $\hat{\mathcal{J}}_q$. Still, in these tasks, the differences produced by gainscheduling were considerably smaller than the differences exhibited by controllers generated by different synthesis strategies. Therefore, the results described below can be considered to apply both to the gainscheduled and non-gainscheduled cases unless otherwise indicated.

The Behavior of Different Plants

A second major result of the simulations is that the *pattern* in the regulation performance measures for PLANTS(0-2) was quite similar across different controllers. Aside from the following specific points, then, the patterns described in the sections below can be considered

to be reflective of all three of these plants.

Comparison of the performances with PLANTS(1,0) for given controllers revealed two noteworthy features. For the time domain indices, $\tilde{\theta}_{max}$, $\tilde{x}_{max}$, σ_θ and σ_x, PLANT(0) fairly consistently had values on the order of 0% to 5% smaller than those of PLANT(1). In particular, for $CTLRS_1(3,12)$, which had the smallest time-domain values among the controllers, the results with PLANTS(1,0) were nearly identical. For measures $\hat{J}$ (Fig. 4-1) and τ_{max}, however, although PLANT(0) resulted in slightly smaller values than PLANT(1) in TASKS(1,3), slightly larger values were obtained with PLANT(0) in TASKS(2,4).

The results with PLANT(2) were overall highly consistent with those obtained with PLANTS(0,1). While PLANT(2), which is more massive than PLANT(1), generated larger errors and input costs, the pattern of regulation performances across different controllers shown with PLANT(2) was largely the same as that with PLANTS(1,0). The most noteworthy difference is that $CTLRS_2(3,5)$ were observed to reduce both σ_θ and σ_x more consistently relative to $CTLR_2(1)$, than $CTLRS_1(3,5)$ relative to $CTLR_1(1)$ with either PLANTs(1,0). This is discussed in greater detail under "Time-domain Measures" below.

Integrated Costs

In all regulation tasks $\hat{J}_u$, comprised at least 80% of $\hat{J}$ for all controllers (see Figs. 4-1-4-3). Therefore, total cost minimization was substantially due to control cost minimization. H_∞ and H_2 controllers normalized according to g_{max2}, (CTLRS(1,2,7,8)) performed quite comparably in terms of $\hat{J}$ minimization on all regulation tasks. It is also apparent that TASKS(1,4), in which initial angular velocities were in the same direction, incur significantly more control cost than do TASKS(2,3) in which initial joint velocities are equal and opposite. Between TASKS(1,4), TASK(1) incurs the greater cost in general.

On all tasks, g_{max1}-normalized H_2 controllers had the greatest $\hat{J}$. When the input torque amplitude was clipped (CTLRS(5,6)), the controllers showed increased $\hat{J}$ and $\hat{J}_u$ on TASKS(1,4) where high τ_{max} was called for (Compare Figs. 4-1a and 4-4a). The performance of CTLRS(5,6) was comparable to that of unclipped controllers (CTLRS(3,4)) on TASKS(2,3) which did not demand as great τ_{max}.

The LPD controllers (CTLRS(9-12)) showed a range of $\hat{J}$ across all regulation tasks and for both linear and nonlinear plants. In general, $\hat{J}$ increases across CTLRS(9,11,12), that is with increasing r. The performances of CTLRS(9,10) were typically very close and

these two controllers have essentially identical values for r (see Table 3.7).

For all controllers, $\hat{\mathcal{J}}_q$ tended to be roughly inversely related to $\hat{\mathcal{J}}_u$ and hence inversely related to $\hat{\mathcal{J}}$. That is, H_∞ designs tended to have the largest $\hat{\mathcal{J}}_q$, while the g_{max1}-normalized H_2 controllers had the least. The g_{max2}-normalized H_2 controllers performed similarly to, or better than the H_∞ controllers while the PD controllers exhibited a range of values as a function of r. The exception to this pattern is that with peak torque clipping, increased $\hat{\mathcal{J}}_u$ was associated with *increased* $\hat{\mathcal{J}}_q$ (Fig. 4-4b).

Time-domain Measures

Overall, unclipped controllers which had large $\hat{\mathcal{J}}_u$, had large τ_{max} with small $\tilde{\theta}_{max}$ and small $\tilde{x}_{max}$. Thus, $\tilde{\theta}_{max}$ and $\tilde{x}_{max}$ changed in parallel and their values correlated closely with small integrated state error (Fig. 4-5). On the other hand, clipped controllers had *increased* $\hat{\mathcal{J}}_u$, or rather in response to, limited peak torque. As such, in TASKS(1,4) the clipped controllers showed comparatively increased $\tilde{\theta}_{max}$ and $\tilde{x}_{max}$ in the presence of increased input cost.

The angular and Cartesian settling times, which moved in parallel, displayed patterns which differed between PLANTS(0,1) and PLANT(2) (Figs. 4-6 and 4-7). For PLANT(2) these measures showed the reciprocal pattern displayed by $\tilde{\theta}_{max}$ and $\tilde{x}_{max}$; being reduced with controllers associated with high $\hat{\mathcal{J}}_u$. For PLANTS(0,1), however, there was a slightly different pattern. Specifically, CTLRS_1(5,6), the g_{max2}-normalized H_2 controllers, produced settling in 0.8 to 0.85 seconds, while the H_∞ controllers, CTLRS_1(1,2), showed more variable settling times (from 0.9 to 1.1 seconds) as did the g_{max1}-normalized H_2 which yielded settling in 0.95 to 1.05 seconds in TASKS(1,4), or near 0.8 seconds in TASKS(2,3). The LPD controllers displayed a wide range of settling times from near 0.6-0.7 seconds, for CTLRS_1(9,10), which is noticeably smaller than those of the other controllers, to near 1.4 seconds with CTLR_1(12). Prolonged settling time was evidently associated with incrasing r. Finally, analogous to the effect of clipping on $\hat{\mathcal{J}}_q$, the clipped controllers displayed slightly prolonged settling time as compared with their unclipped counterparts in TASKS(1,4).

4.1.2 Tracking Tasks using only Reference Trajectory Feedforward

The patterns in the results of the tracking tasks in which $\mathbf{u}_{ff} = \boldsymbol{\theta}_{ref}$ tended to generalize in most respects from the regulation task results.

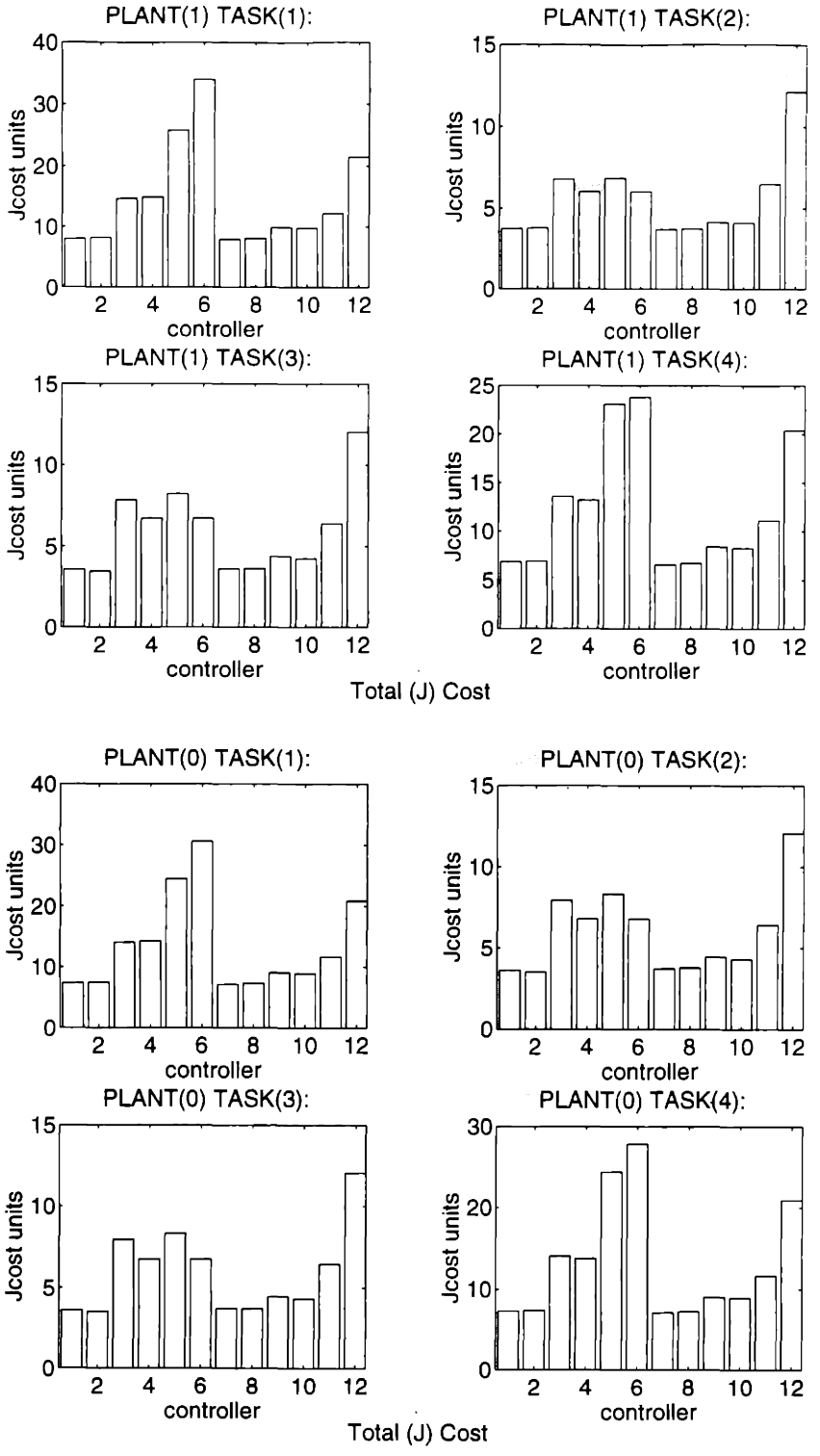

Figure 4-1: a)(top) Integrated total cost, $\hat{\mathcal{J}}$, in regulation tasks for nonlinear PLANT(1) b)(bottom) Integrated total cost, $\hat{\mathcal{J}}$, in regulation tasks for linear PLANT(0).

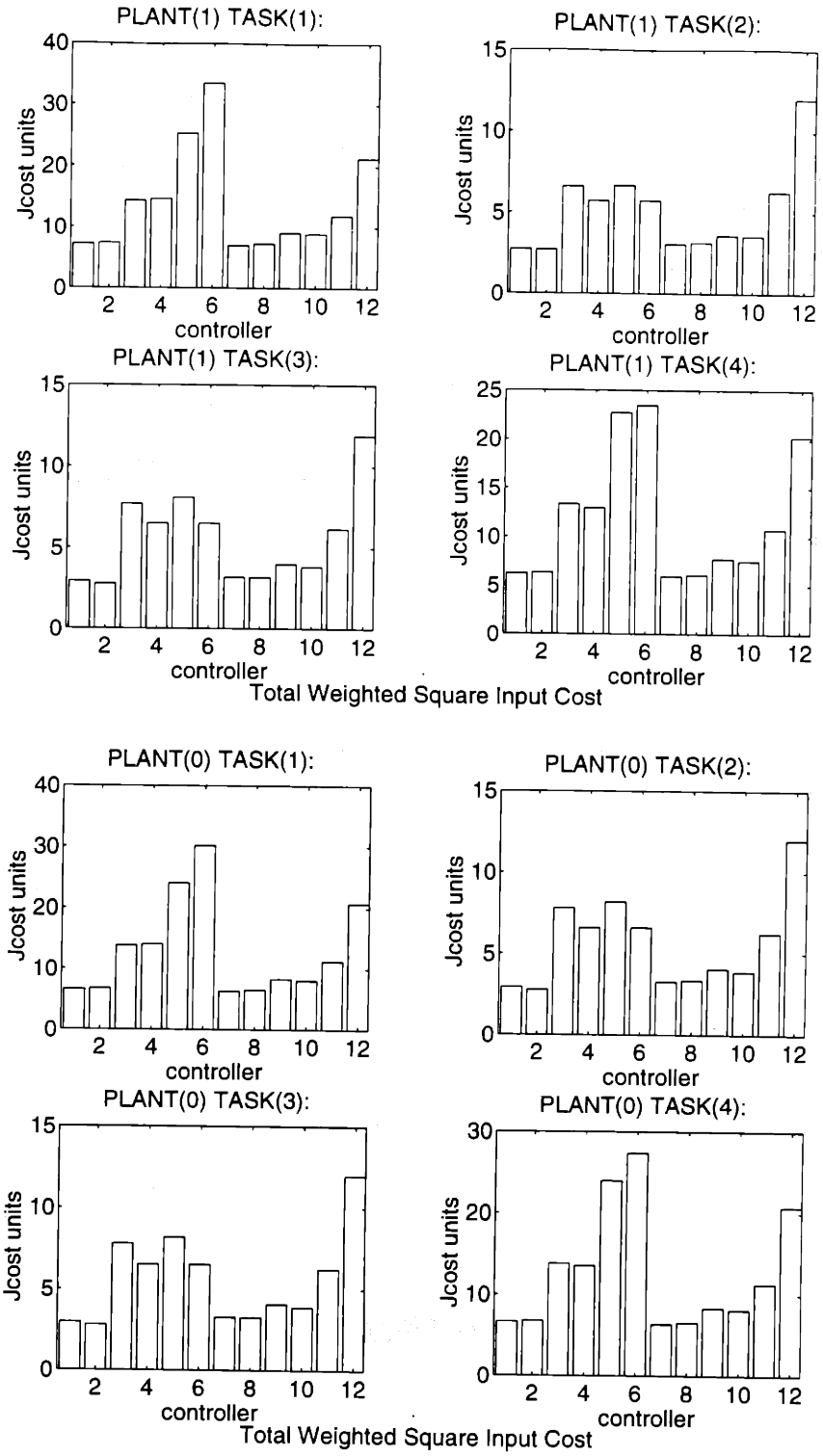

Figure 4-2: Integrated weighted squared input cost, $\hat{\mathcal{J}}_u$, in regulation tasks: a)(top) for nonlinear PLANT(1) b)(bottom) for linear PLANT(0)

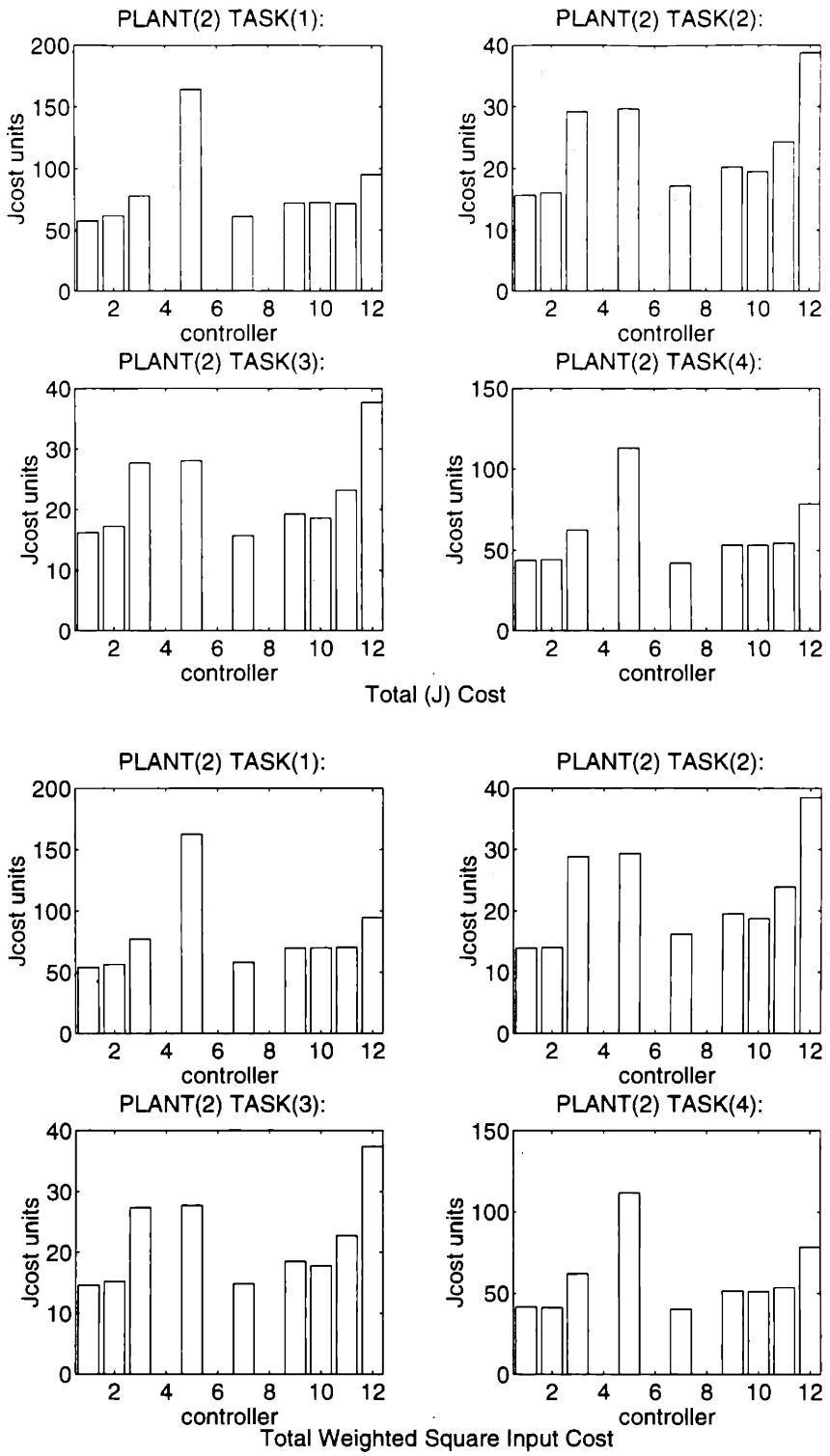

Figure 4-3: For PLANT(2) in regulation tasks: a)(top) $\hat{\mathcal{J}}$, b)(bottom) $\hat{\mathcal{J}}_u$

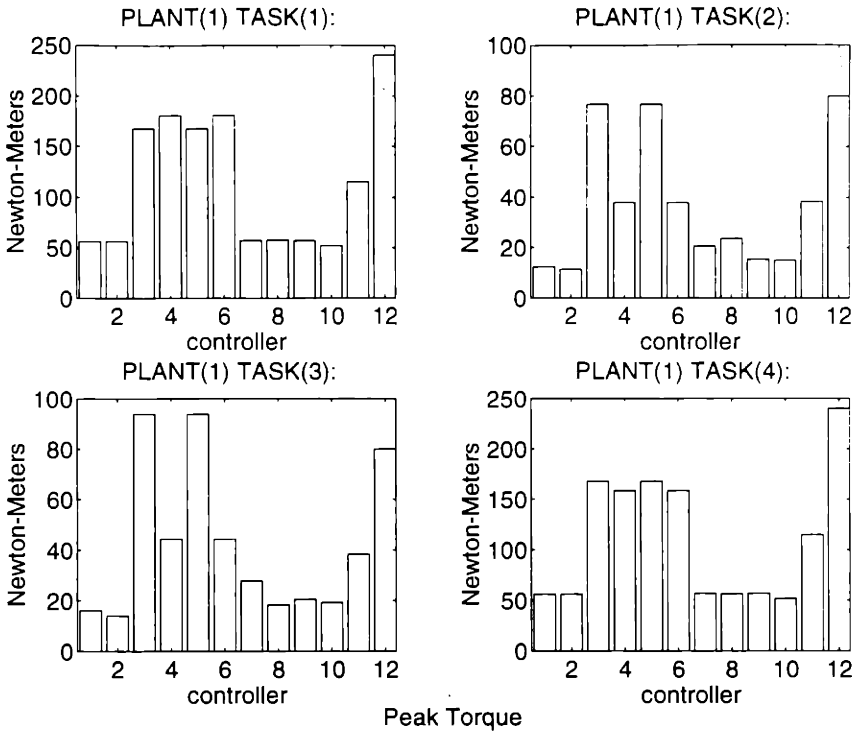

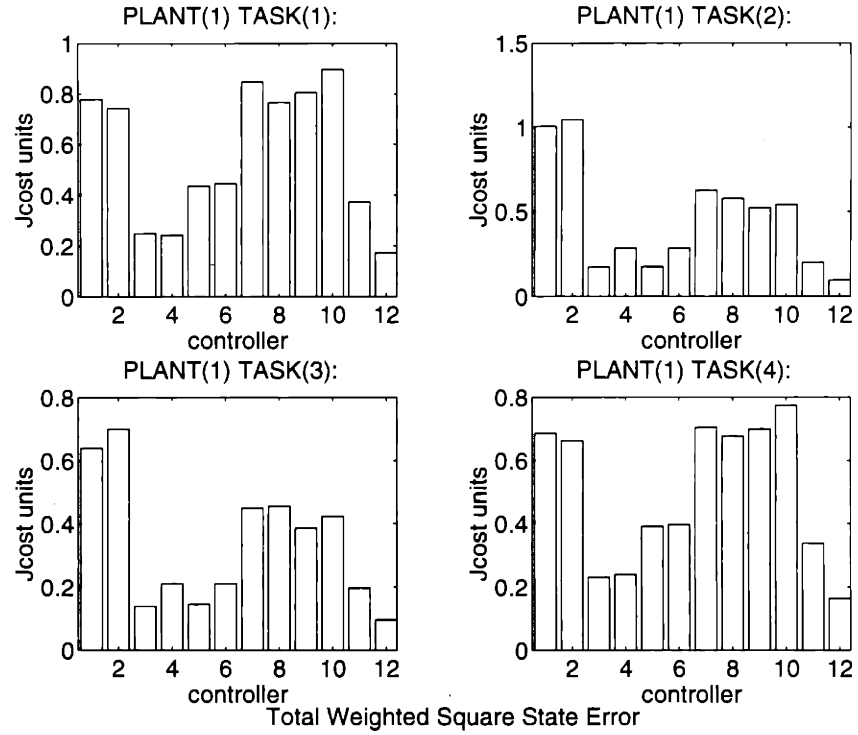

Figure 4-4: For PLANT(1) in regulation tasks: a)(top) peak input torque τ_{max}; b)(bottom) integrated weighted squared state error, $\hat{\mathcal{J}}_q$.

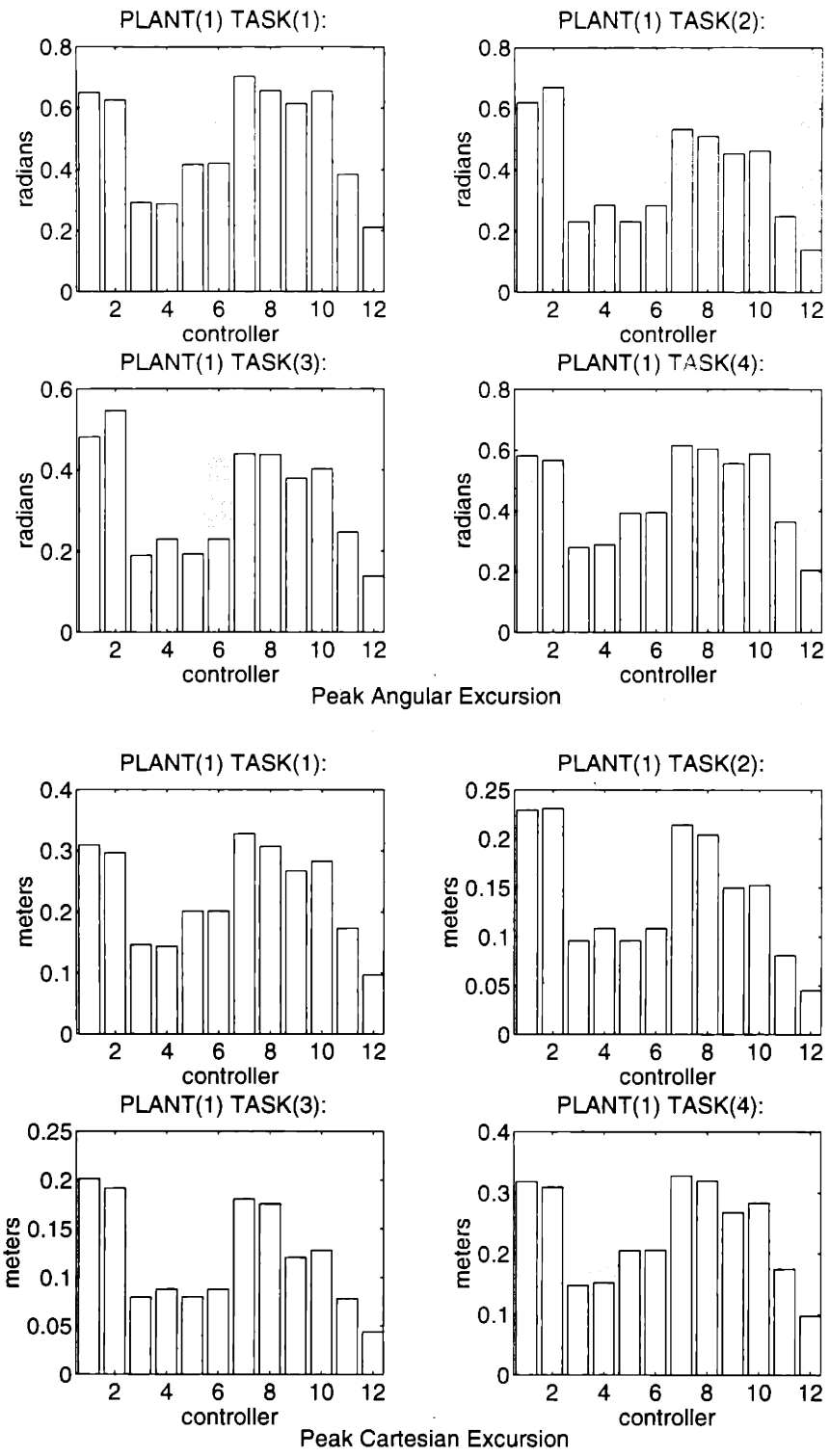

Figure 4-5: For PLANT(1) in regulation tasks: a)(top) Peak angular excursion, $\tilde{\theta}_{max}$; b)(bottom) Peak Cartesian excursion, $\tilde{x}_{max}$.

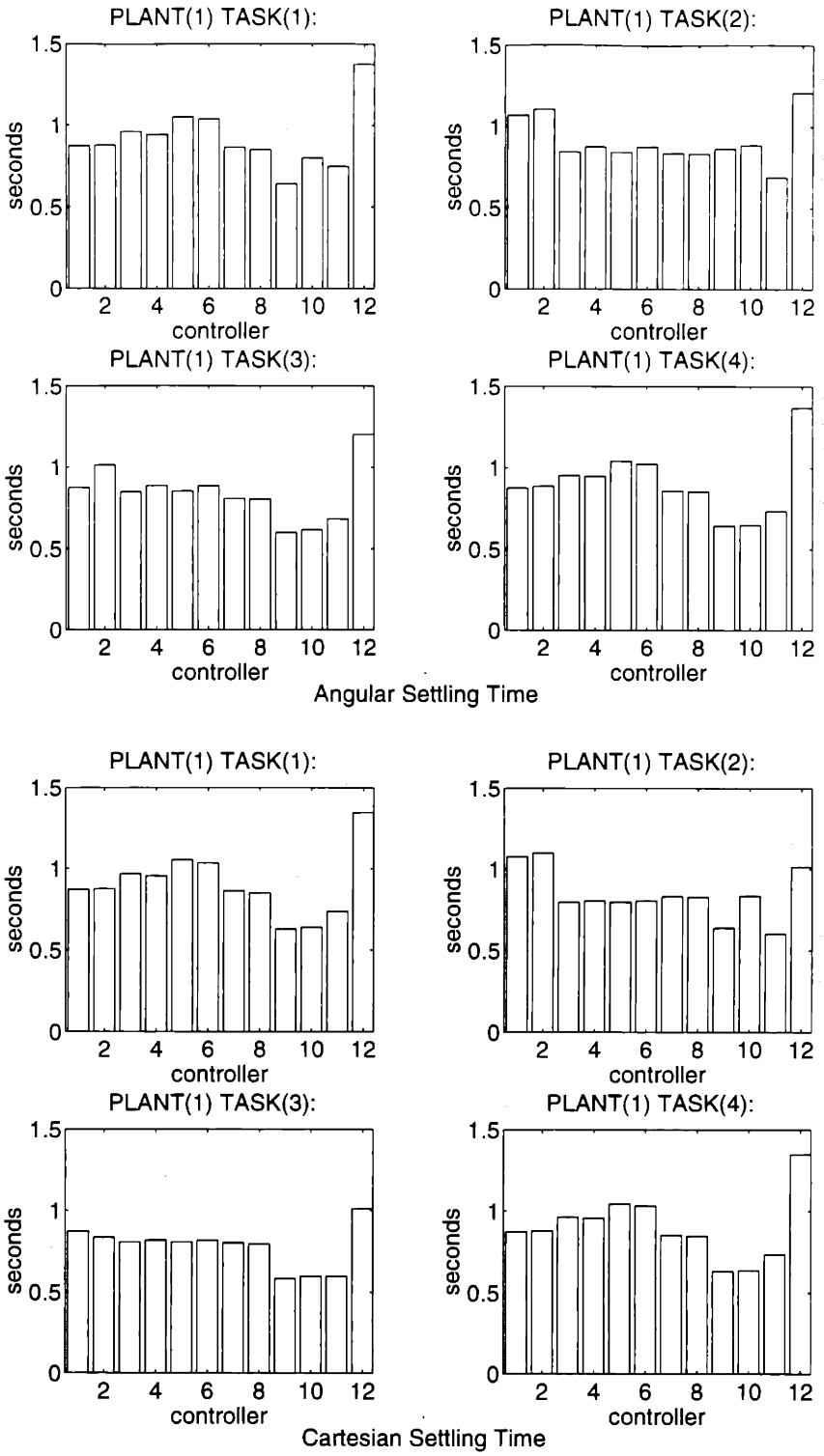

Figure 4-6: For PLANT(1) in regulation tasks: a)(top) Angular settling time, σ_θ; b)(bottom) Cartesian settling time, σ_x.

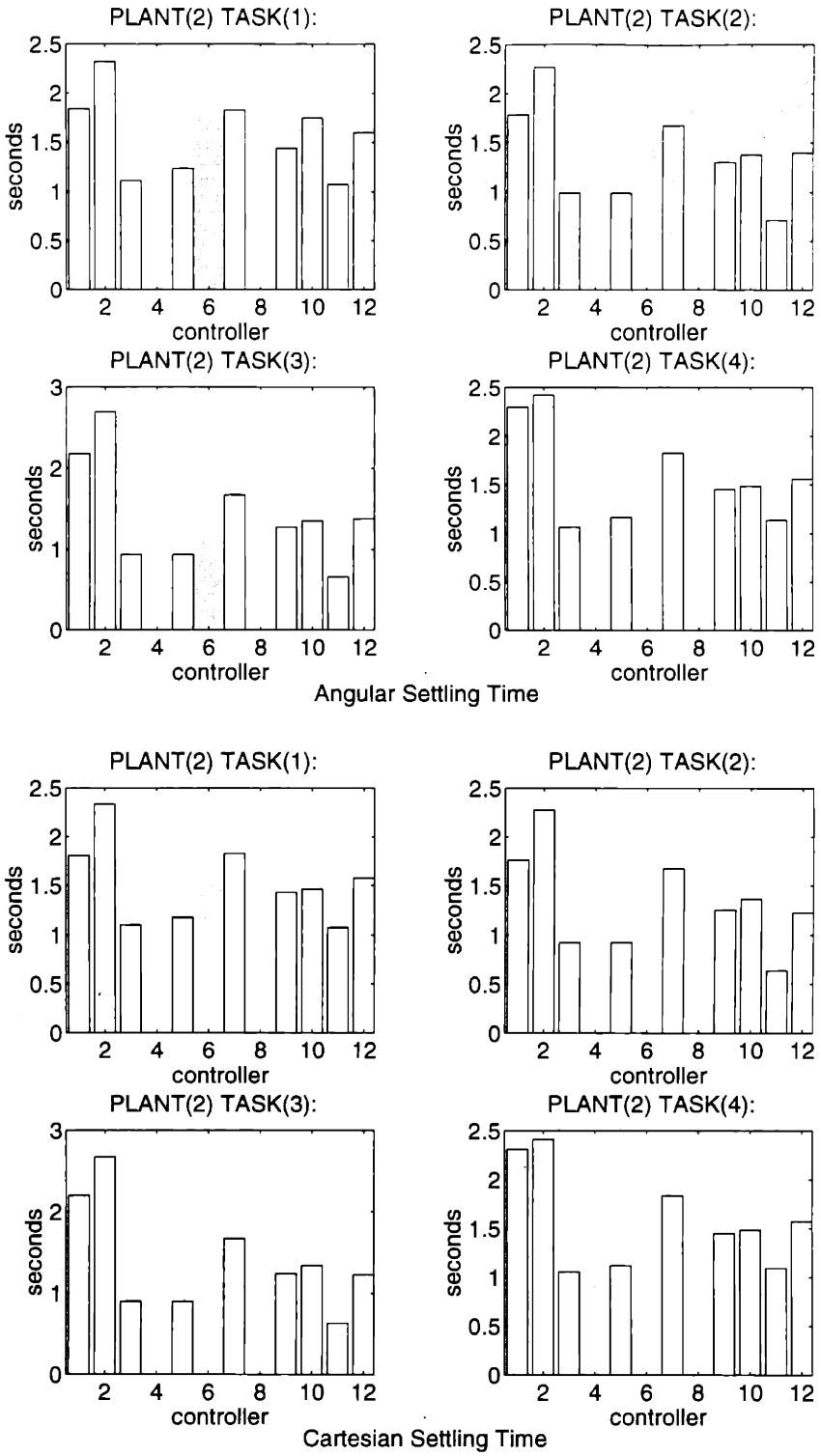

Figure 4-7: For PLANT(2) in regulation tasks: a)(top) Angular settling time, σ_θ; b)(bottom) Cartesian settling time, σ_x.

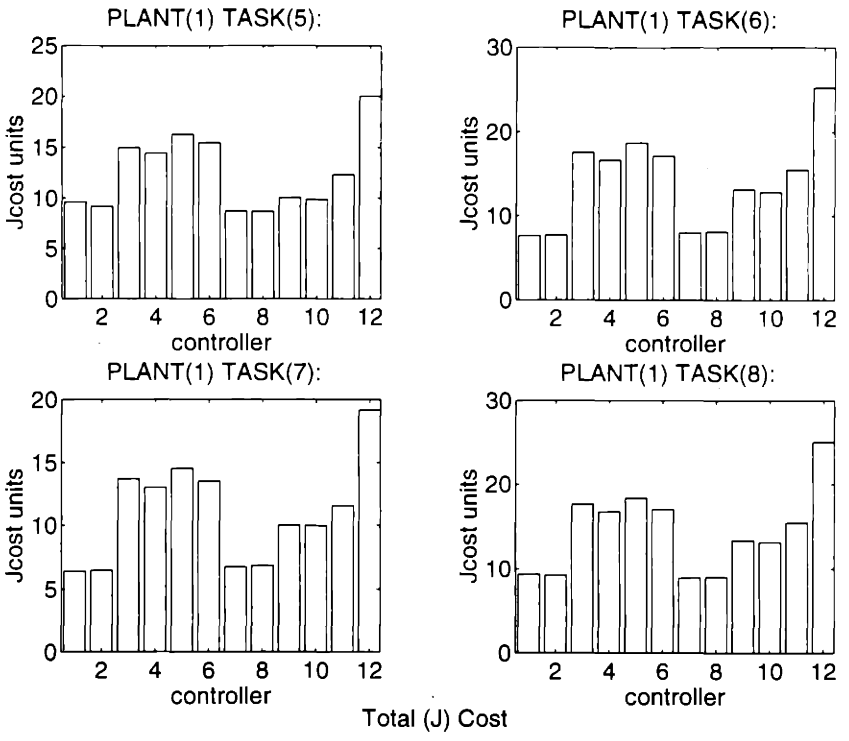

Figure 4-8: $\hat{\mathcal{J}}$ in tracking tasks: a) for PLANT(1); b) for PLANT(0).

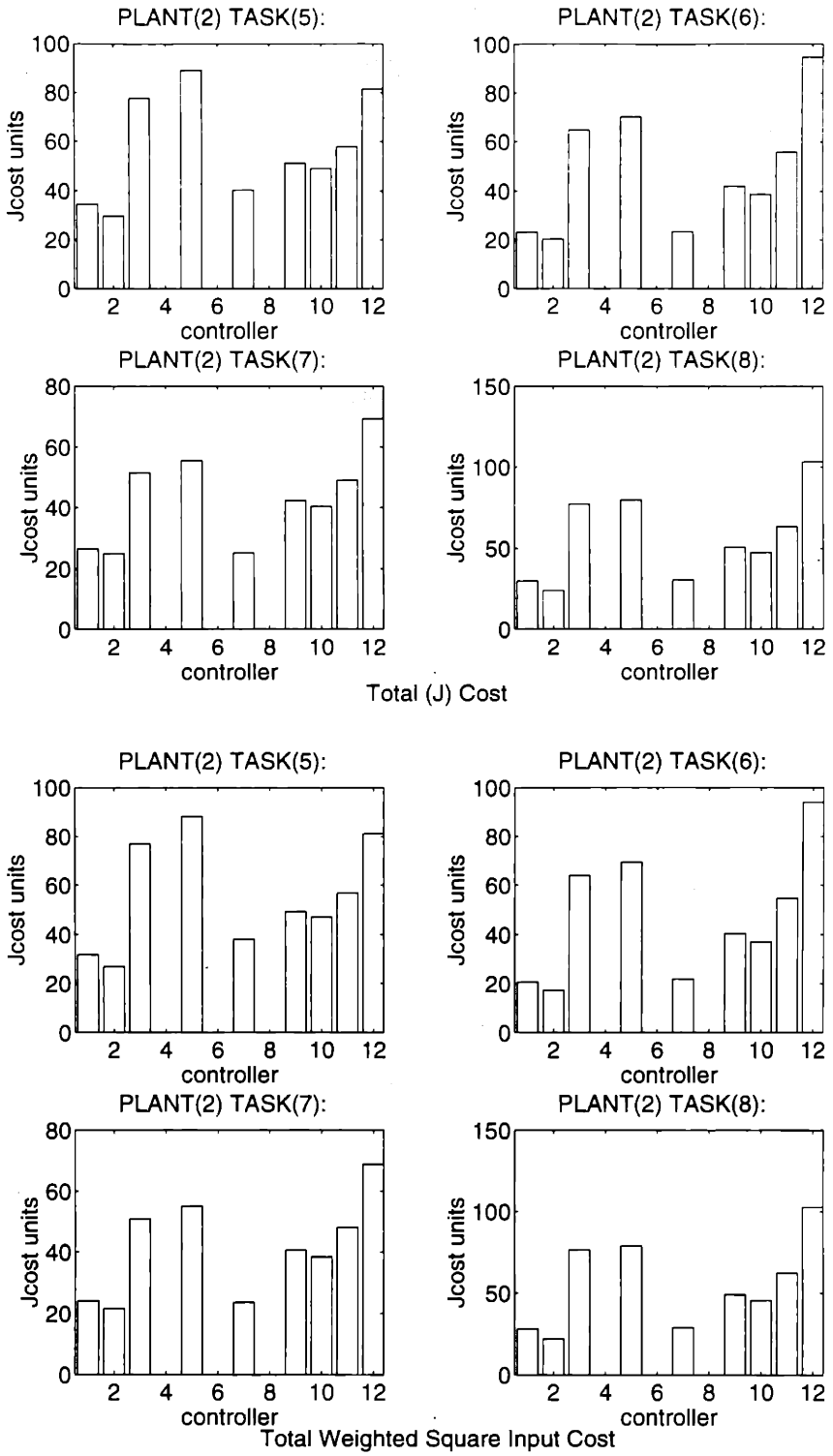

Figure 4-9: For tracking tasks with PLANT(2): a) $\hat{\mathcal{J}}$; b) $\hat{\mathcal{J}}_u$.

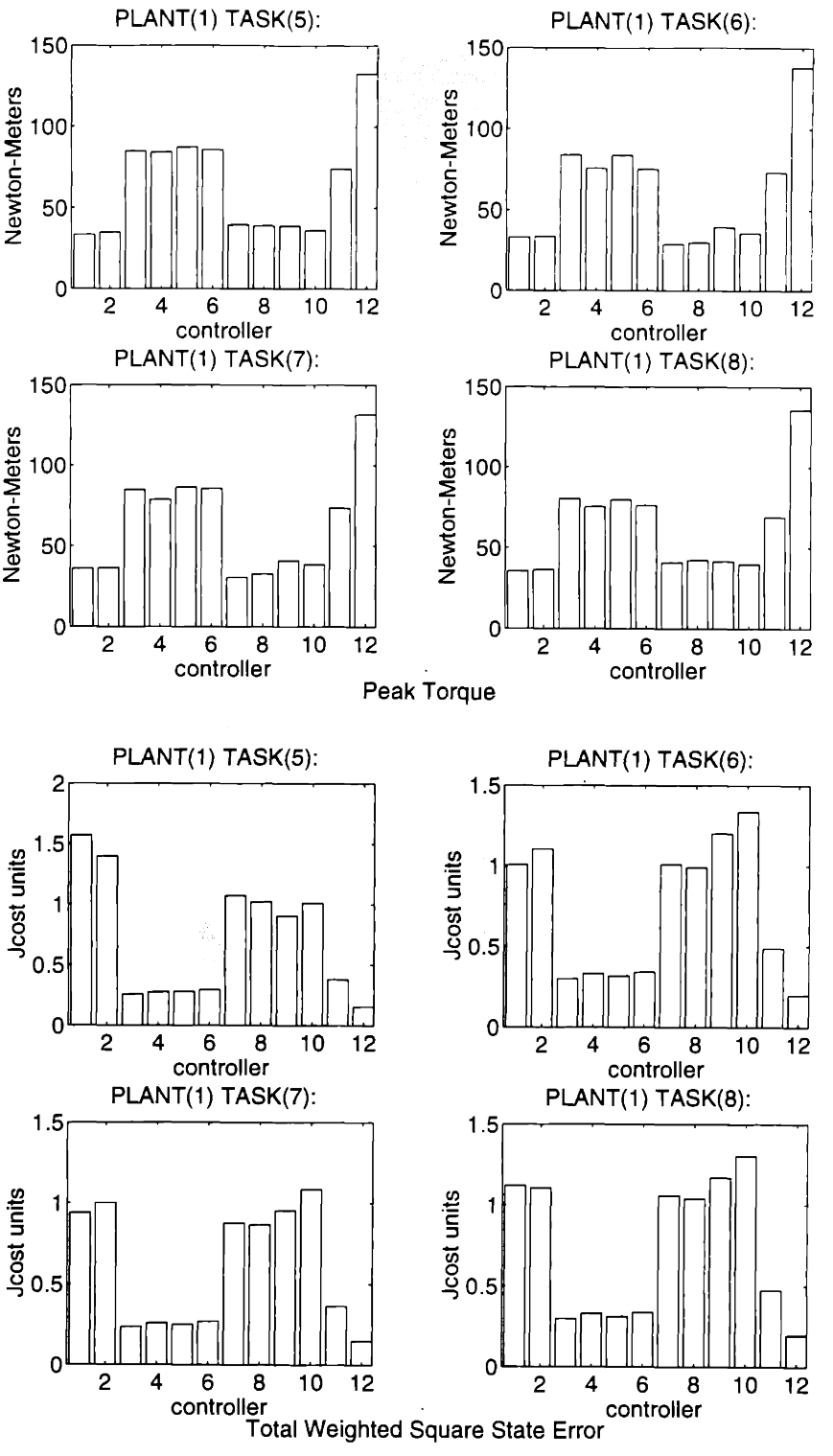

Figure 4-10: For tracking tasks with PLANT(1): a) Peak input torque, τ_{max}; b) Integrated weighted total squared state error, $\hat{J}_q$.

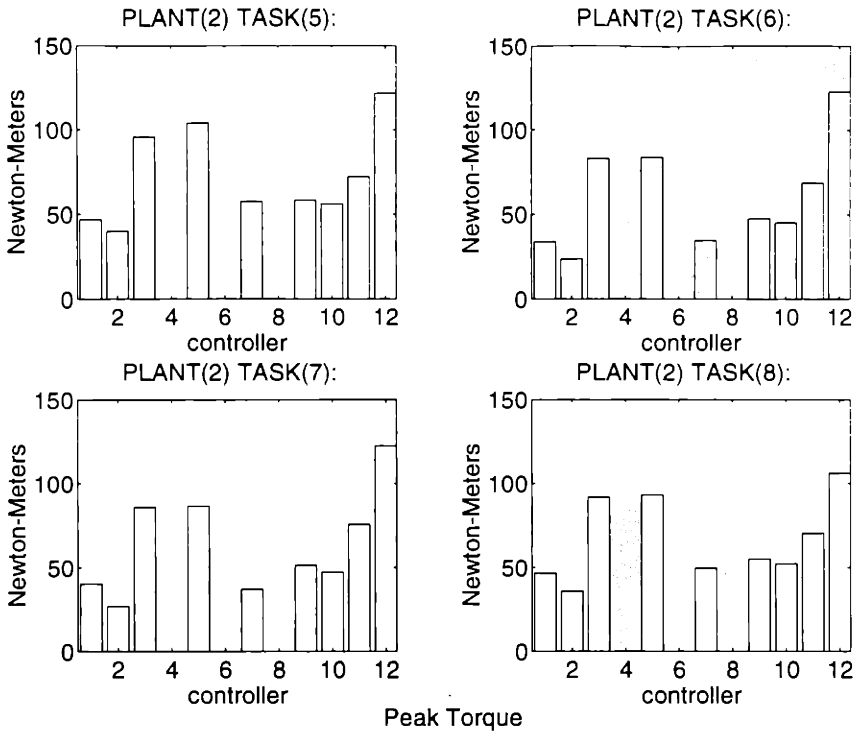

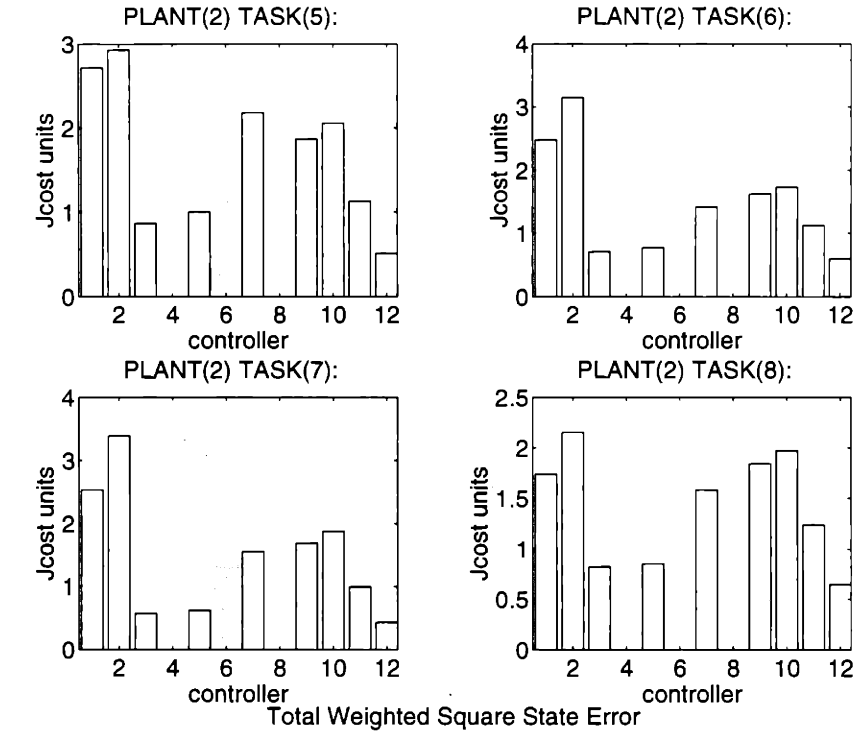

Figure 4-11: For tracking tasks with PLANT(2): a) Peak input torque, τ_{max}; b) Integrated weighted total squared state error, $\hat{\mathcal{J}}_q$.

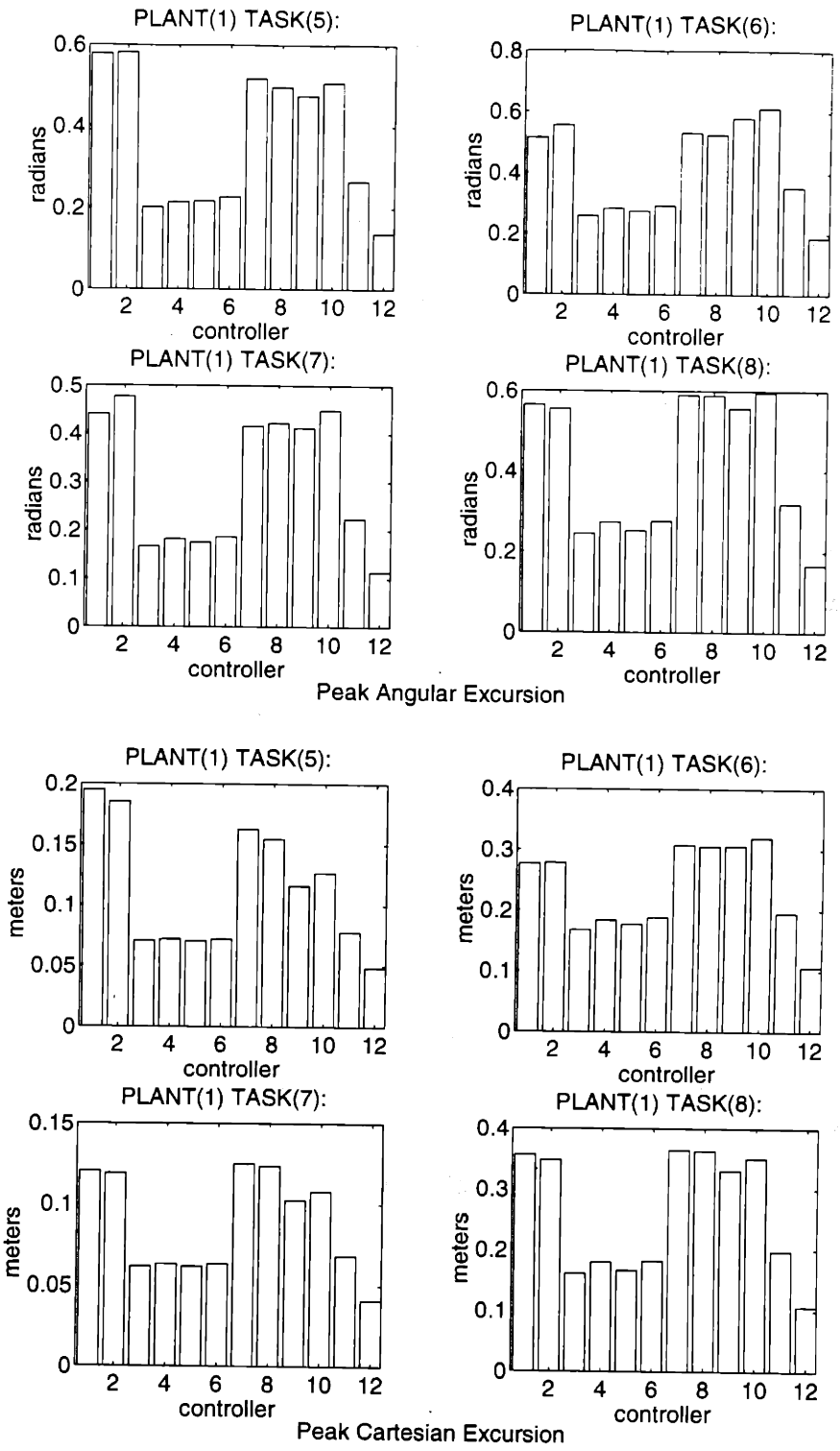

Figure 4-12: For tracking tasks with PLANT(1): a) Peak angular excursion, $\tilde{\theta}_{max}$; b) Peak cartesian excursion, $\tilde{x}_{max}$.

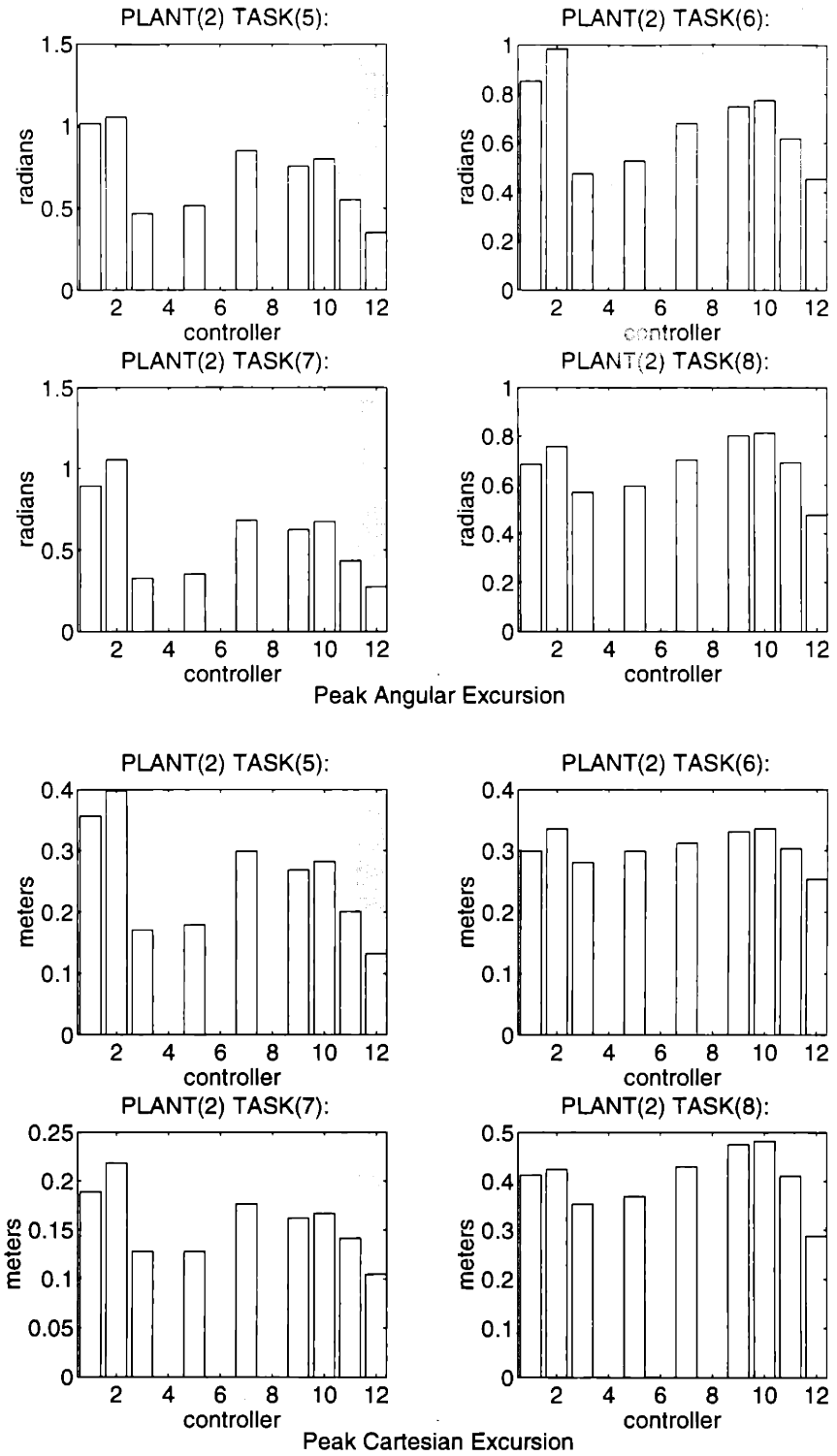

Figure 4-13: For tracking tasks with PLANT(2): a) Peak angular excursion, $\tilde{\theta}_{max}$; b) Peak cartesian excursion, $\tilde{x}_{max}$.

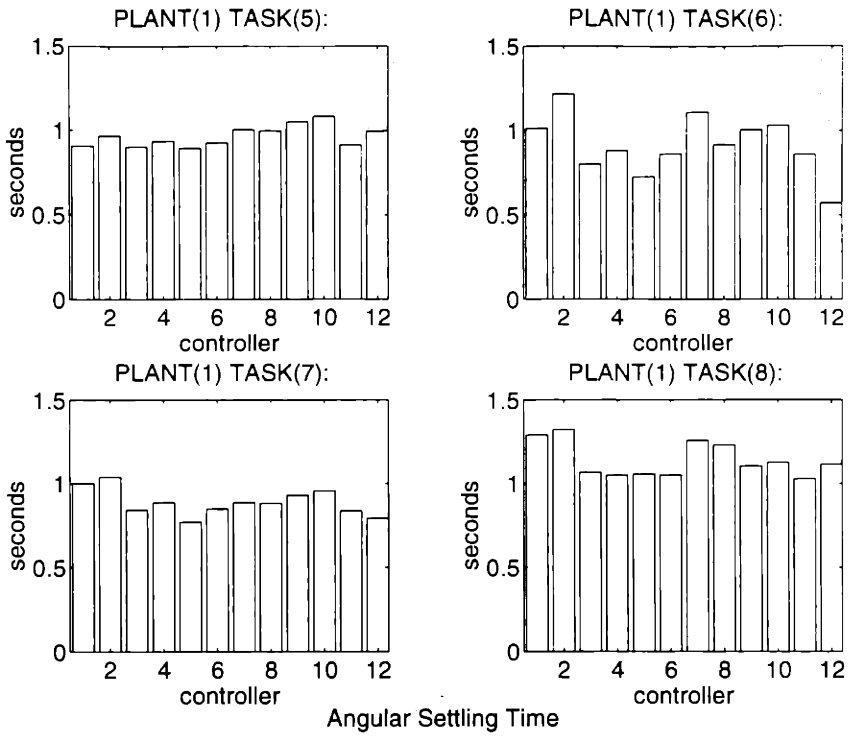

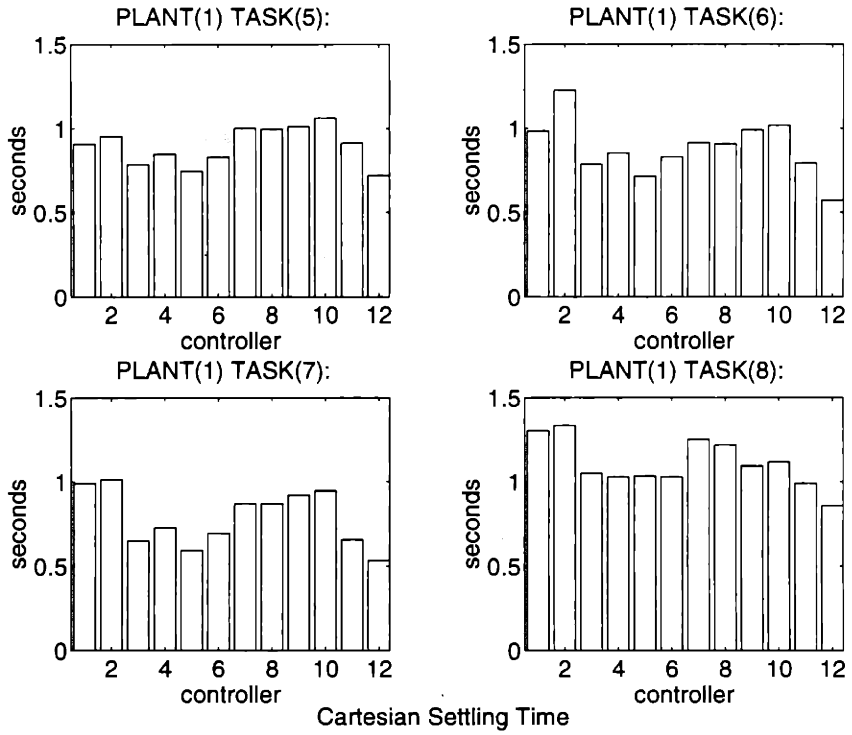

Figure 4-14: For tracking tasks with PLANT(1): a) Angular settling time, σ_θ; b) Cartesian settling time, σ_x.

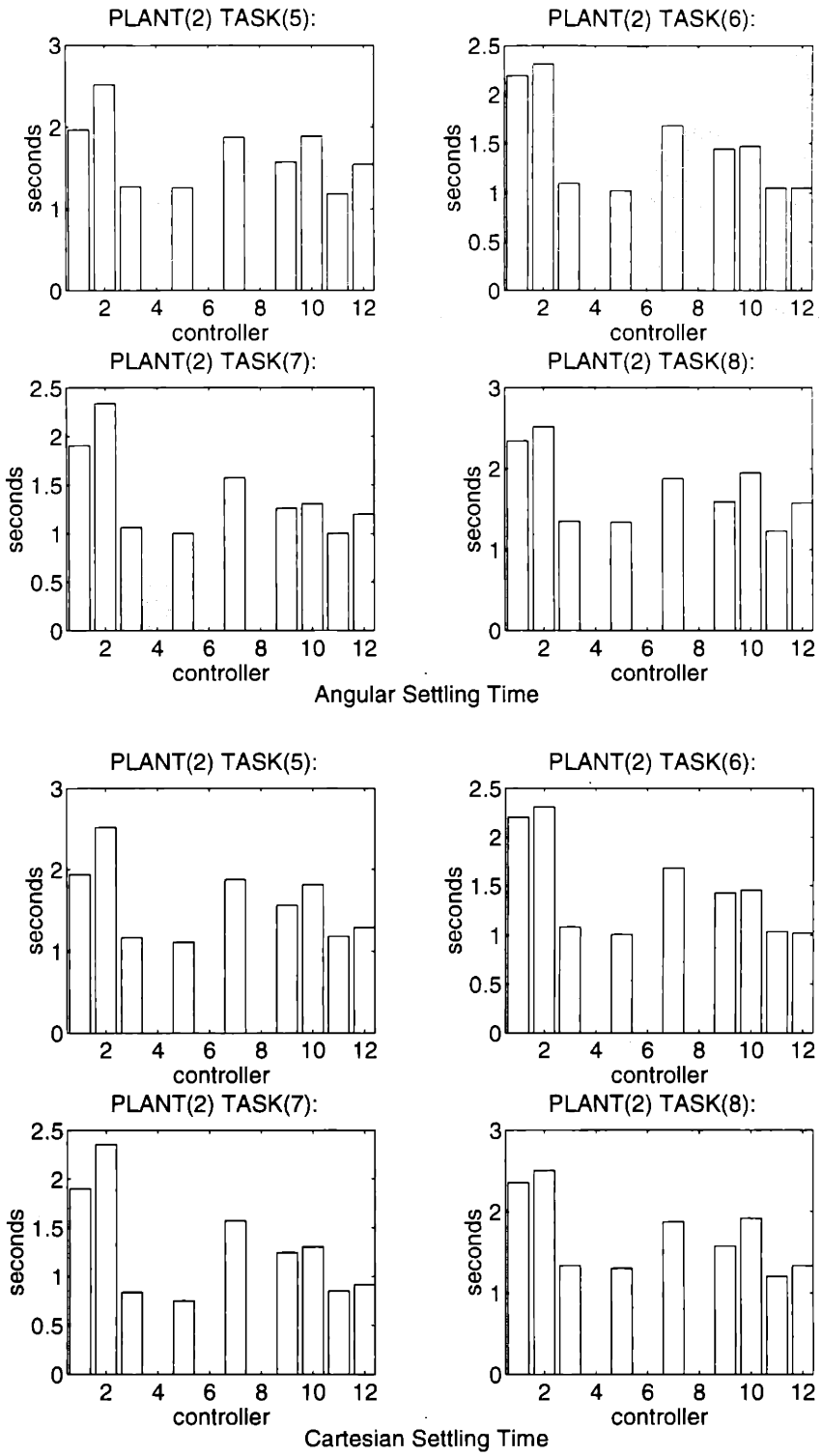

Figure 4-15: For tracking tasks with PLANT(2): a) Angular settling time, σ_θ; b) Cartesian settling time, σ_x.

The Effect of Gainscheduling

As in the regulation tasks, gainscheduling tended to have relatively little effect on $\hat{J}$-cost and other performance measures, and certainly little as compared with differences produced by other factors. When there was a difference, gainscheduling tended to reduce the $\hat{J}$ slightly (Fig. 4-8). This was often associated with a settling time prolongation of about 5% in most tasks (Fig. 4-14). All of the other patterns described, then, hold for both gainscheduled and non-gainscheduled results unless specified otherwise.

The Behavior of Different Plants

In comparison to the situation with TASKS(1-4), the measures for any given controller had less distinct patterns across plants. Both integrated costs and time-domain measures varied between PLANTS(0-2) depending on the task. Just the same, the important finding was that as in TASKS(1-4), results with PLANTS(0,1) were within 10% and often 5% of each other. Otherwise, there are two other minor observations. First, especially in the tracking tasks, with PLANT(2) the gainscheduled H_∞ controller ($\text{CTLR}_2(2)$) generated larger integrated and peak state errors and settling times relative to $\text{CTLR}_2(1)$ than $\text{CTLR}_1(2)$ relative to $\text{CTLR}_1(1)$ with PLANTs(1,0). The effect is not large but is evident. Also, in some tracking tasks $\text{CTLR}_2(2)$ reduced peak excursion relatively less effectively than $\text{CTLR}_1(2)$. These effects are detailed below.

However, as in the regulation tasks, the overall pattern of controller performance across different controllers was the same for PLANTS(0-2) in TASKS(5-8). As such, results reported below can be taken to represent the performances with all three plants unless otherwise indicated. The comparison between all three plants in terms of $\hat{J}$ can be made from Figures 4-8 and 4-9a. The remaining results for PLANT(0) are not reported explicitly.

Integrated Costs

As with the regulation tasks, total cost was dominated by input costs as is shown for PLANT(2) in Fig. 4-9. Across all tasks and plants, CTLRS(1,2,7,8) consistently showed the smallest values for $\hat{J}$; having fromabout 75% to 90% the cost with CTLRS(9,10), about 50% to 70% the cost with CTLRS(3,4,5,6) and about 35% to 60% the cost with CTLRS(11,12) (Figs. 4-8a,b and 4-9a). Similar to the results in the regulation tasks,

$\hat{\mathcal{J}}_u$ parallelled, and $\hat{\mathcal{J}}_q$ often tended to be inversely related to the $\hat{\mathcal{J}}$ (Figs. 4-10b and 4-11b). Thus, CTLRS(1,2,7,8) displayed approximately 3 times the integrated state error as CTLRS(3,4,5,6). The PD controllers again displayed a range of $\hat{\mathcal{J}}_q$ including the smallest values of any controllers which occurs with CTLR(12).

The predominant patterns in $\hat{\mathcal{J}}$ values across TASKS(5-8) and TASKS(1-4) were parallel. Specifically, TASKS(1,4) and TASKS(5,8) incurred greater total costs than TASKS(2,3) and TASKS(6,7), respectively. This was the case with PLANTS(1,0) for CTLRS_1(1,2,7,8) and with PLANT(2) for all controllers except CTLRS_2(11,12). For CTLRS_1(3-6,9-12) and CTLRS_2(11,12), however, TASKS(6,8) in which the second joint's initial velocity was negative, incurred greater control costs than did TASKS(5,7) where it was positive.

Time-Domain Measures

As in the regulation tasks, $\tilde{\theta}_{max}$ and $\tilde{x}_{max}$ correlated well with small $\hat{\mathcal{J}}_q$ (compare Figs 4-12, 4-13, 4-10b while large τ_{max} corresponded to large $\hat{\mathcal{J}}_u$ (compare Figs. 4-9b and 4-11a). Though this was quite consistent across plants and tasks, there were a few additional observations to note. First, CTLRS(9,10) were comparatively less effective in reducing $\hat{\mathcal{J}}_q$ than in reducing peak excursions. CTLRS(11,12) and especially CTLR(12), however, reduced both strongly. Second, with PLANT(2) in TASKs(6,8), $\tilde{\theta}_{max}$, and especially $\tilde{x}_{max}$ were not as dramatically reduced by CTRLRs(3,5) as with PLANTs(0,1). Third, consistent with the procedure for finding "reasonable" G_∞, any given controller type generated similar peak torque levels across PLANTS(1,2). Presumably because for TASKS(5-8) these levels were seldom in excess of the clipping threshold (65 N-m), the behavior of CTLRS(5,6) differed extremely little from that of CTLRS(3,4) in the tracking tasks.

Settling times for the tracking tasks showed a pattern which was different from that of regulation tasks. Specifically, except in TASK(5) with PLANTS(1,0), CTLRS(3,4,5,6) tended to have about 15% to 20% smaller σ_θ and σ_x than CTLRS(1,2). The PD controllers displayed a range of settling times generally spanning the settling times of the other controllers, though especially with PLANT(2) tended to have consistently faster settling times than CTLR(1). Typically, among the PD controllers, CTLR(11) or CTLR(12) had the most rapid settling (Figs. 4-14 and 4-15).

The spatial trajectories produced by CTLRS(1,3,5,12) controlling PLANTS(0-1) in TASK(5) is shown in Figures 4-30-4-35.

4.2 The Reduced Arm Model

4.2.1 Regulation Tasks

Integrated Costs

The integrated costs revealed the same basic pattern with the uncoupled actuator plant (PLANT(3)) as with PLANTS(0-2). Specifically, input costs had a dominant effect in determining total cost and controllers which used incurred large input costs produced small integrated state error (Figs. 4-16 and 4-17b). The general pattern of error magnitude between the tasks was also similar with TASKS(1,4) incurring 2-4 times as much total cost as TASKS(2,3). With PLANT(3), the costs with TASKS(1,4) were slightly more equal than with PLANT(1). In terms of actual magnitude, values for $\hat{\mathcal{J}}_q$ in TASKs(1,4) were comparable to those found with PLANT(1), with values ranging from about 0.2-0.9. In TASKS(2,3), however, the range was approximately 0.1-0.25 with PLANT(3) instead of 0.1-1 with PLANT(1). Similarly, $\hat{\mathcal{J}}_u$ in TASKS(1,4) ranged from 2-6 with PLANT(3), and from 7-25 with PLANT(1). These ranges are fairly comparable if it is noted that the input cost weighting factor, ρ_0, is 5 for PLANT(3) and 20 for PLANT(1). The input cost ranges with TASKS(2,3) are a bit smaller with PLANT(3) (0.5-0.8) than with PLANT(1) (4-6), even taking into account the scaling difference.

With regard to specific controllers used with PLANT(3), $CTLR_3$(1,3) incurred similarly low input cost values (with $CTLR_3$(1) characteristically the lower) but generated large errors in comparison to the other controllers. On the other hand, $CTLRS_3$(12-15) incurred greater input cost, but, in general smaller errors. TASKS(2,3) present slight exceptions to this since $CTLRS_3$(13,14) generate larger errors than all others.

Time-Domain Measures

The ranges of τ_{max} with PLANTS(1,3) in TASKS(1,4) are comparable, excepting the case of $CTLR_1$(12), being about (60-180 N-m) in TASKS(1,4) (compare Figs. 4-4a and 4-17a). In TASKS(2,3), the ranges with the two plants are about (10-90 N-m) and (30-75 N-m), respectively. The latter is narrower, but similarly centered. With the controllers used with PLANT(3), the pattern of τ_{max} closely mirrors the pattern in total input costs.

With PLANTS(1,3), as with the behavior of $\hat{\mathcal{J}}_q$, $\tilde{\theta}_{max}$ and $\tilde{x}_{max}$ fell within similar ranges in TASKS(1,4) but were comparatively smaller with PLANT(3) in TASKS(2,3)

(Figs. 4-17b and 4-18). However, the pattern in peak excursions across controllers used with PLANT(3) was the same as that of $\hat{\mathcal{J}}_q$ for all TASKs. Specifically, $CTLR_3(15)$ exhibited the best overall performance in these measures usually by a margin of at least 10% over the next best controller which was $CTLR_3(12)$ or $CTLR_3(14)$. The only exception was with $\hat{\mathcal{J}}_q$ and $\bar{\theta}_{max}$ which were minimized with $CTLR_3(12)$ in TASKS(2,3).

With PLANT(3), σ_θ and σ_x parallelled each other closely as with PLANT(1). Unlike with PLANT(1), with PLANT(3), the settling times also closely mirrored $\hat{\mathcal{J}}$ (Fig. 4-19). The range in settling times with PLANT(3) was broader, the angular times being from 0.75-1.4 seconds in TASKs(1,4) and 0.65-0.9 in TASKS(2,3) as compared with 0.75-1.0 and 0.8-1.1 respectively, with PLANT(1). In particular, with PLANT(3), $CTLR_3(14,15)$ often generated comparatively long settling times.

4.2.2 Tracking Tasks using only Reference Trajectory Feedforward

As with the FAM, the patterns in the results of the tracking tasks in which $\mathbf{u}_{ff} = \boldsymbol{\theta}_{ref}$ generalized in most respects from the regulation task results.

Integrated Costs

For PLANT(3) the pattern of $\hat{\mathcal{J}}$, $\hat{\mathcal{J}}_u$ and $\hat{\mathcal{J}}_q$ across controllers for TASKS(5-8) followed very closely the patterns of these measures in TASKS(1,4) (Figs. 4-20 and 4-16). Moreover, the ranges of $\hat{\mathcal{J}}_u$: 2-4 and 2.5-5 with PLANT(3) on TASKS(5,8) were quite comparable, after scaling to the ranges 9-15 and 9-17 for the same with PLANT(1). Also, as with PLANT(1), the range of values for TASKS(6,8) were similar, and greater than that for TASKS(5,7).

For $CTLRS_3(12\text{-}15)$, $\hat{\mathcal{J}}_q$ tended to be quite comparable to that exhibited by $CTLR_1(3)$ across all tasks. However, $CTLRS_3(1,3)$ showed 10%-40% smaller $\hat{\mathcal{J}}_q$ than did $CTLRS_1(1,3)$ on corresponding tasks.

Time-Domain Measures

Peak torque ranges were quite similar for PLANT(3) and PLANT(1) for all tracking tasks (compare Figs 4-10a and 4-21a). For PLANT(3), as in the regulation tasks, the τ_{max} pattern across controllers followed that of $\hat{\mathcal{J}}$ and $\hat{\mathcal{J}}_u$ very closely.

Peak excursion measures in TASKS(5-8), followed $\hat{\mathcal{J}}_q$ very closely and the ranges were quite close to those observed in the same tasks with PLANT(1). This closeness was the case

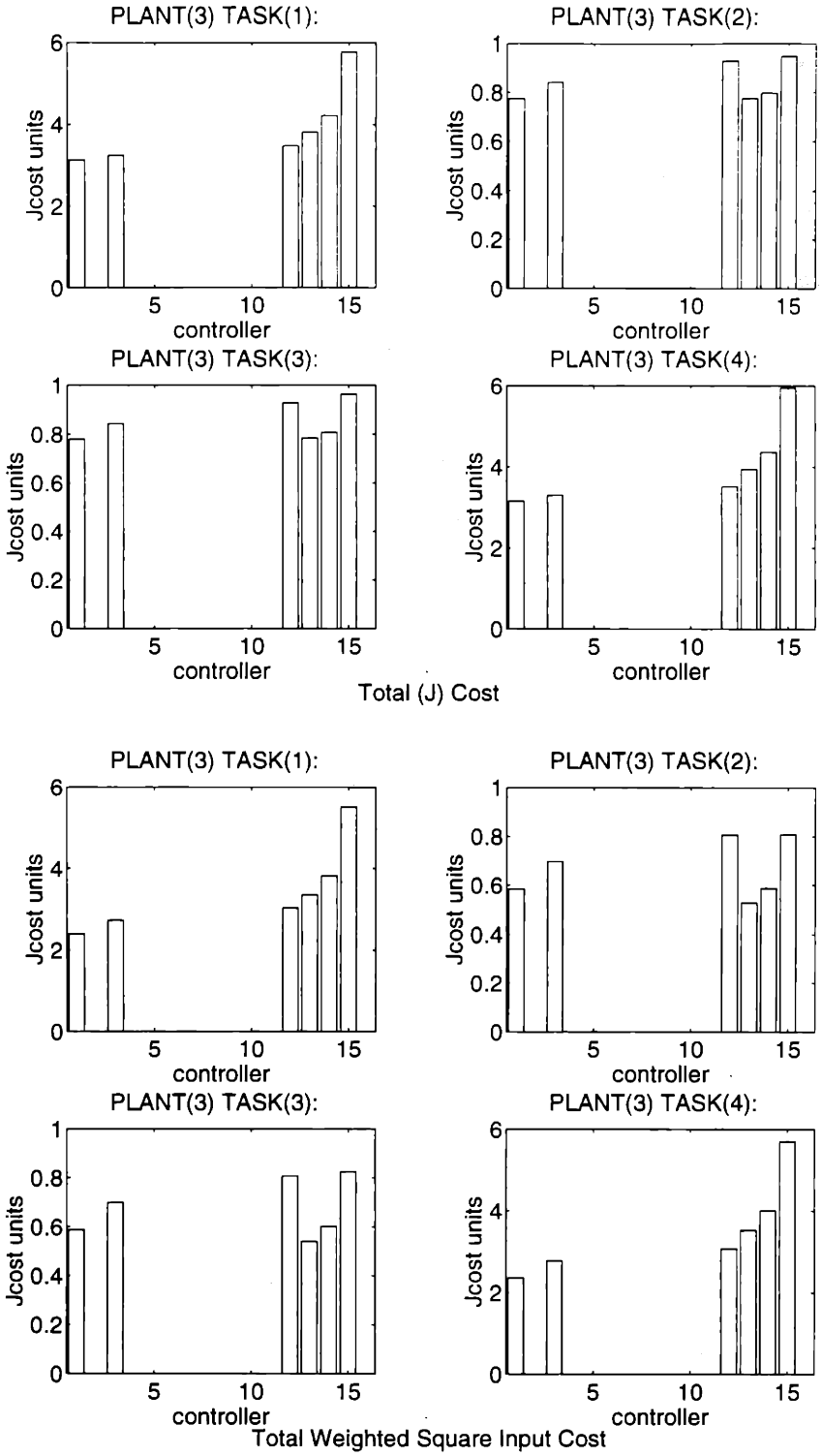

Figure 4-16: For PLANT(3) in regulation tasks: a)(top) $\hat{\mathcal{J}}$ b)(bottom) $\hat{\mathcal{J}}_u$

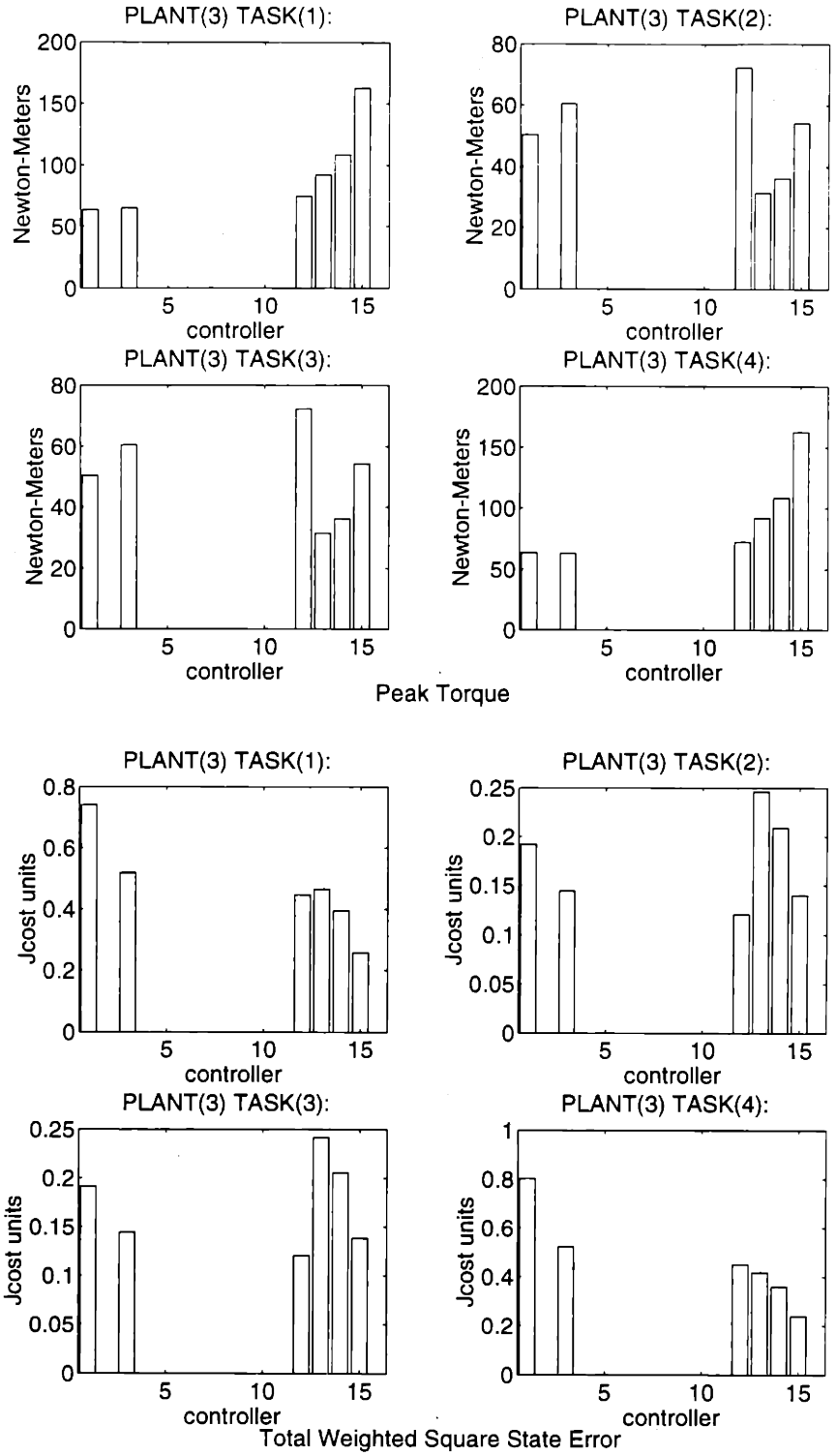

Figure 4-17: For PLANT(3) in regulation tasks: a)(top) τ_{max} b)(bottom) $\hat{\mathcal{J}}_q$.

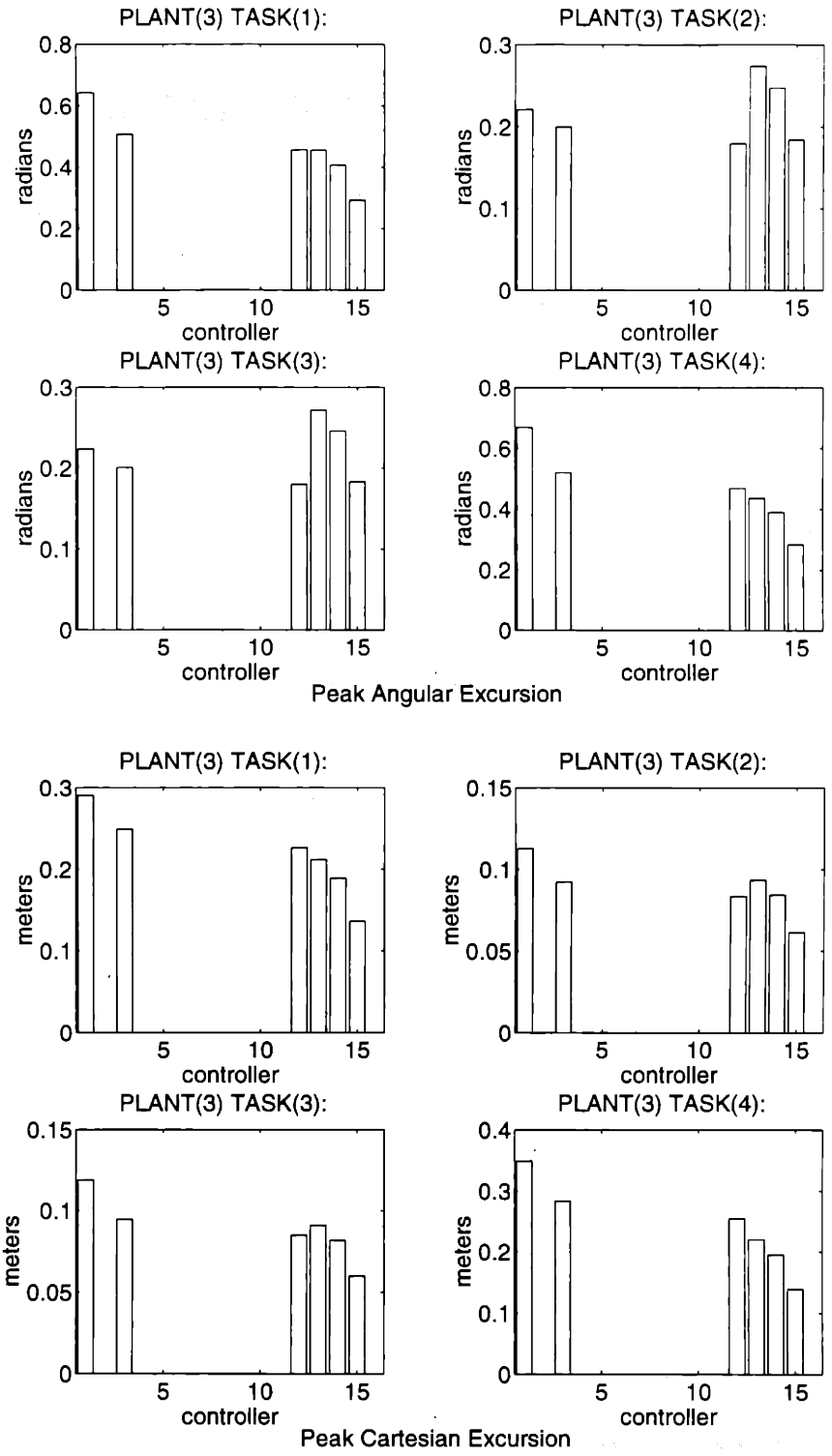

Figure 4-18: For PLANT(3) in regulation tasks: a)(top) $\tilde{\theta}_{max}$; b)(bottom) $\tilde{x}_{max}$.

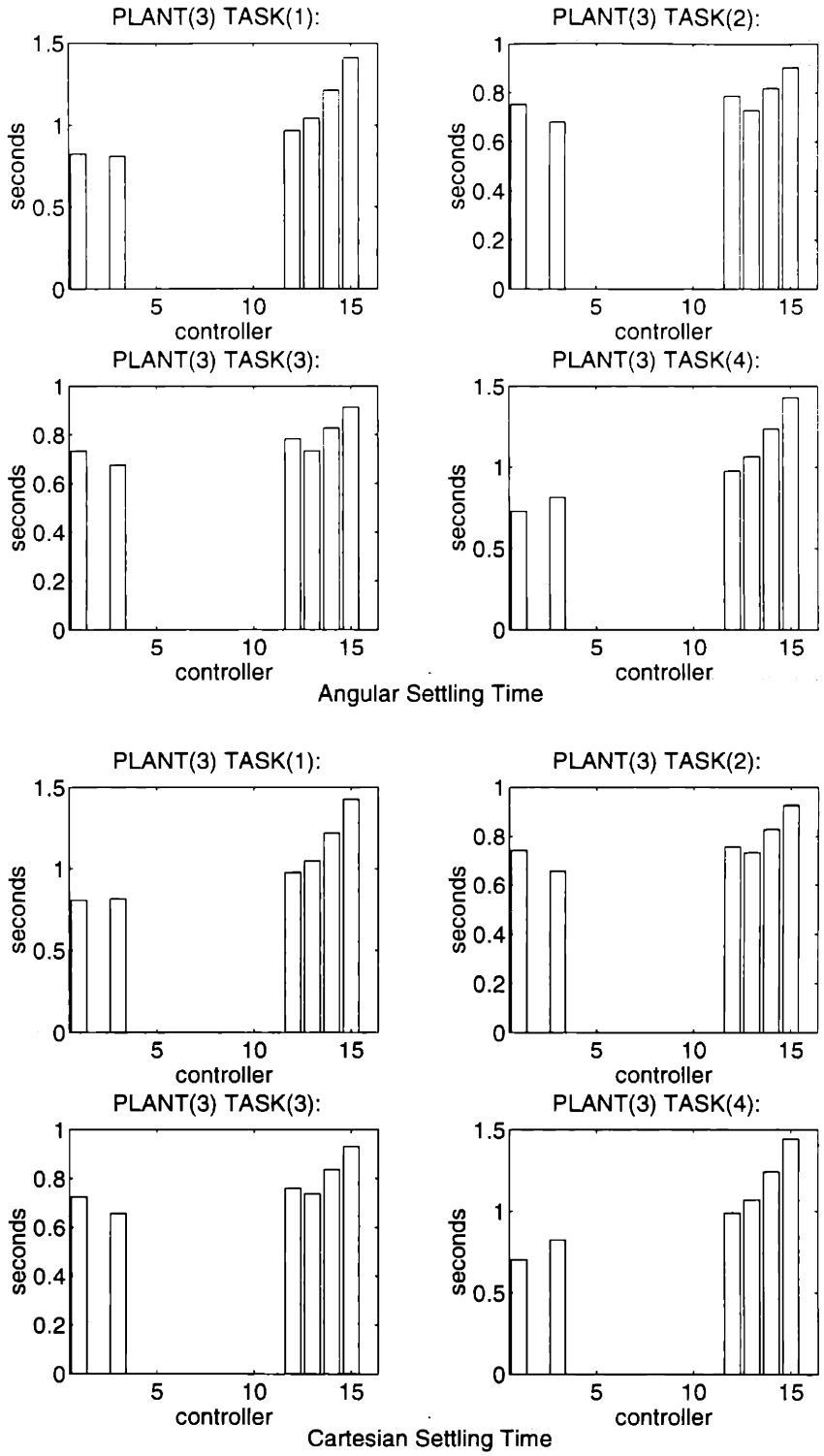

Figure 4-19: For PLANT(3) in regulation tasks: a)(top) σ_θ; b)(bottom) σ_x.

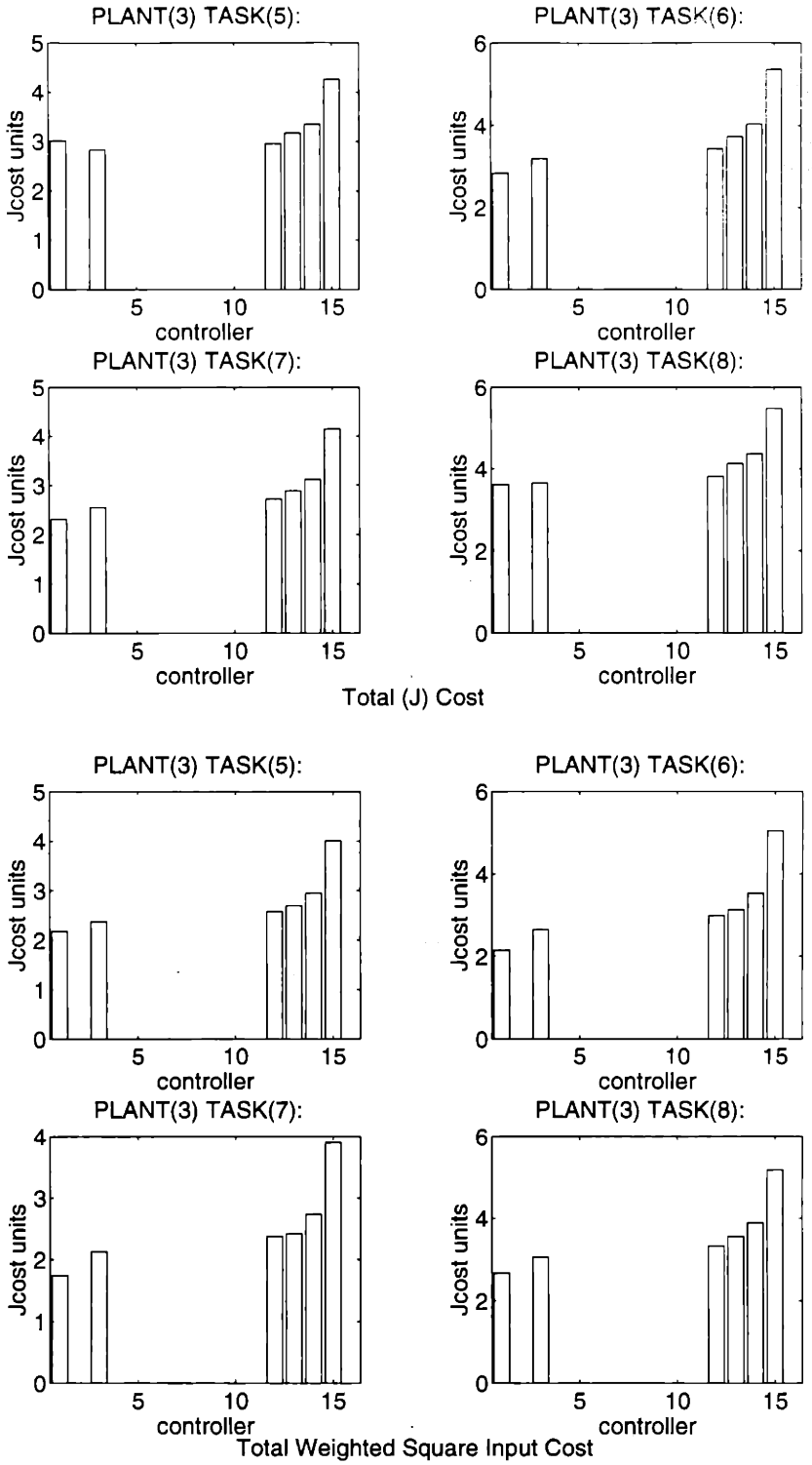

Figure 4-20: For PLANT(3) in tracking tasks: a)(top) $\hat{\mathcal{J}}$ b)(bottom) $\hat{\mathcal{J}}_u$.

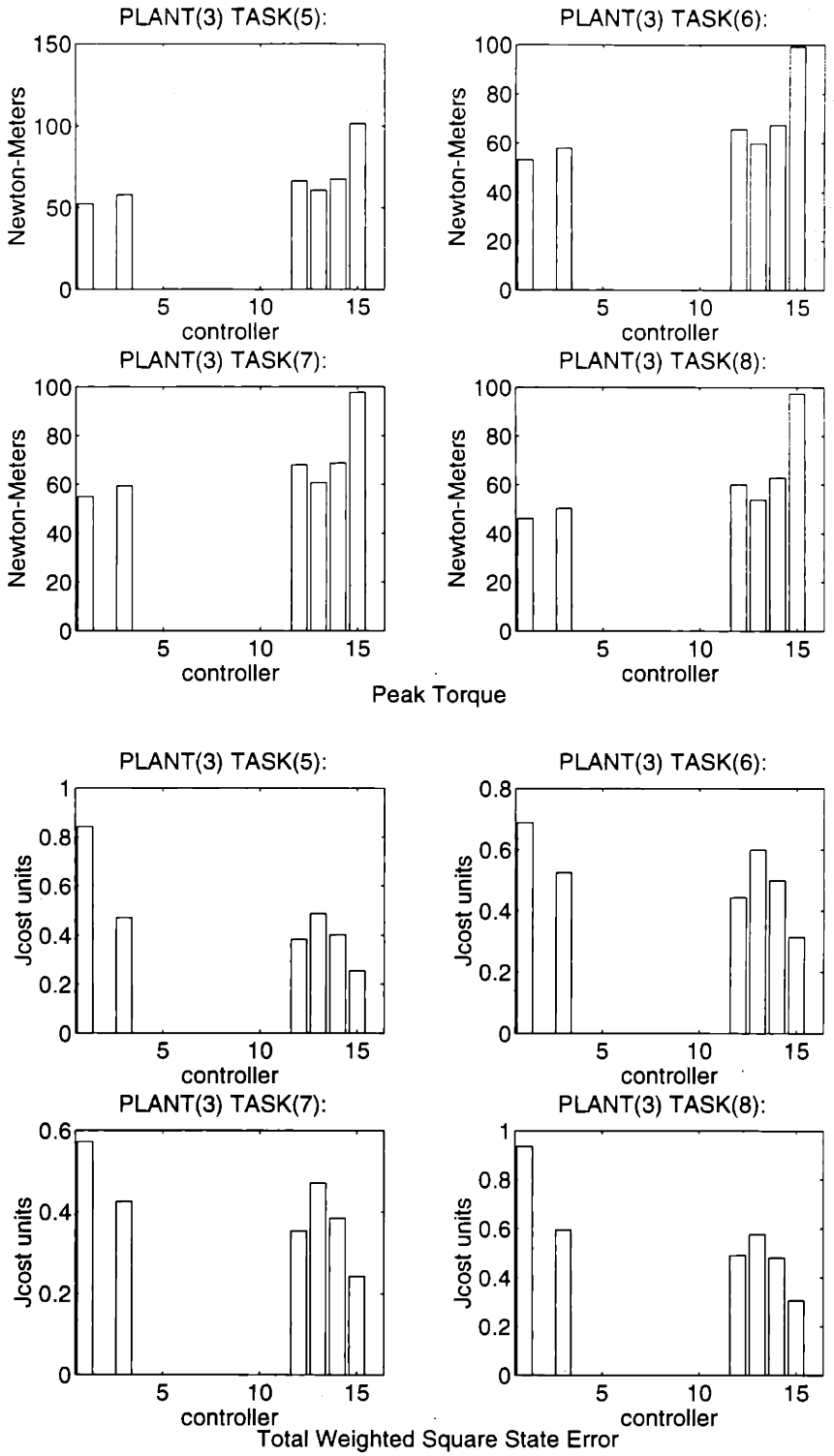

Figure 4-21: For PLANT(3) in tracking tasks: a)(top) τ_{max} b)(bottom) $\hat{\mathcal{J}}_q$.

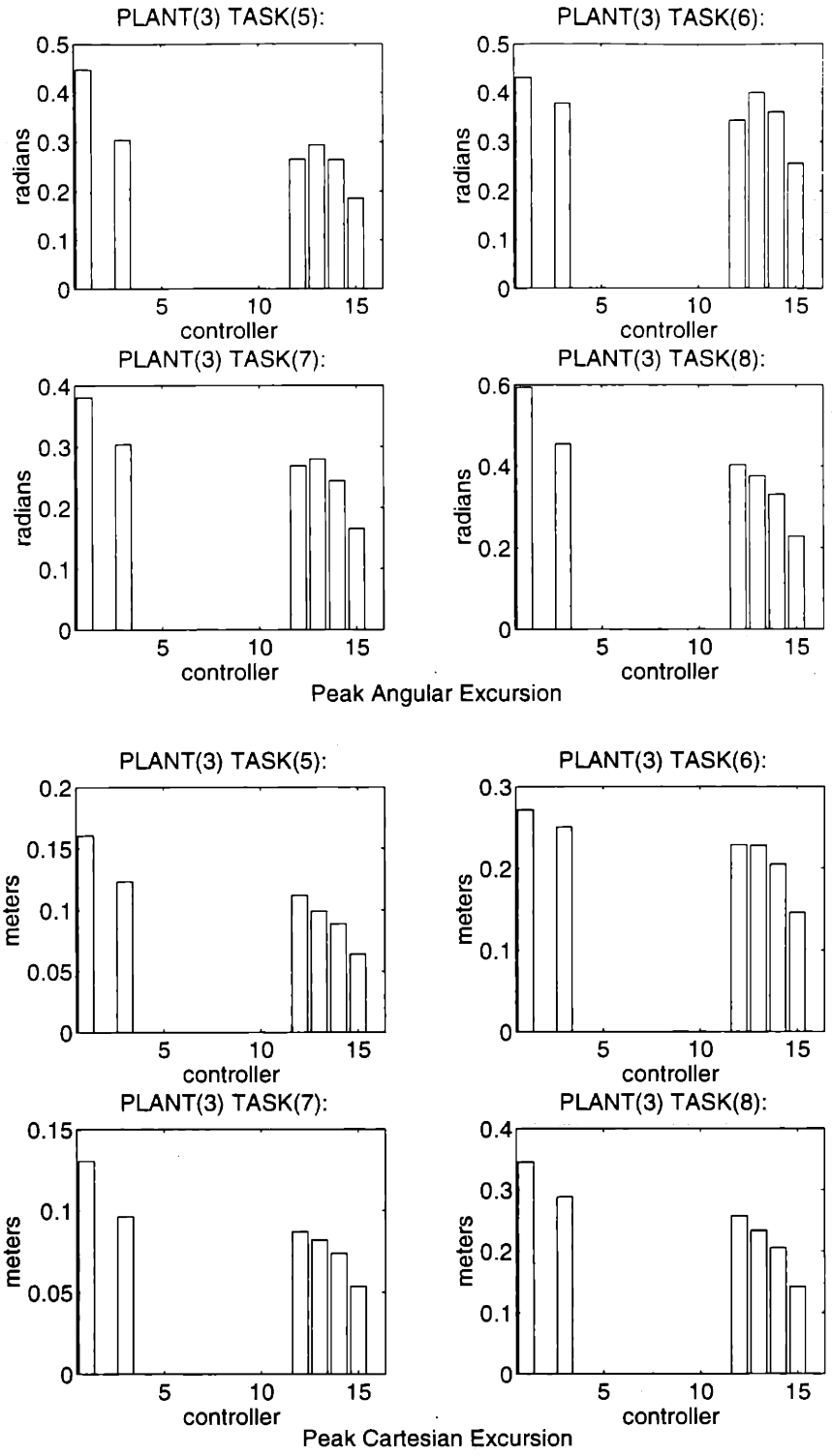

Figure 4-22: For PLANT(3) in tracking tasks: a)(top) $\tilde{\theta}_{max}$ b)(bottom) $\tilde{x}_{max}$.

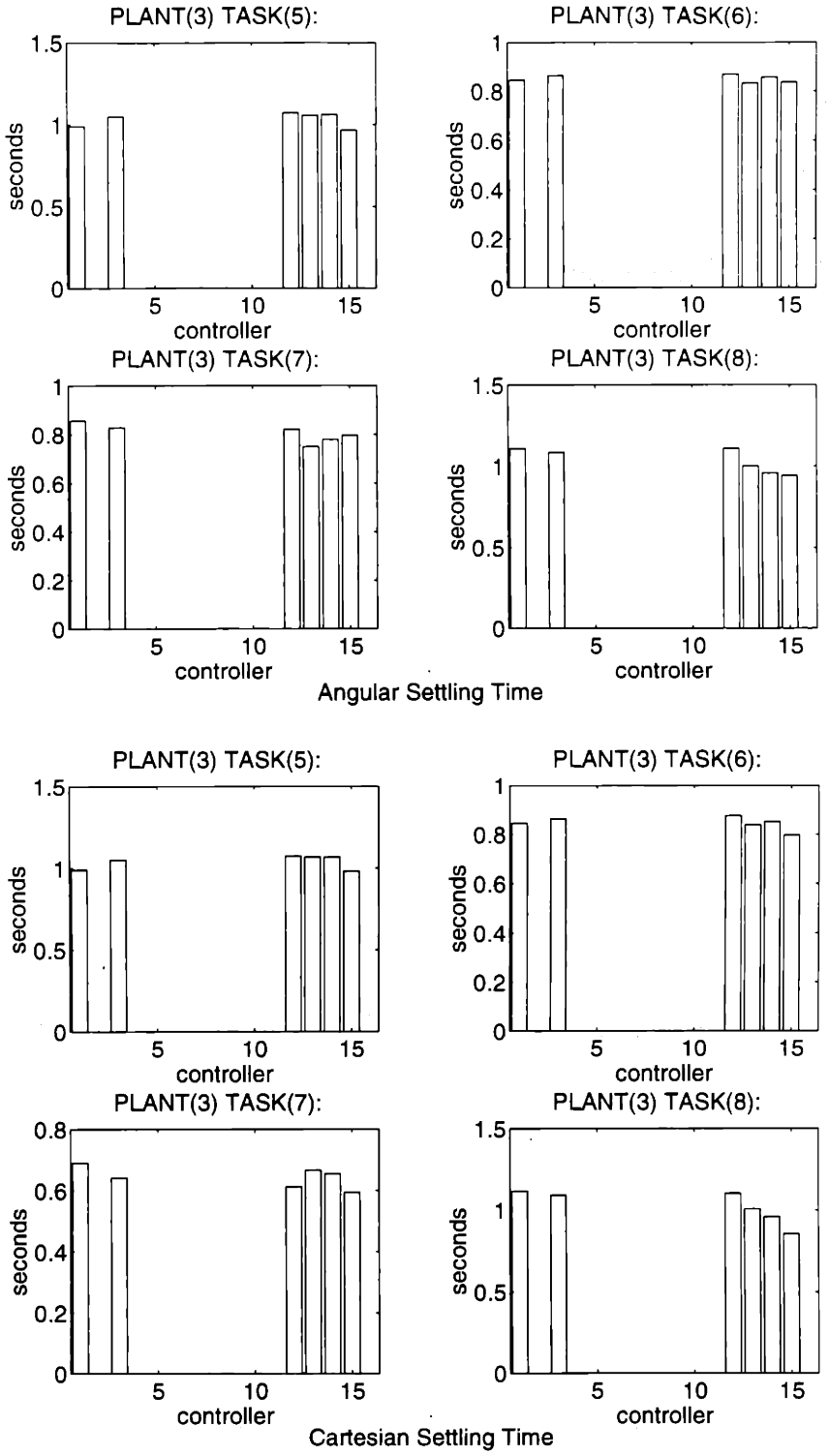

Figure 4-23: For PLANT(3) in tracking tasks: a)(top) σ_θ b)(bottom) σ_x.

with all tasks, not just two of the tasks as in the regulation case. Angular and cartesian settling times were also quite similar for PLANTS(1,3) for corresponding tasks. In the tracking tasks as a whole, CTLR(15) consistently outperformed the other controllers in terms of $\hat{\mathcal{J}}_q$, peak excursion and settling time (see Figs. 4-21-4-23).

The spatial trajectories for CTLRS_3(12,15) in TASK(5) are shown in Figure 4-36.

The effect of Clipping

The effect of actuator saturation for PLANT(3) was the same as that for PLANT(1), namely, that clipping had significance only for the regulation and not the tracking tasks wherein the peak torques required were lower. In TASKS(1,4), clipping increased $\hat{\mathcal{J}}_u$ and $\hat{\mathcal{J}}$ for CTLRS_3(14,15) in particular, and negated their performance advantage over the other controllers in terms of $\hat{\mathcal{J}}_q$ and peak excursions. It also increased these controllers' settling times relative to unclipped values. Other than these effects, the patterns of the clipped and unclipped controllers were quite similar and so the simulation results are not presented explicitly.

4.3 Dynamic Feedforward

The performances achieved with the FAM and RAM using dynamic feedforward ($\mathbf{u}_{dyn} \neq 0$) to linearize the feedback were almost identical in terms of $\hat{\mathcal{J}}$ (when the scaling factor of four is noted in the input cost measures) as assessed by TASK(5) (Fig 4-24). With both models, dynamic feedforward (FFTYPS(2-4)) utilized peak input torques which were in the range 120-160 N-m as compared with 35-90 N-m for simple reference trajectory feedforward (FFTYP(1)). As such, $\hat{\mathcal{J}}_u$ (not shown) and $\hat{\mathcal{J}}$ were larger with dynamic feedforward. But they differed significantly between (unclipped) controllers only for FFTYP(1).

Similarly, at least with PLANT(3), $\hat{\mathcal{J}}_q$ was almost independent of the controller designs used regardless of the feedforward type. On the other hand $\hat{\mathcal{J}}_q$ *does* differ by controller design when dynamic feedforward is used with PLANT(1), with CTLRS_1(3,4,12) always yielding less error than CTLRS_1(1,2) and CTLRS_1(7-11) intermediate. This effect became considerably less pronounced with FFTYP(4) as compared with FFTYPS(2,3) (Fig. 4-25). The magnitude of $\hat{\mathcal{J}}_q$ yielded by the *best* controllers for each plant were comparable for each type of feedforward. In terms of magnitude, FFTYPS(2,3) reduced $\hat{\mathcal{J}}_q$ by about 90% from

the value with FFTYP(1) for the best controllers. FFTYP(4) provided just slightly greater reduction.

Clipping, as associated with $CTLRS_1$(5,6) and $CTLR_3$(17) produced an increase in $\hat{J}_q$ by nearly a factor of three relative to the best controller's performance with FFTYPS(2-4). Though observable, the effect of clipping is much less marked with FFTYP(1).

The above remarks regarding $\hat{J}_q$ hold for $\tilde{\theta}_{max}$ and $\tilde{x}_{max}$ as well except that first, advancing FFTYP reduces peak excursion values by slightly different factors (Figs. 4-26 and 4-27). Examinining the best controller performances for each of PLANTS(1,3), FFTYPS(2,3) displayed a 30% to 50% reduction in $\tilde{\theta}_{max}$ and a 60%-70% reduction in $\tilde{x}_{max}$ relative to FFTYP(1). And FFTYP(4) produced a 75% to 85% reduction in $\tilde{\theta}_{max}$ and $\tilde{x}_{max}$. Second, clipping produces a four to five-fold as opposed to three-fold degradation in peak angular excursion with FFTYP(4).

Settling times tended to vary little across controllers regardles of plant or type of feedforward and the best controllers for each plant yielded comparable settling times for each type of feedforward: FFTYP(1) about 0.9 sec, FFTYPS(2,3) about 0.75 seconds and FFTYP(4) about 0.5 seconds (Figs. 4-28 and 4-29). Clipping produced increases in settling times of 25% to 40% in FFTYPS(2,3) and up to 100% with FFTYP(4). With FFTYP(1), however, clipping *reduced* settling time by about 15%.

A spatial trajectory of $CTLR_3$(15) in TASK(5) with FFTYP(3) is shown in Figure 4-37.

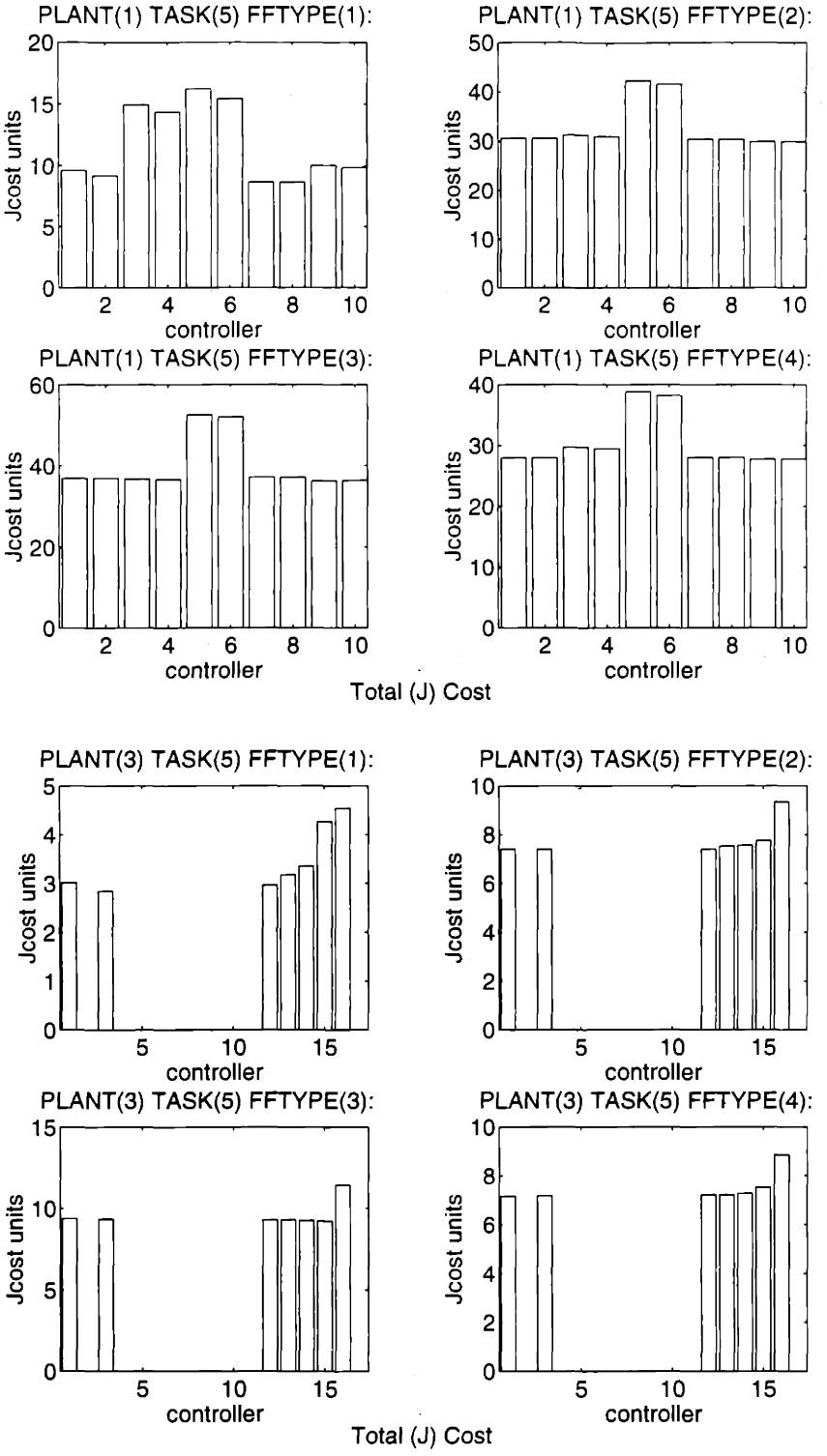

Figure 4-24: $\hat{\mathcal{J}}$ in tracking TASK(5) for various feedforward signals: a) with PLANT(1) b) with PLANT(3).

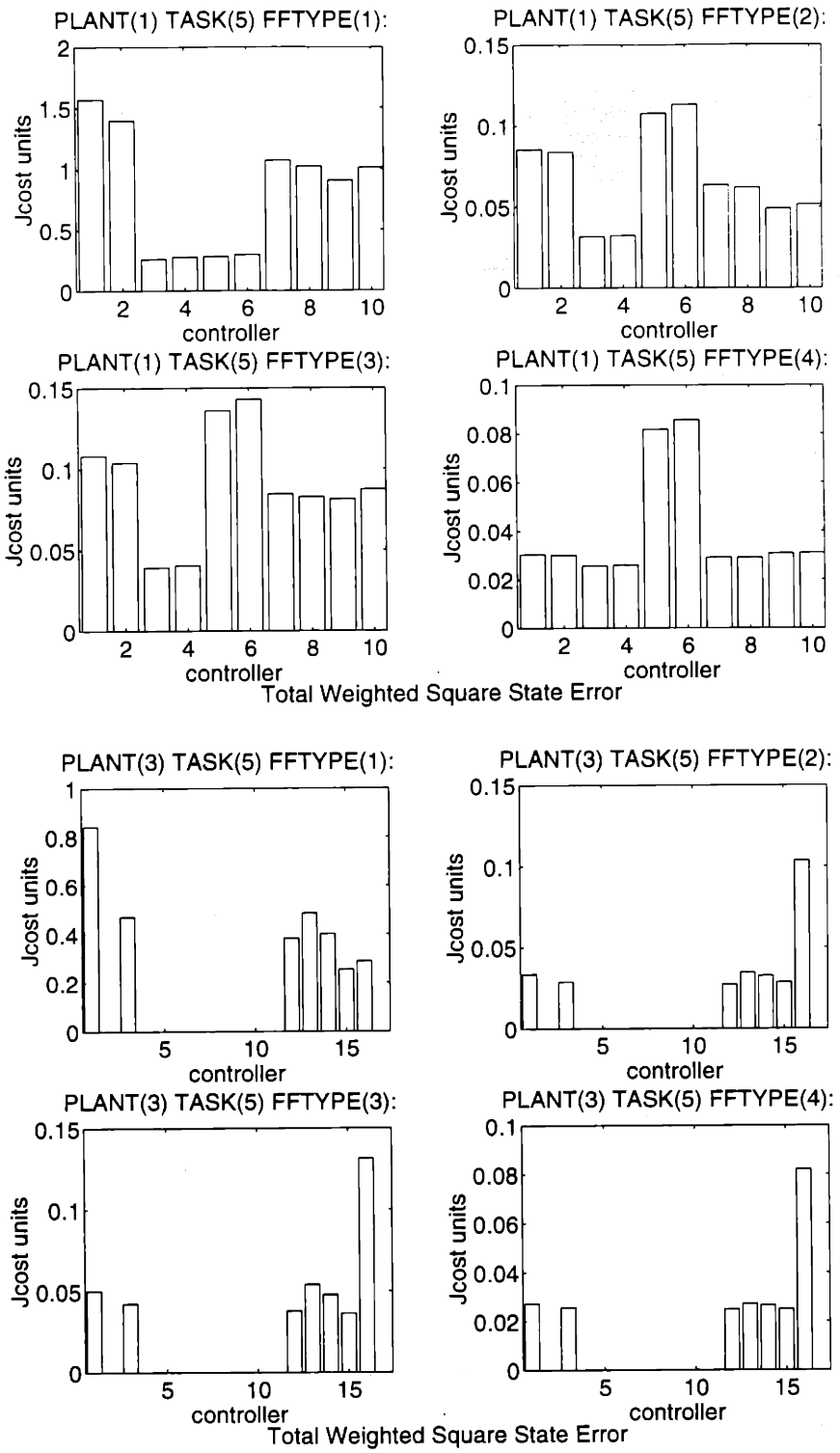

Figure 4-25: $\hat{\mathcal{J}}_q$ in TASK(5) for various feedforward singals: a)(top) with PLANT(1) b) (bottom) with PLANT(3).

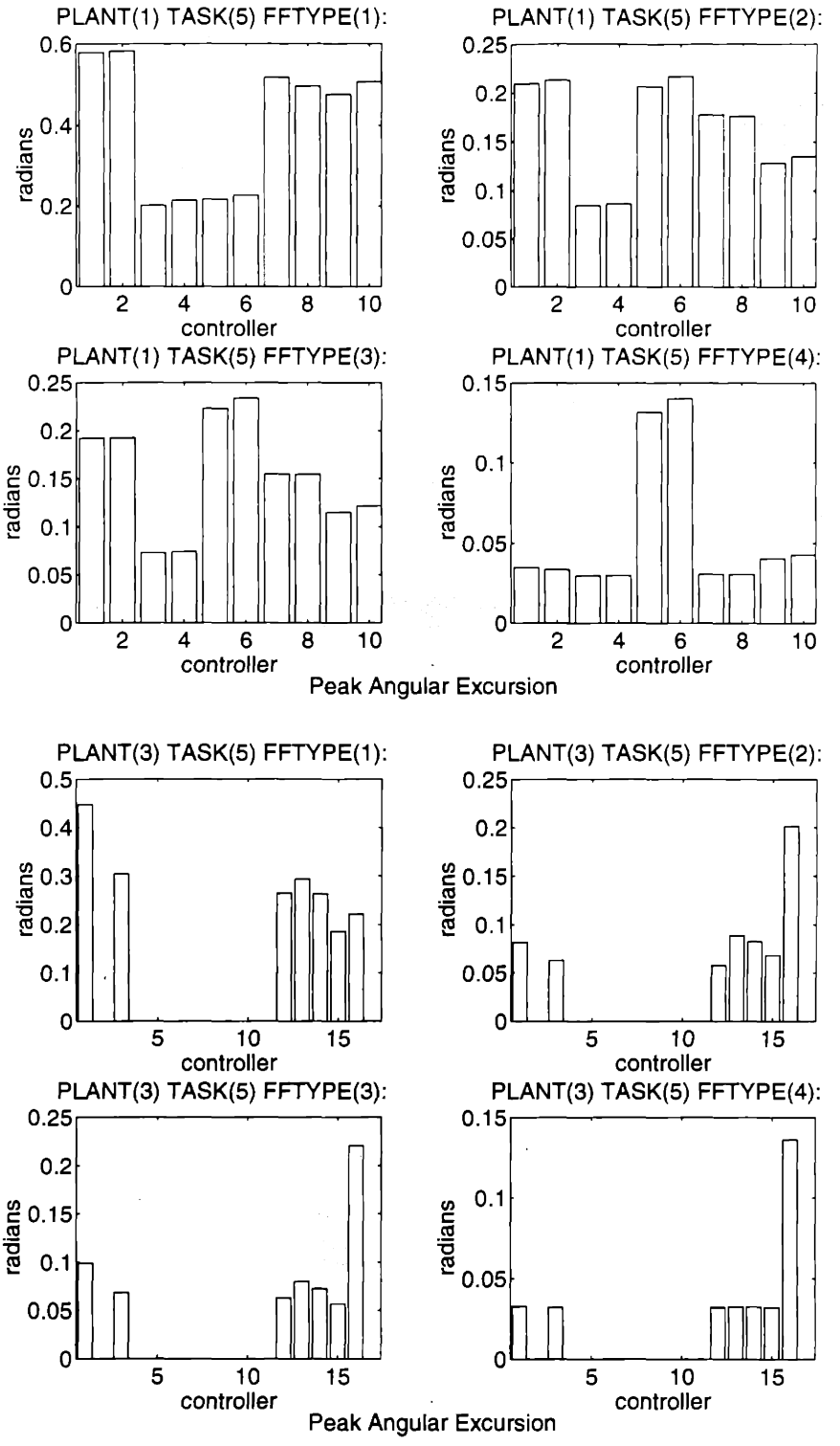

Figure 4-26: $\tilde{\theta}_{max}$ in TASK(5) for various feedforward singals: a)(top) with PLANT(1) b) (bottom) with PLANT(3).

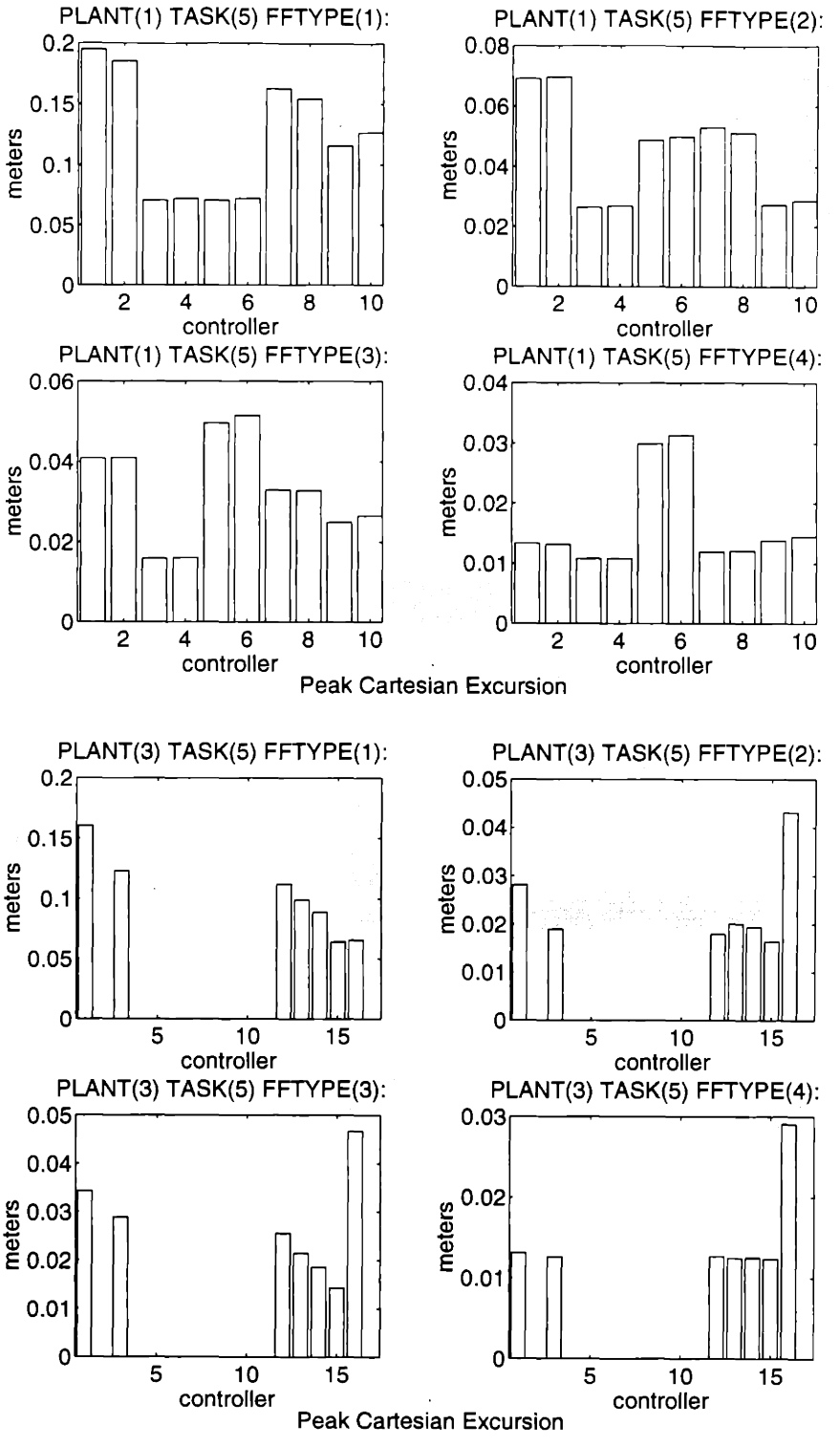

Figure 4-27: $\tilde{x}_{max}$ in TASK(5) for various feedforward singals: a)(top) with PLANT(1) b) (bottom) with PLANT(3).

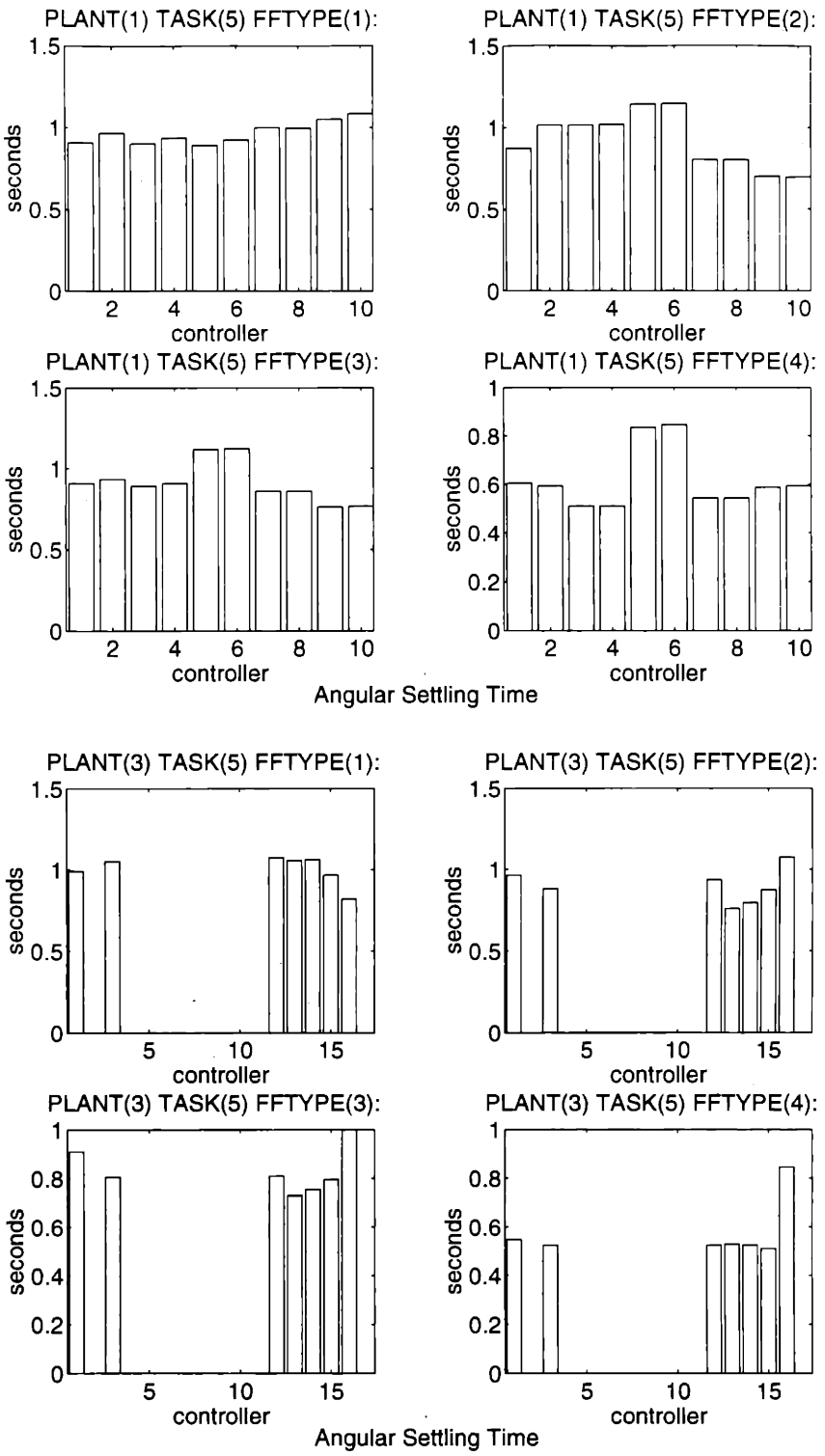

Figure 4-28: σ_θ in TASK(5) for various feedforward singals: a)(top) with PLANT(1) b) (bottom) with PLANT(3).

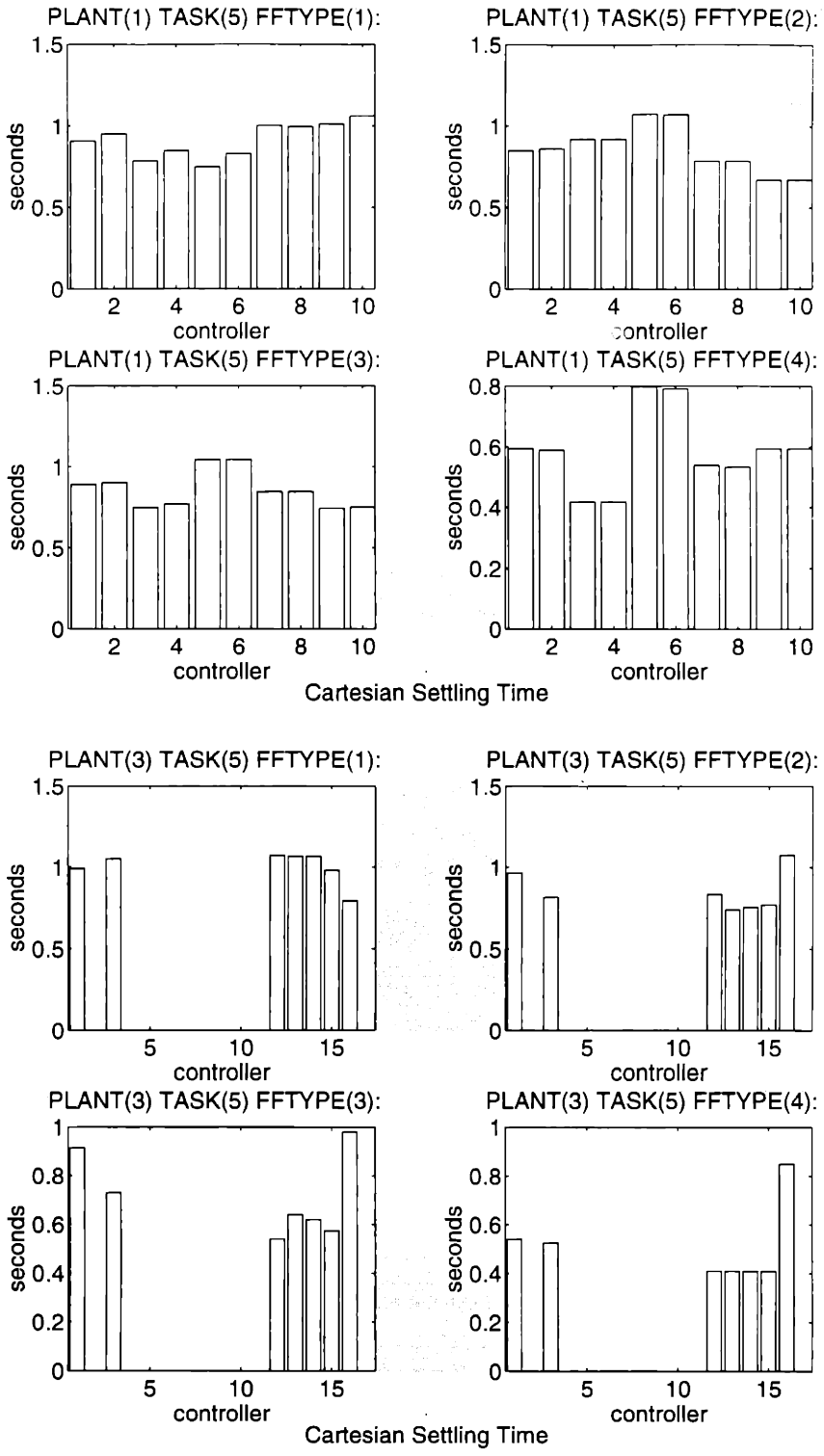

Figure 4-29: σ_x in TASK(5) for various feedforward singals: a)(top) with PLANT(1) b) (bottom) with PLANT(3).

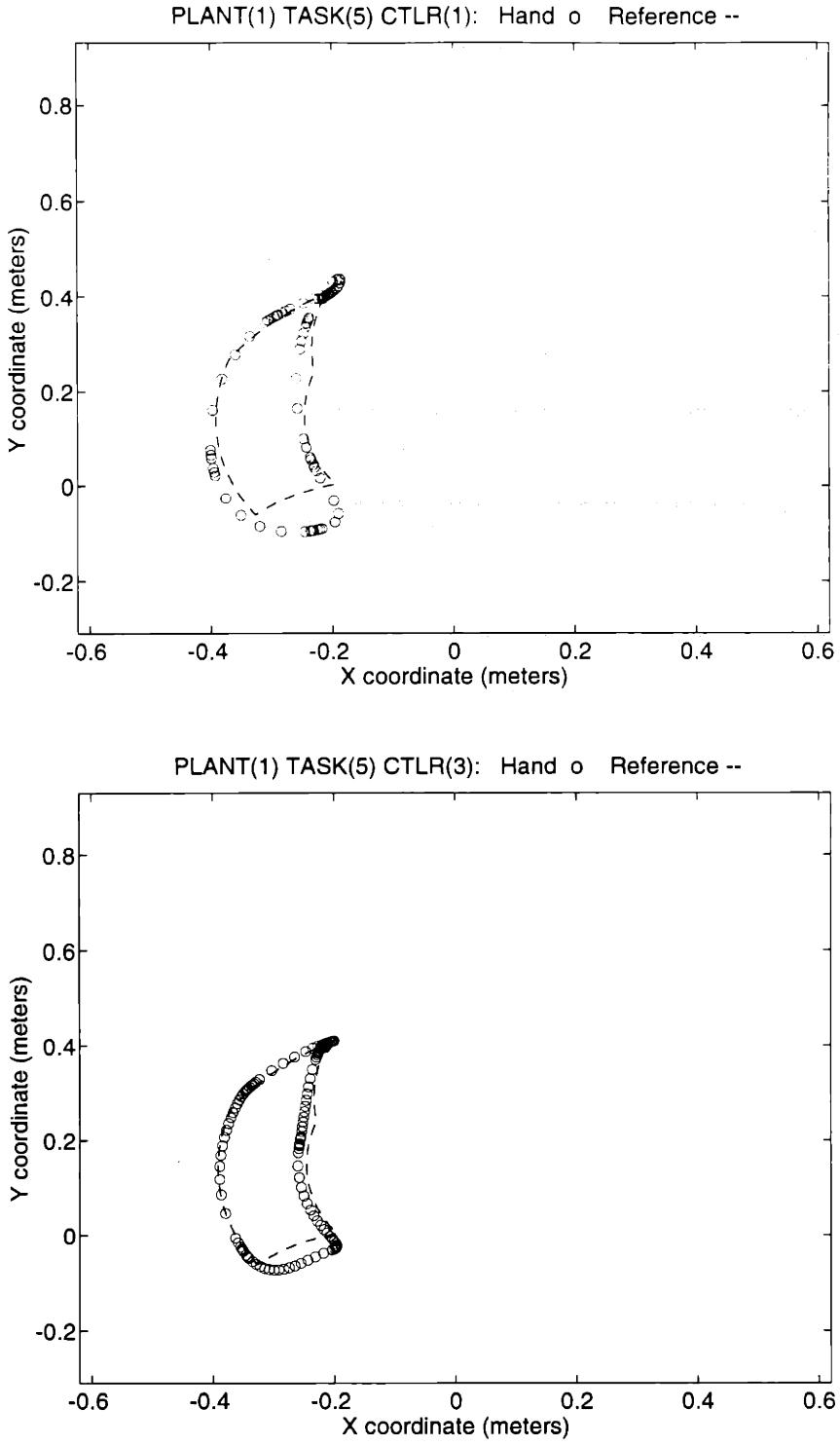

Figure 4-30: Tracking TASK(5) for PLANT(1).

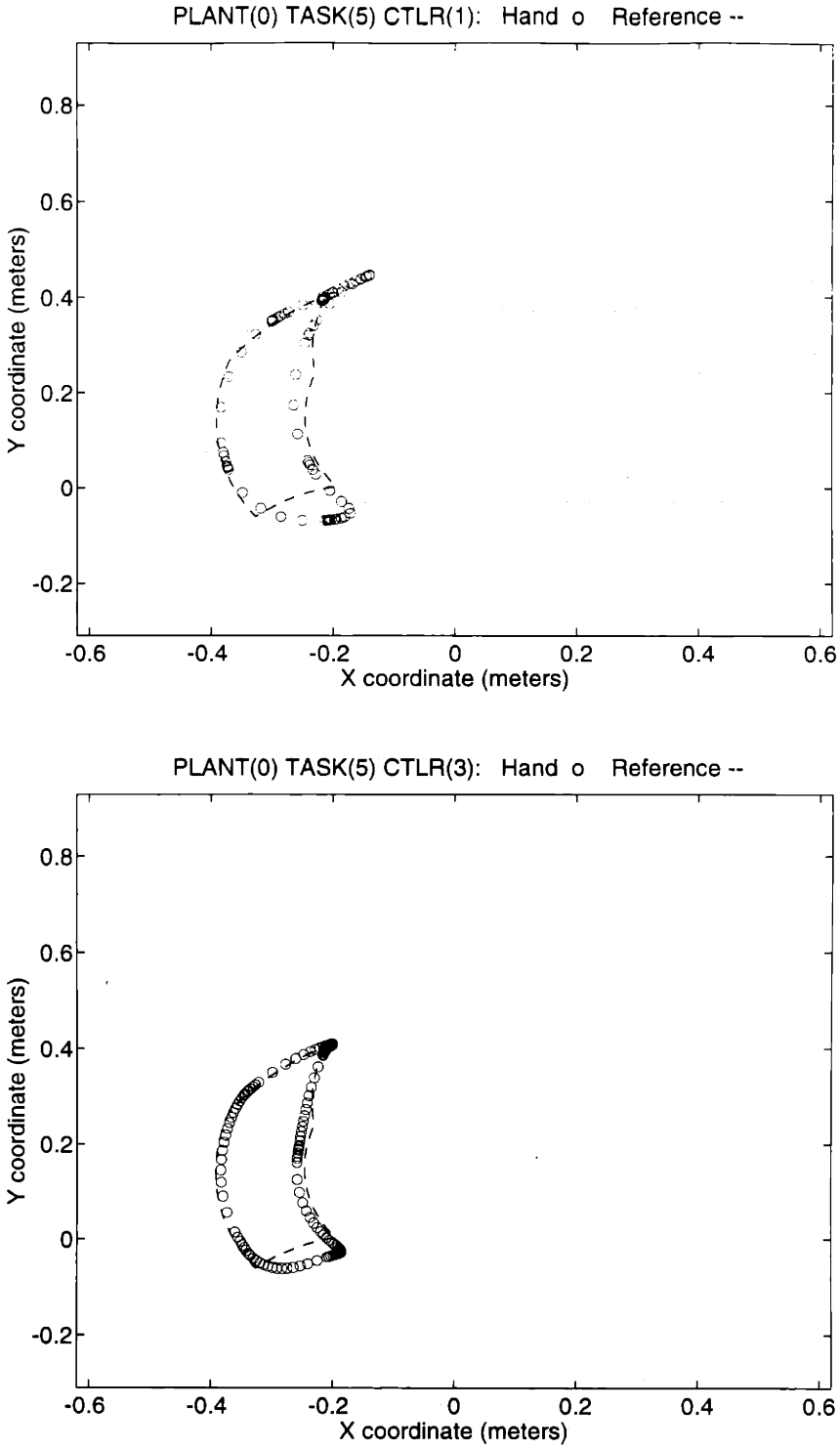

Figure 4-31: Tracking TASK(5) for PLANT(0).

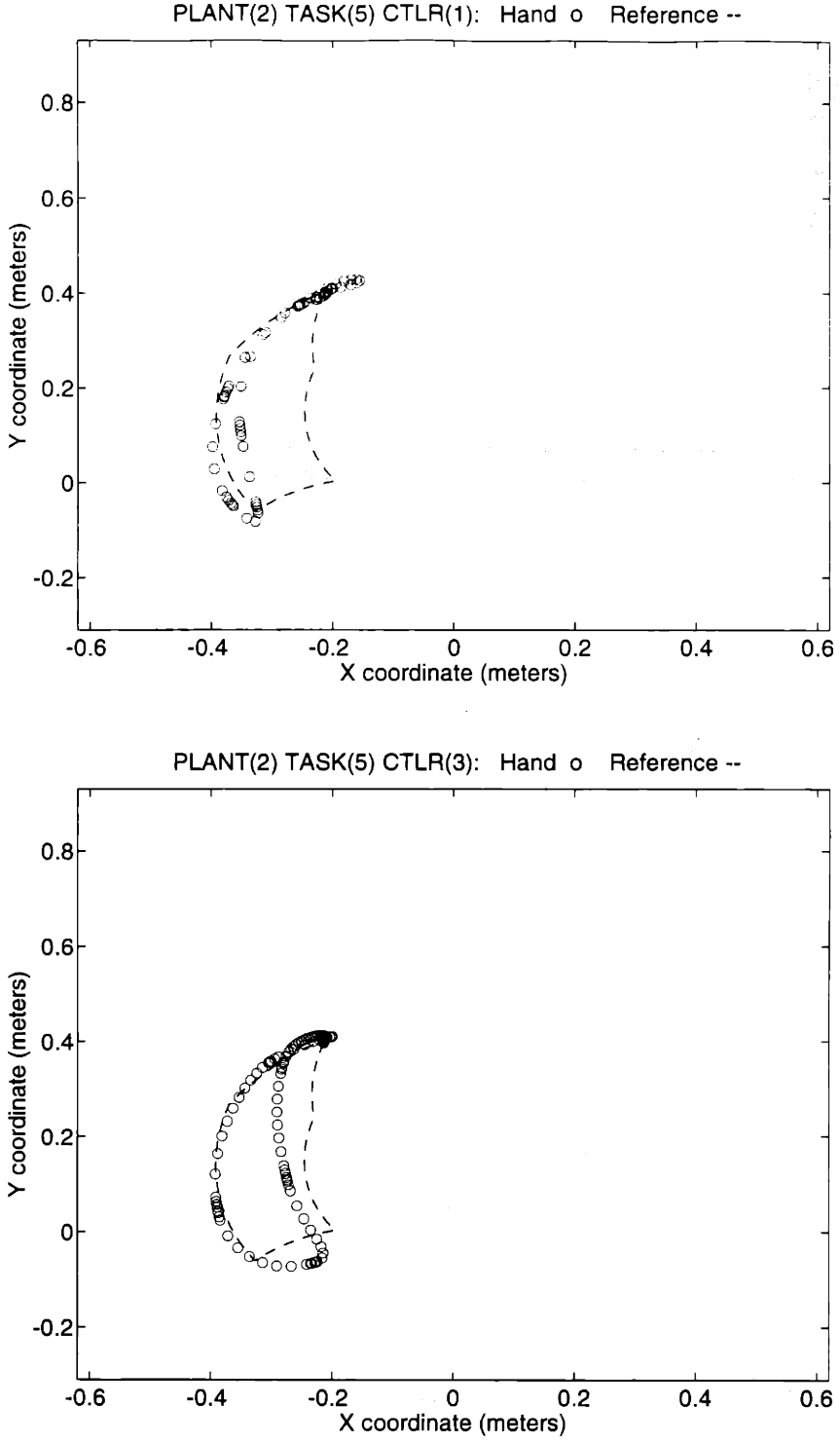

Figure 4-32: Tracking TASK(5) for PLANT(2).

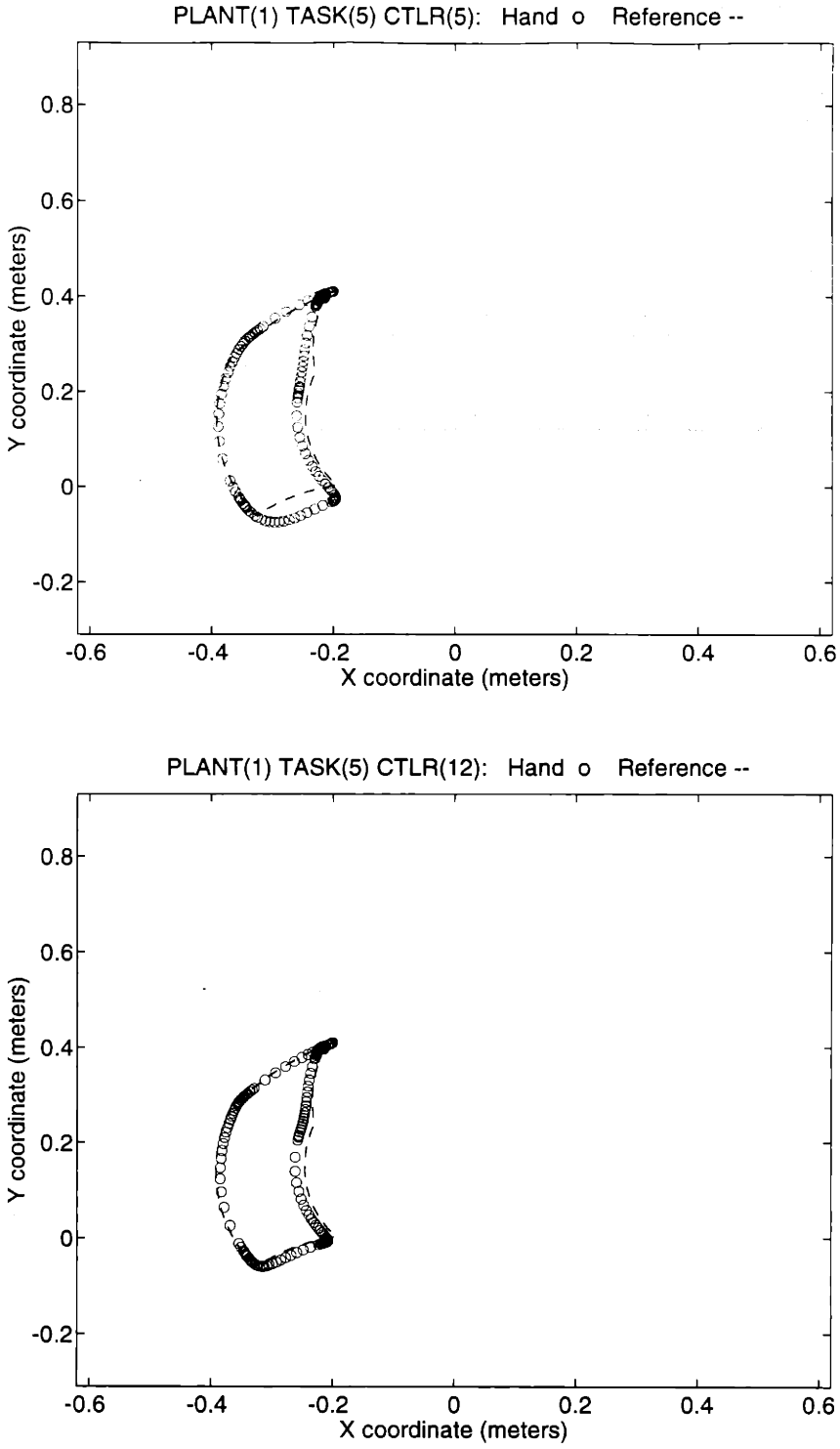

Figure 4-33: Tracking TASK(5) for PLANT(1).

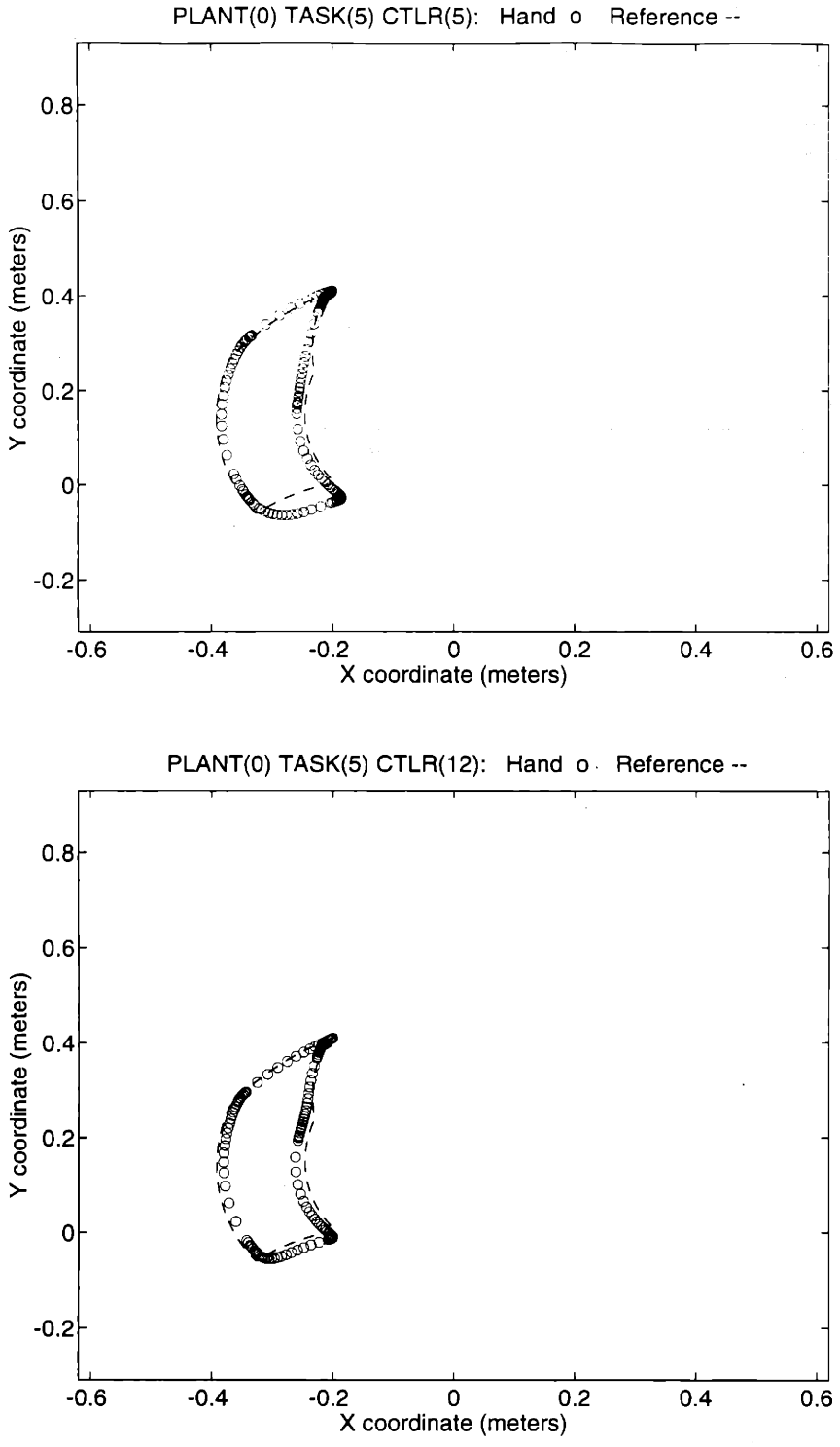

Figure 4-34: Tracking TASK(5) for PLANT(0).

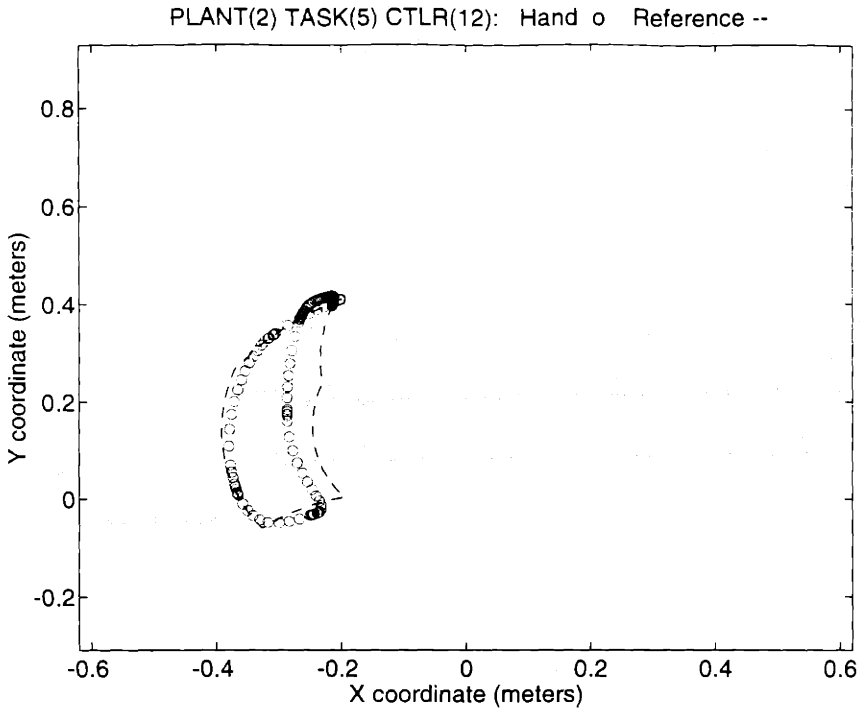

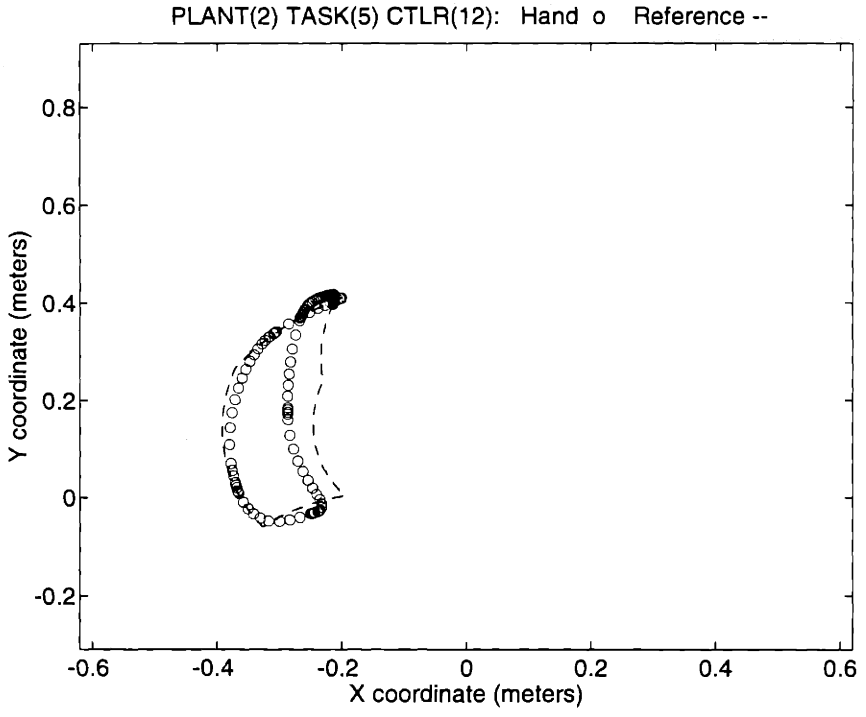

Figure 4-35: Tracking TASK(5) for PLANT(2)

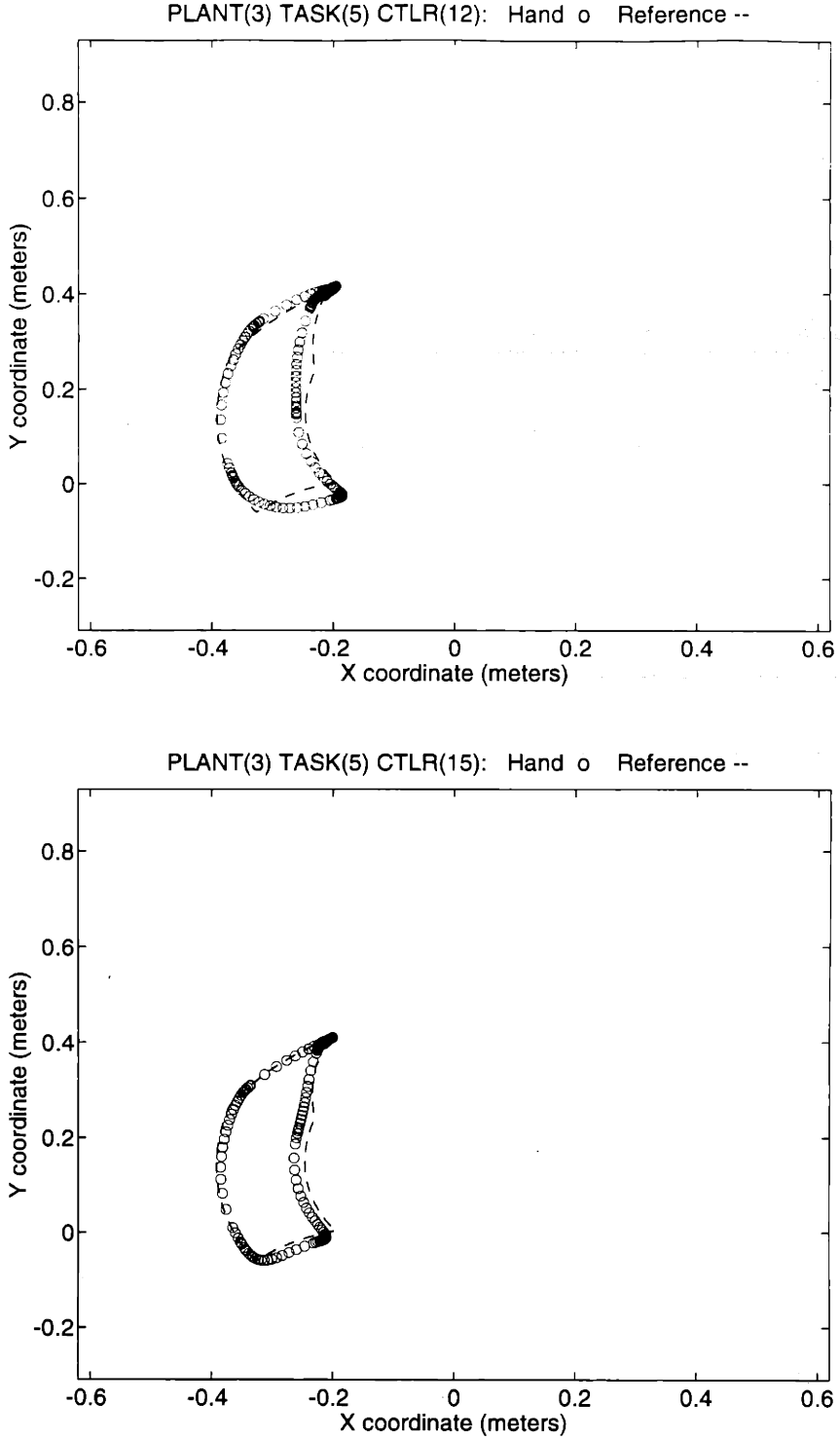

Figure 4-36: Tracking TASK(5) for PLANT(3) (with FFTYP(1)).

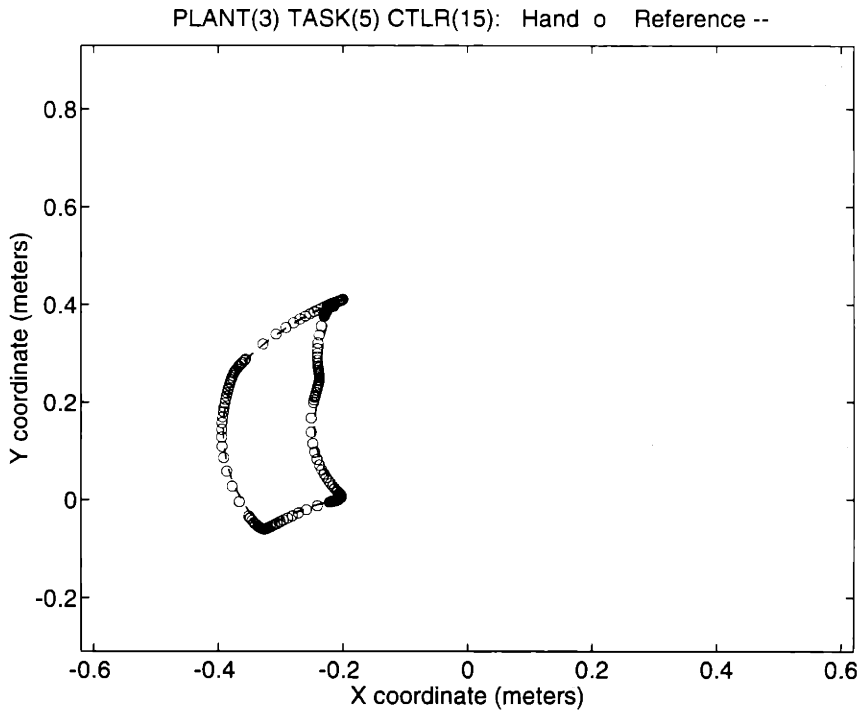

Figure 4-37: Tracking TASK(5) for PLANT(3) with FFTYP(3).

Chapter 5

Discussion

5.1 The Small Effect of Velocity-Space Gainscheduling

The FAM simulations verified the relatively small effect of gainscheduling across the two-dimensional angular velocity-space. This was most likely the result of two principal effects. First, the angular velocities encountered in these tasks, which were chosen to represent feasible movements by a human, are not *persistently* large. In the regulation TASKS(1,4) the *initial* angular velocities are 10 rad/sec. However, within 0.08 seconds, which was about 10% of the settling time, the values were on the order of 2 rad/sec. In the tracking tasks peak velocities of 5 rad/sec and for much of the movement the velocities are smaller. Thus, the system spends very little time using the high velocity controllers. Since the low-velocity controllers are very similar numerically to the non-gainscheduled controllers (identical, in the H_2 case), the similarity in the gainscheduled and non-gainscheduled results is not surprising.

Second, for some controllers, there is, moreover, comparatively little important difference between the high and low-velocity controllers. The small gainscheduling effects which *are* observed are due to differences in the magnitudes of the velocity feedback gains in the different controllers. This is because $\hat{\mathcal{J}}$ is dominated by $\hat{\mathcal{J}}_u$, which is, in turn, most heavily determined by the feedback response to the velocity error (since it tends to be much larger than the position error). Examination of the controller feedback gains (Table 3.6) reveals that, for example, $\text{CTLRS}_1(4_2, 4_3)$ have considerably smaller velocity feedback gains than do $\text{CTLRS}_1(4_1, 4_4)$. Correspondingly, gainscheduled $\text{CTLR}_1(4_i)$, in TASKS(2,3,5-8), which each include significant periods of equal and opposite angular velocities and thus utilize $\text{CTLRS}_1(4_2, 4_3)$, has reduced $\hat{\mathcal{J}}$. Conversely, increased $\hat{\mathcal{J}}$ occurs with $\text{CTLR}_1(4_i)$ in

TASKS(1,4) which utilize $\text{CTLRS}_1(4_1, 4_4)$ heavily because of significant periods of same-direction angular velocities. On the other hand, the velocity gains of $\text{CTLRS}_1(8_1, 8_2, 8_3, 8_4)$ do not differ nearly as much. As a result, gainscheduling involving $\text{CTLR}_1(8_i)$ produces no significant increase or decrease in $\hat{\mathcal{J}}$.

The small effects of velocity-space gainscheduling were not limited to $\hat{\mathcal{J}}$ (which the schemes were designed to optimize). For all other measures, as well, gainscheduling was not nearly as significant a variable as was controller design. These findings are of interest for they suggest that for the type of natural activities in which human's engage, velocity-space gainscheduling would not be an important feature of a feedback control system.

On the other hand, the variation in $\hat{\mathcal{J}}$ with task, with comparatively larger $\hat{\mathcal{J}}$ occuring in TASKS(1,4-6,8) where there are significant periods of extension of joint 2 (which increases moment of inertia matrix), suggests that gainscheduling across the the two-dimensional angular position-space may be useful, especially for tracking tasks which use a larger portion of the angular workspace. It is interesting that there may be a physiological substrate for this type of gainscheduling. Muscle sensors apparently provide position and velocity *error* signals. However, signals from joint receptors appear to provide information regarding absolute joint position. While this system is not felt to have high spatial resolution, it might be adequate for gainscheduling. Whether the system actually serves this purpose, however, is not known. On the other hand, that there does not appear to be a similar system for absolute velocity is perhaps consistent with the lack of value of velocity-space gainscheduling.

5.2 The Effect of Plant Variations

The overall consistency in the pattern of results across controllers for all four plants supports the generality of the findings with regard to controller design. These findings are discussed in detail in the next section.

In comparing the results with PLANTS(0,1) for any given controller, it is clear that for most tasks, the presence of nonlinearities reduces the performances of all controllers especially in terms of $\tilde{\theta}_{max}$, $\tilde{x}_{max}$, σ_θ and σ_x. However, the effects were not profound ($\leq 10\%$ and often $\leq 5\%$ difference). It is evident that especially the higher gain feedback controllers, as measured by ω_c, are quite effective in suppressing the effects of nonlinearities

associated with natrual arm movements. This is at least true for the unweighted arm. For the weighted arm, the presence of nonlinearities may be more significant. This remains to be evaluated.

In any case, the addition of distal weighting itself, however, clearly degrades performance significantly, often doubling the peak excursions. This is, of course, intimately related to the fact that CTLR(1) was always designed to produce "reasonable" levels of torque. Larger gains and hence larger torques would be necessary to provide comparably small errors with the more massive plant. Since the "reasonable" levels of torque were taken from average human male values, it is certainly possible that higher torque limits could be used to model the higher performance of athletic subjects. Since the average ω_c for the controllers for PLANT(2) were smaller than those for PLANT(1) by a factor of about 2.5, there remains considerable margin for increasing the controller or actuator gain before the effects of noise and/or unmodelled dynamics become significant.

As was discussed in section 3.3.3, however, other concerns may preclude the use of higher gains. In particular, although the results presented in the next section suggest that actuator saturation is not catastrophic with regard to control, it may not be tolerated physically, especially if high torque levels are long in duration. Thus, it may be necessary in practice for feedback gains to be up or down-regulated according to the loads present. In addition, examination of the gain element values for the CTLRS(1,3,5,7,9,10,11) in Table 3.7 shows that not only are the gain magnitudes increased for the less massive plant, but the values of r are decreased. That is, the less massive plant uses proportionately less velocity feedback.[1] $\text{CTLR}_1(12)$ presents an exception to this rule, and apparently the adverse consequence is prolonged settling times. These considerations suggest that feedback control should be adaptive. That the cerebellum is highly adaptive, then, is quite consistent with its hypothesized role as a feedback controller.

[1]Because the more massive plant was not tested as a reduced arm model (see section 5.3.2 below), it is not clear whether the use of off-diagonal gain elements is also more or less important with different plant loadings. Simulation with a loaded version of PLANT(3) could be used to elucdiate this issue.

5.3 The Significance of Controller Design

5.3.1 The Full Human Arm Model

H_∞ and H_2 designs

For most tasks and almost all measures, the different controller design schemes produced significantly different results. Very generally, among the controllers with nonzero off-diagonal gains, the H_∞ and g_{max2}-normalized H_2 designs were best at minimizing $\hat{\mathcal{J}}$ with either sometimes being a bit better depending on the task and plant, while the g_{max1}-normalized H_2 design incurred considerably higher $\hat{\mathcal{J}}$ and τ_{max}, but performed better with $\hat{\mathcal{J}}_q$ and the time-domain indices $\tilde{\theta}_{max}$, $\tilde{x}_{max}$, σ_θ and σ_x. Of note, the clipped g_{max1}-normalized H_2 designs frequently underperformed the unclipped versions, but still outperformed the other controllers in terms of the time domain indices. This was only untrue for TASKS(6,8) with PLANT(2).

That especially the gainscheduled H_∞ design did not consistently fare better than the g_{max2}-normalized H_2 in regulation tasks with PLANTS(1,2) may be due to several factors. First, as discussed in section 5.1, that the gainscheduling was not done across angular position-space as well as angular velocity-space. Second, the H_∞ and H_2 controllers were not exactly matched for ω_c. Although explicit normalization by ω_c was not done, $\text{CTLRS}_1(1,7)$ were quite close in terms of ω_c, at 323 and 314 rad., respectively. $\text{CTLRS}_2(1,7)$ also were close, at 122 and 125 respectively. Still, it is conceivable that even these differences were significant given the closeness of the H_∞ and H_2 performances.[2] Finally, it likely reflects the fundamental inability of the gainscheduling schemes to optimize cost for a nonlinear plant. In any case, relative to the performance of the g_{max1}-normalized H_2 controller, the H_∞ and g_{max2}-normalized H_2 designs are quite comparable in terms of total cost minimization.

The g_{max1}-normalized H_2 design had a ω_c values of 530, 189 and 539 for PLANTS(1-3), respectively, and were by this measure, "more powerful" than the H_∞ controllers with ω_c values of 323, 122 and 440, respectively. Therfore, the superiority of the former set of controllers in term of time-domain indices was not surprinsing. Normalization by maximal gain element size had this effect because the H_2 designs have a narrower range between the largest and smallest elements than did the H_∞ design. In particular, the H_∞ controller

[2] This could also account for the occasional small lack of relative optimality of the H_2 controller with PLANT(0).

places a larger gain emphasis on position feedback from joint 2 to joint 1. This can be understood in mechanical terms since in the "worst-case", joint angular velocities are maximal and positive.[3] In such circumstances, with the arm in the initial configuration used for these tasks, $\tilde{\theta}_2$ is predominantly positive while $\dot{\theta}_2^2$ and $\dot{\theta}_1\dot{\theta}_2$ are acting to increase the acceleration of joint 1. Moreover, since $\dot{\theta}_1^2$ is strongly decelerating joint 2, any secondary acceleration of joint 2 produced by braking action at joint 1 is minimized so long as $\dot{\theta}_1$ is large.

LPD designs

The results with CTLRS(9-12) indicate that the LPD designs subjected to the same normalizations generate a range of performances depending on the value of derivative to proportional control employed. With PLANT(1) in TASKS(1-4), when $r = r_1$, in $\text{CTLR}_1(8)$, $\hat{\mathcal{J}}$ was reduced to levels approaching, but not precisely equaling, the values incurred by the H_∞ and g_{max2}-normalized H_2 designs. In tracking tasks, however, the LPD controllers used were not as close. With PLANT(2), the H_∞ and H_2 designs were both more diagonal. So, trivially, their results matched those of the PD controllers much more closely.

To be sure, the further flexibility of allowing the diagonal elements within the proportional and derivative parts of the LPD controllers to be unequal was not employed. It is quite possible that use of these degrees of freedom would have enabled better performance, but systematic exploration of that flexibility was beyond the scope of this project. Extrapolating from the case of a linear plant, however (since most of the results with PLANT(1) followed those with PLANT(0) quite closely), we my suspect that whenever the H_∞ or H_2 solutions to a linearized nonlinear problem employ large off-diagonal gains, there will also be, in general, no diagonal solution which minimizes $\hat{\mathcal{J}}$ for the nonlinear plant. However, as discussed in section 2.2.2, minimization of $\hat{\mathcal{J}}$ it is not necessarily meaningful in practical human or robotic movement. Therefore, we pay particular attention to the other measures.

With regard to integrated state error and time-domain indices, LPD designs, as a group, were able to surpass H_∞ and H_2 designs in performance on all tasks despite the fact that the ω_c values for these controllers was not higher than that used by the g_{max1}-normalized LH_2 designs. It should be noted, however, that among the designs studied here, for any given

[3] This impression is supported by the slightly higher $\hat{\mathcal{J}}$ incurred in TASK(1) than in TASK(4).

LPD controller, superior reduction of peak excursion was usually associated with longer settling time, and vice versa. Still, among the fixed-gain type feedback controllers considered in this study, it can be concluded the diagonal designs displayed a greater performance range.

5.3.2 The Reduced Arm Model

That the diagonal designs exhibited greater performance range in several measures in the FAM does not, of course, imply that local joint control is superior to global multijoint control. Since any FAM controller operates through the stiffness matrix K which is non-diagonal because of the biarticular muscles, unless G is of the form: $[(K^{-1}K_{d1}-I)\ K^{-1}K_{d2}]$, where K_{di} are arbitrary diagonal matrices, the effective feedback to the joints, as represented by $G_\tau = K([I_2\ 0]+G)$ will not be local. Indeed, inspection of G_τ in Table 3.7 indicates that because of the biarticular actuators, none of the controllers was effectively exerting local control. Since the RAM does not have biarticular actuators, any interjoint control must be generated by the controller directly.

Simulations with PLANT(3) indicate that, at least in the cases of regulation or simple reference trajectory feedforward tracking tasks (FFTYPS(0,1)), global MIMO control exerted by $\text{CTLR}_3(15)$ is superior to the local control exerted by $\text{CTLR}_3(12)$ with respect to $\hat{\mathcal{J}}_q$ and peak excursion measures in almost all tasks. The improvement is freqently on the order of 20%-30%. Settling time was typically poorer with the global controllers in regulation tasks; however, it was better in tracking tasks. The exceptional cases are TASKS(2,3) in which $\text{CTLR}_3(12)$ was superior to $\text{CTLR}_3(15)$ in terms of $\hat{\mathcal{J}}_q$, $\tilde{\theta}_{max}$ and σ_θ. It is important to note, however, that the performance difference between $\text{CTLRS}_3(12,15)$ in this situation is small in relative terms (<5%) (except with settling time prolongation) and extremely small in absolute terms since TASKS(2,3) produce considerably smaller $\hat{\mathcal{J}}_q$ and $\tilde{\theta}_{max}$ and peak angular excursion values than do TASKS(1,4).

The results for CTLR(14), which represents the simple addition of off-diagonal elements to $\text{CTLR}_3(12)$ were often superior to those with $\text{CTLR}_3(12)$, but not as consistently nor by as large a margin. In TASKS(2,3), $\text{CTLR}_3(14)$ performed significantly more poorly than both $\text{CTLRS}_3(12,15)$. Thus, the addition of interjoint feedback control is not in of itself advantageous for all tasks. And, in fact in the particular case of equal and opposite initial angular velocities may be slightly disadvantageous. This can again be understood in mechanical terms since the value of the off-diagonal gain elements is to counteract reaction

movements at a second joint resulting from feedback correction of errors at the first joint. In the case where movements are equal and opposite, reaction forces are beneficial and thus performance deteriorates slightly when they are reduced.

However, the second and major effect of the addition of interjoint control in the manner done here, was the simultaneous decrease in ω_c. This allowed the overall gain of the controller to be rescaled upward without exceeding allowable crossover frequency limits. Hence, a performance improvement can be obtained which applies to all tasks.

A third effect seen here, is a moderate reduction in intrinisic stability as indicated by increasing settling time in regulation tasks. Interestingly, the overall settling time in tracking tasks is *reduced* with addition of interjoint control. This is apparently because σ_θ and σ_x are times until settling to a fixed threshold, and not to a certain small fraction of peak excursion. Hence, by these measures, settling time may be reduced if peak excursions are minimized strongly enough, as appears to occur with tracking tasks.

Finally, it is interesting that interjoint control generally assists in minimizing $\tilde{x}_{max}$ more effectively than it does $\tilde{\theta}_{max}$. This is presumably because interjoint control is particularly effective at improving stabilization when angular errors are in the same direction (e.g. TASKS(1,4)) and therefore would generate the largest Cartesion errors. Thus, analogously to improvement afforded by interjoint actuators to end-effector stiffness uniformity described by Hogan [11], interjoint position and velocity control, preferentially assists end-effector stabilization. Presumably, if *integrated* Cartesian position error had been measured, it would have been improved here even more dramatically than integrated state (angular) error. This conjecture, however, must still be verified.

5.4 Variations in the Feedforward Signal

While the variations in the feedforward signals were not extensive, the results were clear and were not surprising. Simply put, in conjunction with effective feedback controllers, the more complete the feedforward signals in terms of representing the plant dynamics, the better the performance. Accordingly, when the feedforward signal is crude, as with FFTYP(1), the structure of the feedforward controller is much more significant than when the feedforward signal is extremely accurate, as with FFTYP(4). Still, $\text{CTLR}_3(15)$ is equal or better than $\text{CTLR}_3(12)$ in all measures except $\tilde{\theta}_{max}$ with FFTYP(2), and σ_x with FFTYP(3), where

$CTLR_3(15)$ slightly underperformed $CTLR_3(12)$.

It is also noteworthy that using $CTLR_3(15)$, the error reduction using FFTYP(2) was typically at least 90% as effective as with FFTYPS(3,4). This means that for natural arm movements, there is relatively little additional benefit provided by taking nonlinearities into account in the feedforward signal. If this observation holds for other tasks and plants, it would raise the consideration that the nervous system may not use feedback linearization to explicitly cancel nonlinear terms. It is conceiveable that a reference trajectory, together with a crude dynamic feedforward signal which takes only inertia into account may be sufficient for satifactorily high performance in the presence of good feedback control.

To be sure, a much larger number of tasks and feedforward signal variants must be examined to clarify the full importance of feedback controller design in feedback linearization schemes. Nevertheless, there does not appear to be any significant disadvantage in using global controllers, and there is likely to be considerable advantage when misestimation of plant dynamics is severe.

That actuator saturation may severely compromize the performance advantages gained by interjoint control and of feedforward control is not surprising since these both typically demand higher torque levels. Just the same, the presence of clipping at 65 N-mwas not sufficient to result in instability. This study did not examine which of the controller types is more advantageous in the presence of actuator saturation, but this question is an interesting and important one.

Chapter 6

Conclusion

6.1 Summary of Findings

In this project a number of simplifying assumptions were made about the structure and physiology of human arm control. Specifically, these were that 1) The brain, including the cerebellum generates muscle force commands consisting of a reference trajectory, a feedforward dynamic compensation signal and state feedback. 2) Signal transmission delays are adequately compensated for by the cerebellum or other motor control circuitry. 3) The ascending output of the plant consists of linear combinations of joint angle and angular velocity error signals. 4) The S-mCBLM functions as a linear feedback controller. A selected group of linear control schemes was then evaluated in terms of its performance in controlling two arm models one of which included interjoint actuators and the other without. These controllers were used with and without different types of feedforward signals. This was done for both postural maintenance (regulation) and trajectory formation (tracking) tasks.

With regard to the central questions of the investigation, it was determined that all of the design procedures did produce controllers for the nonlinear plant which were stabilizing at least within the region of the state space tested. Next, it was demonstrated that, although the study was in no way exhaustive, variations in performance with controller design which were broadly consistent across tasks and plants. The specific findings were as follows.

First, it appears that angular velocity-space gainscheduling of the feedback controller is not a consistently valuable control strategy. Gainscheduling across angular position was not evaluated though given the large variation in arm inertia matrix associated with large movements, coarse angular position-space gainscheduling may have utility.

Consistent with the first observation is that within the range of angular velocities and arm configurations studied, the presence of plant nonlinearities did not have major effects on closed loop performance of the non-gainscheduled controllers, especially those with high gain as measured by closed-loop crossover frequency. However, varying the limb segment mechanical parameters, specifically increasing the mass and effective length of the second arm link did markedly affect performance. The H_∞ and H_2 controllers with similar ω_c were quite similar in effectiveness at reducing $\hat{\mathcal{J}}$ and were generally superior to the other designs in this regard. The LPD controllers yielded a range of cost values, but none was found to match the performance of the H_∞ or H_2 designs. Although not specifically demonstrated here, it can be argued that interjoint feedback gains will typically be required to optimize integrated total cost.

Third, and quite importantly, if controller gain is normalized by closed-loop crossover frequency and performance is assessed in terms of minimizing integrated state error and peak excursion values, then the incorporation of interjoint feedback was shown to provide superior controller performance.

Interjoint control need not be generated by the controller itself, however. In the presence of interjoint actuators, a set of controllers each of which processes local feedback information and, in turn, apportion the local feedback to the various actuators in a fixed ratio, may effectively provide high performance global control. Thus, this work does not yet imply that the S-mCBLM, which is hypothesized to be a feedback controller, needs to be inherently global in its processing. On the other hand, the tasks studied herein consisted only of controlling the positions of two connected links. Many significant human control tasks, such as upright balance, may involve precise control over body segments which are not contiguous. For example, maintaining body center of mass stationarity in reaction to ankle tilt may utilize compensatory movements of the arms as well as legs. Since there are clearly no actuators which connect ankle joints and shoulder joints, any interjoint control must reside in the controller.

It is threfore quite conceivable that the S-mCBLM exerts inherently global feedback coordination for such behaviors. Even in the situation of simple shoulder-elbow coordination, it is not necessarily the case that the intrinsic stiffness ratios of the muscles are ideal. Global controller action may be used to optimize these ratios. In fact, since the stiffness estimates used were measured in intact subjects, it is not clear to what extent the stiffness

values are the product of intrinsic muscle properties, spinal reflex and cerebellar feedback effects.

Fourth, noting that the H_∞ and H_2 controllers had significantly different gains depending on the massiveness of the plant, it is apparent that a change in gain settings is necessary for optimization of integrated total cost. But it is also likely that a change in gain settings is necessary to optimize performance with regard to peak torque, integrated state error and other time-domain measures. Given the natural variation in limb mechanical parameters (typically due to loads), and of desired behaviors, the possibilities outlined above underscore the need for adaptive control.

Both Kawato and Slotine point out the value and tractablity of adaptive feedforward schemes. We do not know precisely what type of feedforward signal the brain provides, but this work suggests that especially if the feedforward signal is crude, optimization, hence adaptation, of the feedback controller may be useful as well. In particular, if the optimal feedforward signal is being learned by the C-lCBLM, then having a well-adapted S-mCBLM would be especially important during the early phases of the learning process. In any case, this study also shows that in disturbance rejection around an equilibrium position or a nominal trajectory, where the feedforward signal with regard to the (unpredicted) disturbance is zero, linear feedback controller design is significant to performance. Hence, controller adaptation is potentially useful from this perspective as well. In terms of Slotine's theory, this problem corresponds to one of optimizing the sliding surface with respect to the plant being controlled quite possibly at the same time that the feedforward signal is being adapted. This would, then, appear to be also an interesting and potentially fruitful direction for further research.

To be sure, the simplifying assumptions underlying this analysis must continue to be reevaluated. Modifications and refinement of the human arm model are certainly necessary to model actual behavior more accurately. The problem of delay compensation, in particular, must be addressed. Assuming, as do Kawato and others, that appropriate compensation does exit, the central issues and results herein, appear to be generally applicable to the problem of controlling *human-like* arms in natural tasks. Therefore, it is likely that, whether or not it is in precisely the manner hypothesized in this study, the brain and spinal cord cooperate to execute global feedback control, with or without position-space gainscheduling. This thesis is consistent with Kawato's framework but emphasizes the importance of

understanding more deeply the structure and role of the feedback control portion.

6.2 Plans for Further Research

The results of this project encourage further work in refining models of cerebellar function from the perspective of feedback linearization with linear MIMO feedback control. Because kinematic arm movement data from human patients having cerebellar dysfunction has already been collected previously by the author, the next step is to attempt to simulate this data using the cerebellar model considered here. Since this data reveals systematic trajectory aberrations in patients versus normal control subjects, it would be very interesting if the abnormal trajectories may be easily generated by reducing the strength of controller feedback below values estimated for normal subjects. This might be done in terms of overall gain reduction, i.e. by scaling G by a factor smaller than unity, as well as by scaling down specific elements within G. This might indicate, for example, whether the physiological derangement consists of global gain attenuation, or predominantly intrajoint, interjoint, general position or general velocity feedback alteration.

A second important goal is to integrate the concepts of dynamic postural force field and dynamic viscosity fields. Flash [26] and Shadmehr et al.[23], have studied postural force fields during multijoint arm movements. Shadmehr, who studied relatively slow (peak velocities on the order of 0.2 m/sec), small amplitude movements found that forces generated during goal-driected movement were consistent with the hypothesis that the center of the postural force field had merely been shifted to the target position; a result which is entirely consistent with, and supportive of the equilibrium trajectory hypothesis for limb movement control.

Flash, however, studied and simulated arm movements with a range of velocities, some exceeding 2.5 m/sec. The study was also consistent with the equilbrium point control hypothesis but only if the magnitude of the stiffness fields was allowed to be scaled upward with increasing hand velocities. Also, the shape of the field and damping ratio of the arm had to be varied somewhat for movement directions. Thus, Flash clearly identified dynamic modifications of the postural fields. Flash points out that muscle stiffness automatically increases with level of muscle activation and so an increase in stiffness field magnitude is not unexpected. However, this observation begs the question of how the appropriate level

of muscle activation increase is specified for a given desired movement velocity.

A possibly simplifying hypothesis is that in addition to the shift in postural stiffness field which occurs with movement, there is an accompanying shift in a *dynamic* viscosity field which is mediated by the cerebellum. Perhaps a significant component of the *apparent* increase in stiffness during movement is due to angular velocity feedback. Velocity feedback might account for much of the "automatic" scaling of muscle activation with intended velocity. This would enable equilibrium trajectory specification to be the only feedforward signal; the dynamics being entirely determined by position and velocity feedback relative to this trajectory. Moreover, it is conceivable that the apparent variation in stiffness scaling with different movement directions may be related to a variation in velocity feedback which occurs for different movements. This could be due to feedback gainscheduling across arm configuration-space, or it might result from fixed feedback gains operating on velocity error signals which vary according to movement.

Finally, a third and major goal for the future, is the investigation of adaptive changes in feedback gain. Mussa-Ivaldi [17] has noted that normal subjects can vary the magnitude, but not necessarily the shape or orientation of stiffness fields on command. If stiffness is substantially due to intrinsic muscle properties, then the fields are likely to have truly invariant shapes and orientations. If, however, a significant amount of effective limb stiffness is the product of cerebellar action, then plastic changes may occur after prolonged (hours to days) training under the proper environmental conditions. If such changes can be demonstrated, then the basis for a model of adaptive cerebellar control could be established.

F

Appendix A

Muscular Plant Model and Equilibrium Control

A.1 The Single-Joint Case

To a first approximation, muscles may be considered springs which have adjustable rest lengths. The equilibrium trajectory hypothesis for limb movement control [2] asserts that joint angle is determined by the equilibrium lengths for the muscles spanning the joint. When the rest lengths of a pair of antagonistic muscles spanning a joint are changed as in Figure A-1a, the joint angle changes until the muscles reach the equilibrium angle for the new rest length settings. Thus, in principle, a movement may be specified entirely by a shift in muscle rest length settings after which the dynamics are determined passively by the spring-like properties of the muscles. Essentially, the muscles provide continuous position error feedback relative to the equilibrium or reference angle setting. Although, experimental support for this hypothesis is variable it remains an active hypothesis regarding limb movement control.

To be sure, for geometrical reasons there is a nonlinear relationship between muscle rest lengths and equilibrium angle so that even linear muscle (linear) stiffness does not imply linear joint (angular) stiffness. Nevertheless, as argued in chapter 2, it may be the case that the spinal cord functions to minimize the effect of the nonlinear relationship so that effectively linear joint stiffness results.

It is also likely, however, that the effective stiffness of the muscles changes (increases)

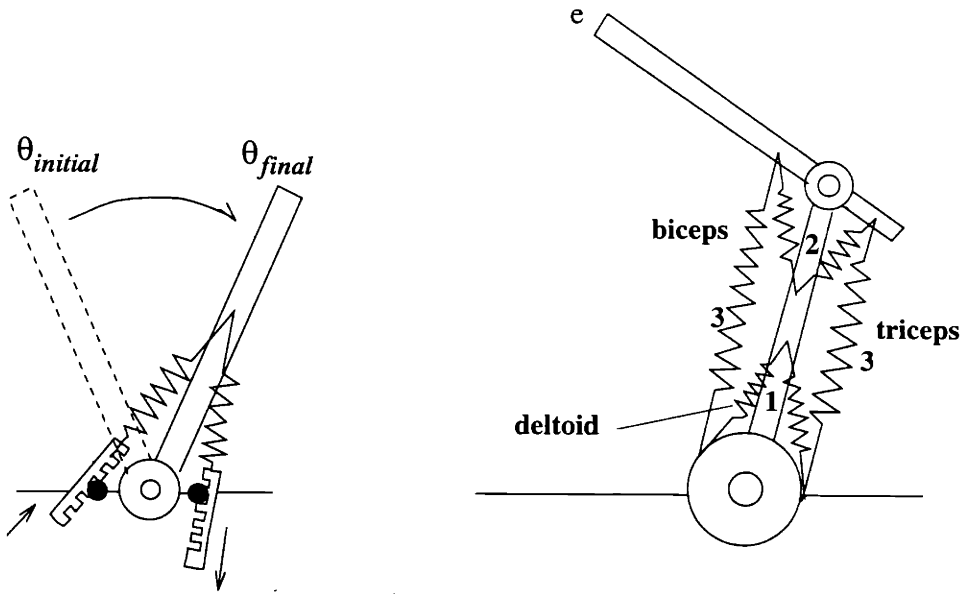

Figure A-1: Representation of human muscular control in terms of pairs of antagonistic springs. a)(left) The position of a single joint is determined by the equilibrium angle for the pair of muscles spanning the joint. This equilibrium angle is in turn determined by the setting of the rest lengths as represented by the ratchets. b)(right) In the two-joint case, single and double joint muscles are required to provide optimal stiffness characteristics at the limb end effector (e). (Figure adapted from Hogan, see text).

during movement [26] presumably to improve tracking of the intended trajectory. The source of this increase is not known, but in this thesis it is hypothesized that it is at least in part mediated by the cerebellum. That is, if the cerebellum served as a position feedback controller, its action would appear as an augmentation of muscle stiffness during movement or active resistance to perturbations.

A.2 The Multijoint Case

The equilibrium trajectory control hypothesis can be extended to the multijoint movement case, but the situation is a bit more complicated. First of all, as pointed out by Hogan [11], the issue of stiffness in a multiarticulated limb is more complex. In this case, the joint stiffnesses create a 2-dimensional postural force field [23] around the arm. In order to optimize the symmetry of this stiffness field at the *end-effector* (e.g. hand or foot), it is essential to have both mono- and multiarticular stiffnesses. This implies that there need to be muscles which span single joints and other muscles which span both joints of an arm. Indeed, as illustrated in Figure A-1b, in a human arm the deltoid spans the shoulder while the short heads of the biceps and triceps span the elbow. The long heads of these muscles span both shoulder and elbow joints. Since an equivalent arrangement exists for the muscles of the leg, credence is strongly added to the idea that end-effector stiffness field optimization is a natural design constraint.

Thus, the limb angular stiffness field which relates angular displacement to the torque generated by the stiffness, τ_s, represented by a matrix, K, of stiffness constants:

$$\text{(A.1)} \qquad \begin{bmatrix} \tau_{1,s} \\ \tau_{2,s} \end{bmatrix} = \begin{bmatrix} -k_1 - k_3 & -k_3 \\ -k_3 & -k_2 - k_3 \end{bmatrix} \begin{bmatrix} \theta_1 - \theta_{1,ref} \\ \theta_2 - \theta_{2,ref} \end{bmatrix} = -K \begin{bmatrix} \tilde{\theta}_1 \\ \tilde{\theta}_2 \end{bmatrix},$$

where k_1 refers to the effective stiffness of the deltoid muscle, k_2 the effective stiffness of the antagonistic muscle pair consisting of the short heads of the biceps and triceps, and k_3 is the effective stiffness of the muscle pair consisting of the long heads of the biceps and triceps.

For the purposes of simulation, Flash uses a variety of effective stiffness matrices which include various scaling factors to account for configuration- and movement-dependent stiffness changes, and which presumably include the effects of cerebellar control. The underlying values for the k_i however, are approximately: $k_1 = k_2 = k_3 = 10$ N-m/rad. Hence the underlying stiffness matrix used for the main plant in this thesis is:

$$K = \begin{bmatrix} 20 & 10 \\ 10 & 20 \end{bmatrix}.$$

The value of 20 N-m/rad for the elbow stiffness also corresponds to the mean value in the "do not resist" condition of Lacquaniti [15].

With regard to control of the multiarticulated limb via the equilibrium trajectory scheme, because of the redundancy in actuators, an additional constraint of some type must included. With multiple joints, limb end-effector position no longer has a one-to-one relationship with pairs of joint angles (i.e. there may be two different pairs of joint angles which yield the same end-effector position). Still, any *given* combination of joint angles yields only one end-effector position and therefore, specification of the joint angles still defines the end-effector position. The difficulty, however, is that the joint angles at equilibrium no longer necessarily correspond to the reference angles.

This is because, from the perspective of independent muscular control via reference angle specification, the torque equation is slightly different from (A.1). Instead, it is of form:

$$\text{(A.2)} \qquad \begin{bmatrix} \tau_{1,s} \\ \tau_{2,s} \end{bmatrix} = \begin{bmatrix} k_1 & k_3 & 0 \\ 0 & k_3 & k_2 \end{bmatrix} \begin{bmatrix} \theta_1 - \theta_{1,ref} \\ (\theta_1 + \theta_2) - \theta_{(3),ref} \\ \theta_2 - \theta_{2,ref} \end{bmatrix} = K' \begin{bmatrix} \tilde{\theta}_1 \\ \tilde{\theta}_{(3)} \\ \tilde{\theta}_2 \end{bmatrix},$$

where $\theta_{(3),ref}$ is the equilibrium angle specification for the third muscle pair.

Since this system is overdetermined, it is possible to have $[\tau_1, \tau_2]^T = 0$ while

$$[\tilde{\theta}_1, \tilde{\theta}_{(3)}, \tilde{\theta}_2]^T \neq 0.$$

Moreover, there is typically an infinite number of angular positions different from the reference values which satisfy this (A.2). To eliminate this problem a further constraint is required. A simple solution is if $\theta_{(3),ref} = \theta_{1,ref} + \theta_{2,ref}$. In this case, equation A.2 becomes equivalent to A.1 and for a wide range of reasonable values for the k_i, the matrix K is positive definite, hence invertible and able to force the equilibrium joint angles to match the reference values.

Pellionisz [22] recognizes the problem of muscle redundancy as a major one and suggests that a primary function of the cerebellum is its solution. Whether the cerebellum is *necessary* for this calculation is not known definitively. However, since *static* end-effector

position specification is not fundamentally abnormal individuals with cerebellar impairment (aside from the presence of a persistent tremor which is sometimes seen), it does not seem likely that this is the case; at least not in posture maintenance or slow movements. Because arm-muscle redundancy can be managed by the simple constraint outlined above, which could presumably be executed by the spinal cord, the arm model used in this study neglects the potential independence of muscular control and uses K rather than K' as the effective stiffness matrix.[1]

In any case, the action of the cerebellum in augmenting the stiffness field of a multiarticulated limb during movement is likely to be more complex than with a single joint. And it is in the derangement of high-velocity multijoint movements that the presence of cerebellar impairment is dramatically evident. A central issue of the thesis, then, is whether interjoint feedback is required for optimal control of multijoint tracking and regulation, analogously to the requirement for biarticular muscles in optimally shaping the static postural force field.

Finally, it is hypothesized herein that the cerebellum provides not only angle error, but angular velocity error feedback signals as well. If this is so, then the action of the cerebellum is not only to provide dynamic augmentation of the limb's postural force field, but to provide in addition a "dynamic viscous force field". That is, it creates an effective "dynamic viscosity" which rejects deviations from the limb reference velocity instead of from zero. It is presumed that the strength of this dynamic viscosity is sufficient to dominate the effects of the intrinsic viscosity of the muscle tissue.

[1]That the cerebellum may not be necessary to handle muscle redundancy, of course, does not imply that its operation does not take redundancy into account. More sophisticated models of cerebellar function *may* profitably include independent muscular control.

Appendix B

Mathematical Results

B.1 Observability and Controllability of the Plant

The plant $\mathcal{P}$ is trivially observable because the availablilty of full state information has been assumed.

Controllability is established by observing that:

$$[B \quad AB] \quad = \quad \begin{bmatrix} 0 & H^{-1}K \\ H^{-1}K & -H^{-1}CH^{-1}K \end{bmatrix}.$$

Since H^{-1} is invertible, it has full column rank. Therefore, since K is nonzero, $H^{-1}K$ also has full column rank, and so does $[B \quad AB]$. Hence, the plant is controllable for any value of C.

B.2 Stability of H_2 and H_∞ Controllers in Adaptive Feedback Linearization

As mentioned in section 2.2.2, Slotine and Li [24, pages 404-405] present an adaptive feedback linearization scheme for which global stability is assured. The argument relies on a particular adaptive law which is based on a linear combination of state errors represented by the summary variable "s". s is defined as:

$$\mathbf{s} = (\Lambda\tilde{\boldsymbol{\theta}} + \dot{\tilde{\boldsymbol{\theta}}})$$

for some matrix Λ where $-\Lambda$ is Hurwitz.[1]

They demonstrate that if feedback is of the form:

(B.1) $$K_D \mathbf{s}$$

where K_D is positive definite matrix, then the adaptive law:

$$\dot{\hat{\mathbf{a}}} = -\Gamma Y^T \mathbf{s}$$

where $\dot{\hat{a}}$ is a vector of parameter estimates, Γ is an arbitray symmetric positive definite gain matrix, Y is a matrix of system dynamics in terms of $\mathbf{s}$, guarantees global stabilization of the plant $\mathcal{P}'$ given by:

(B.2) $$\mathcal{P}': \qquad \dot{\mathbf{q}} = A'\mathbf{q} + B_1\mathbf{u}$$

where

$$A' = \begin{bmatrix} 0 & I_2 \\ 0 & -H^{-1}C \end{bmatrix}$$

and B_1 is as in (2.4).

Evidently, $\mathcal{P}'$ is the same as $\mathcal{P}$ in (2.4) except that there is no stiffness K within the plant itself. Thus, for $\mathcal{P}'$, feedback gain is determined entirely by the controller K_D.

The proof presented below, establishes that state feedback controllers, G, resulting from H_2 and H_∞ design methodologies produce globally stable adaptive control for $\mathcal{P}'$ because under a mild condition to be specified, they provide feedback which is of form (B.1). The proof does not, however, extend completely to plant $\mathcal{P}$ at present. Extension to cover $\mathcal{P}$ is the subject of ongoing work.

First, we know from (3.1) that for $\mathcal{P}'$, G will be of form: $G = R^{-1}B_1^T X$, where X solves the appropriate algebraic Riccati equation. Hence we have that:

$$G = [G_1\ G_2] = R^{-1}[0\ \ (H^{-1})^T]X$$

$$G = R^{-1}[(H^{-1})^T X_{21}\ \ (H^{-1})^T X_{22}]$$

where

[1]Note the difference between this notation and that used by Slotine and Li. Specifically, in this thesis $\mathbf{q}$ is defined differently.

$$X = \begin{bmatrix} X_{11} & X_{12} \\ X_{21} & X_{22} \end{bmatrix},$$

and therefore, $X_{21} = X_{12}^T$ and X_{11}, X_{22} are both symmetric positive definite by the symmetry and positive definiteness of X.

Now since $H > 0$ and hence $(H^{-1})^T > 0$, we have $(H^{-1})^T X_{22} > 0$ and therefore $((H^{-1})^T X_{22})^{-1} = X_{22} H^T$ exists. So we may write:

(B.3) $$G = (R^{-1}(H^{-1})^T X_{22})[X_{22}^{-1} X_{21} \quad I_2].$$

Because $R > 0$ we have $R^{-1} > 0$ and so $(R^{-1}(H^{-1})^T X_{22}) > 0$ as well.

Therefore, we can define $\Lambda = X_{22}^{-1} X_{21}$ and $\Lambda_2 = R^{-1}(H^{-1})^T X_{22}$ and write (B.3) as:

$$G = \Lambda_2[\Lambda \quad I_2],$$

so that state error feedback can be written:

$$G\tilde{\mathbf{q}} = \Lambda_2[\Lambda \quad I_2]\tilde{\mathbf{q}} = \Lambda_2(\Lambda\tilde{\boldsymbol{\theta}} + \dot{\tilde{\boldsymbol{\theta}}}).$$

From its definition, we have that $\Lambda_2 > 0$, then if $-\Lambda$ is Hurwitz, then $G\tilde{\mathbf{q}} = \Lambda_2 \mathbf{s}$ is of form (B.1).

It is now simply necessary to show that $-X_{22}^{-1} X_{21}$ is Hurwitz. Let $eig(A)$ stand for the set of eigenvalues of A. It can be shown [25, pages 262-263] that if $B > 0$ then $eig(B^{-1}A) > 0$ iff $eig(A) > 0$. Thus, we seek to show that $eig(X_{21}) > 0$.

Well, given the algebraic Riccati equation:

$$0 = XA' + (A')^T X + \begin{bmatrix} Q_1 & 0 \\ 0 & Q_2 \end{bmatrix} - XB_1 R^{-1} B_1^T X$$

with A' and B_1 as defined above, we obtain the four matric equations:

$$Q_1 = X_{21} H^{-1} R^{-1} (H^{-1})^T X_{21}$$

(B.4) $$0 = X_{11} + X_{12}(-H^{-1})C - X_{12} H^{-1} R^{-1} (H^{-1})^T X_{22}$$

(B.5) $$0 = X_{11} + (-H^{-1}C)^T X_{21} - X_{22} H^{-1} R^{-1} (H^{-1})^T X_{21}$$

$$Q_2 = -X_{21} - X_{21}^T - (H^{-1}C)^T X_{22} - X_{22}H^{-1}C + X_{22}H^{-1}R^{-1}(H^{-1})^T X_{22}$$

Combining (B.4, B.5) we have:

$$-2X_{11} = X_{12}M_2 + M_2^T X_{21} \tag{B.6}$$

where $M_2 = -H^T[C + R^{-1}(H^{-1})^T X_{22}]$. Now suppose that M_2 is Hurwitz *and diagonalizable*, then $M_2 = PJP^{-1}$ for some diagonal matrix J which is negative definite and some nonsingular matrix P. So:

$$-2X_{11} = X_{12}PJP^{-1} + (P^{-1})^T JP^T X_{12}^T,$$

or

$$-2P^T X_{11}P = P^T X_{12}PJ + JP^T X_{12}^T P$$

Because $X_{11} > 0$, $P^T X_{11}P > 0$ so $-2P^T X_{11}P < 0$. This is a Lyapunov equation where $J < 0$ hence $-P^T X_{12}P$ is stable. This means that $eig(P^T X_{12}P) > 0$ and, hence, $eig(X_{12}) > 0$. The last result is because a congruence transformation does not change the signs of the eigenvalues.

With regard to the conditions on M_2, it can be demonstrated that M_2 is Hurwitz as follows: Since all H_2 and H_∞ controllers are stabilizing, $A' - B_1 G$ is Hurwitz. We note that

$$A' - B_1 G = \begin{bmatrix} 0 & I_2 \\ M_1 & M_2 \end{bmatrix}$$

where $M_1 = R^{-1}H^{-1}X_{21}$ and M_2 is as defined above.

Now if $Z = W + W^T$ then W is nonsingular if Z is positive or negative definite. Since otherwise, if det(W)=0, then there exists x such that $Wx = 0$ and $x^T Zx = x^T Wx + x^T W^T x = 0$ which contradicts the definiteness of Z. Therefore, from (B.6), $X_{12}M_2$ is nonsingular. So X_{12} and M_2 are each nonsingular.

Finally, we note the following congruence transformation on $A' - B_1 G$:

$$M(A' - B_1 G)M^T = \begin{bmatrix} -M_2^{-1}M_1 & 0 \\ M_1 - M_2(M_2^{-1})^T & M_2 \end{bmatrix}, \tag{B.7}$$

where

$$M = \begin{bmatrix} I_2 & -M_2^{-1} \\ 0 & I_2 \end{bmatrix}.$$

Thus, the RHS of (B.7) is Hurwitz implying, because of its block-triangular form, that M_2 is also.

The condition that M_2 be diagonalizable remains necessary for the proof at the present time.

B.3 Stability of *ad hoc* Feedback Controllers

The stabilizing property of LPD controllers for which the on-diagonal elements are positive is evident given the arguments of Slotine [24, pages 89-90]. For the *ad hoc* controllers (defined in section 3.3.3) of form:

$$G = [G_1 \;\; G_2] = \begin{bmatrix} a & \frac{a+b}{4} & c & \frac{c+d}{4} \\ \frac{a+b}{4} & b & \frac{c+d}{4} & d \end{bmatrix},$$

to invoke Slotine's argument we must to determine under what circumstances the G_i are positive definite. Taking G_1 without loss of generality, we note that:

$$\det G_1 = |G_1| = ab - \frac{a^2 + 2ab + b^2}{16}$$

so that

$$16|G_1| = 14ab - a^2 - b^2, \quad \text{and therefore } |G_1| = 0 \text{ implies: } a^2 - 14ab + b^2 = 0$$

or

$$a = b(7 \pm 4\sqrt{3})$$

hence:

$$|G_1| > 0 \text{ iff } 0.07179 \leq \frac{a}{b} \leq 13.928,$$

and G_1 will be positive definite iff, in addition, $a > 0$ (and so $b > 0$).

Bibliography

[1] J. S. Albus. A theory of cerebellar functions. *Mathematical Bioscience*, 10:25–61, 1971.

[2] E. Bizzi, A. Polit, and P. Morasso. Mechanisms underlying achievement of final head position. *Journal of Neurophysiology*, 39:435–444, 1976.

[3] James R. Bloedel and Jacques Courville. *Handbook of Physiology – The Nervous System II: Chapter 16.* American Physiological Society, 1981.

[4] Daniel Bullock and Jose Contreras-Vidal. How spinal neural networks reduce discrepancies between motor intention and motor realization. *Boston University Center for Adaptive Sytems: Technical Report*, CAS/CNS-91-023:1–35, 1991.

[5] Stephen C. Cannon and George I. Zahalak. The mechanical behavior of active human skeletal muscle in small oscillations. *Journal of Biomechanics*, 15(2):25–61, 1982.

[6] P.M. Fitts. The information capacity of the human motor system in controlling the amplitude of movement. *Journal of Experimental Psychology*, 47(6):381–391, 1954.

[7] H.J. Freund and V. Dietz. *Physiological Tremor, Pathological Tremor and Clonus*, pages 66–89. Karger, Basel, 1978.

[8] M. Fujita. Adaptive filter model of the cerebellum. *Biological Cybernetics*, 45:195–206, 1982.

[9] S. Gilman and W.I. MacDonald. Relation of afferent fiber conduction velocity to reactivity of muscle spindle receptors after cerebellectomy. *Journal of Neurophysiology*, 30:1513–1522, 1967.

[10] R. Granit, B. Holmgren, and P.A. Merton. The two routes for excitation of muscles and their subservience to the cerebellum. *Journal of Physiology, London*, 130:213–224, 1955.

[11] Neville Hogan. The mechanics of multi-joint posture and movement control. *Biological Cybernetics*, 52:315–331, 1985.

[12] James C. Houk and Zev W. Rymer. *Handbook of Physiology – The Nervous System II: Chapter 8.* American Physiological Society, 1981.

[13] J.C. Houk, J. Keifer, and A.G. Barto. Distributed motor commands in the limb premotor network. *Trends in Neuroscience*, 16(1):27–33, 1993.

[14] M. Kawato, K. Furakawa, and R. Suzuki. A hierarchical neural-network model for control and learning of voluntary movement. *Biological Cybernetics*, 57:169–185, 1987.

[15] F. Lacquaniti, F. Licata, and J.F. Soechting. The mechanical behavior of the human forearm in response to transient perturbations. *Biological Cybernetics*, 44:35–46, 1982.

[16] D. Marr. A theory of the cerebellar cortex. *Journal of Physiology*, 202:437–470, 1982.

[17] Bizzi E Mussa-Ivaldi FA, Hogan N. Neural, mechanical and geometrical factors subserving arm posture in humans. *Journal of Neuroscience*, 5:2732–2743, 1985.

[18] P.D. Neilson. A computational model of central information-processing in motor control. *International Journal of Neuroscience*, 35(1-2):140–141, 1987.

[19] P.D. Neilson, N.J. O'Dwyer, and M.D. Neilson. Central processes underlying the movement disorders of cerebral palsy: a computational model of brain function. *Unpublished Manuscript.*

[20] W. L. Nelson. Physical principles for economies of skilled movements. *Biological Cybernetics*, 46:135–147, 1983.

[21] C.E. Osborn and R.E. Poppele. Parallel distributed network characteristics of the DSCT. *Journal of Neurophysiology*, 68(4):1100–1112, 1992.

[22] A. Pellionisz and R. Llinas. Tensor network theory and the metaorganization of functional geometries of the nervous system. *Neuroscience*, 16(2):245–273, 1985.

[23] Reza Shadmehr, Ferdinando. Mussa-Ivaldi, and Emilio Bizzi. Postural force fields of the human arm and their role in generating multi-joint movements. *Journal of Neuroscience*, 13(1):45–62, 1993.

[24] Jean-Jacques Slotine and Weiping Li. *Applied Nonlinear Control.* Prentice-Hall, Inc., 1991.

[25] Gilbert Strang. *Linear Algebra and its Applications.* Harcourt Brace Jovanovich., 1980.

[26] Flash T. The control of hand equilibrium trajectories in multi-joint arm movements. *Biological Cybernetics*, 57:257–274, 1987.

[27] W.T. Thach, H.P. Goodkin, and J.G. Keating. The cerebellum and the adaptive coordination of movement. *Annual Review of Neuroscience*, 15:403–442, 1992.

[28] Y. Uno, M. Kawato, and R. Suzuki. Formation and control of optimal trajectory in human multijoint arm movement. *Biological Cybernetics*, 61:89–101, 1989.

[29] T. Villis and J. Hore. Central neural mechanisms contributing to cerebellar tremor produced by limb perturbations. *Journal of Neurophysiology*, 43(2):279–291, 1980.